Multiple Antenna Concepts in OFDM Transmission Systems

Vom Promotionsausschuss der
Technischen Universität Hamburg-Harburg

zur Erlangung des akademischen Grades

Doktor-Ingenieur

genehmigte Dissertation

von
Christian Stimming

aus
Gießen

2009

1. Gutachter: Prof. Dr. Hermann Rohling
2. Gutachter: Prof. Dr.-Ing. habil. Udo Zölzer
Tag der mündlichen Prüfung: 12. Juni 2009

Persistent Identifier:
urn:nbn:de:gbv:830-tubdok-5778

Contents

Acknowledgments

The research work described in this thesis has been carried out during my stay at the Institute of Telecommunications at the Technische Universität Hamburg-Harburg.

I would like to thank Prof. Dr. Hermann Rohling for the helpful support at all times during the years of my research. Furthermore I am thankful for all the colleagues and students who created a great work environment at the Institute of Telecommunications. In particular, the support and fruitful discussions with Alexandre Vanaev, Jianjun Ran, Christian Fellenberg, Volker Ohlen, and Rainer Grünheid have been a great inspiration to me.

Finally I would especially like to thank my wife Anne for her continuing support during challenging tasks such as raising our wonderful children or finishing this thesis. Together with her "we will in all things grow up into him who is the head, that is, Christ."[1]

Hamburg, June 2009 Christian Stimming

[1] The Bible, Ephesians 4:15

1 Introduction

With the expected development of new mobile multimedia services in the coming years, radio systems will have to meet demands for much higher data rates than today. Those variable and high data rates (20 Mbps and more) will be requested at all different levels of mobility, even at high vehicular speeds. Therefore future radio systems will have to offer data services at a high degree of flexibility, where additionally high adaptivity to the actual transmission situation is necessary. To meet this demand for higher data rates, new technologies need to be implemented.

In general, the design of communication systems depend strongly on the properties of the radio channel. Broad-band radio propagation is characterized by a multitude of propagation paths ("multi-path") which lead to a frequency selective behavior of the radio channel. In high data rate applications this leads to strong Inter-Symbol Interference (ISI), which requires a high equalization complexity at the receiver. Multicarrier techniques have been proposed to deal with the frequency selectivity while still keeping the implementation feasible. In these techniques, a high rate source data stream is distributed onto multiple parallel low rate substreams which are modulated individually and transmitted simultaneously. In *Orthogonal Frequency Division Multiplexing* (OFDM), those substreams are chosen to be orthogonal subcarriers. Due to this, OFDM is an effective transmission technique to deal with the frequency selectivity with low complexity.

An interesting new technology proposes to use multiple transmit and receive antennas simultaneously, denoted as *Multiple Input Multiple Output* (MIMO, figure 1.1), which will be used in combination with OFDM in this thesis. The multiple antennas will transmit simultaneously and in the same radio frequency. Even though conventionally this would result in degraded performance due to interference, suitable MIMO techniques exist so that this simultaneous transmission can be used to increase the resulting data rate significantly [Fos96, RC98, TSC98, Ala98]. With this MIMO techniques, the radio channel can have a much higher capacity, enabling very high data rates.

However, this improved channel capacity depends strongly on the properties of the radio channel: If there are a lot of different radio propagation paths

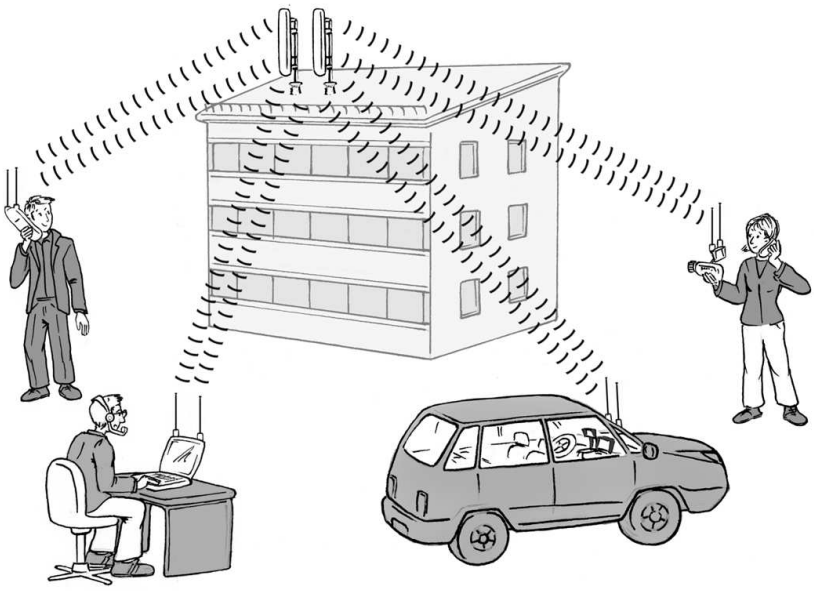

Figure 1.1: Multiple users using MIMO radio communication

through reflection and rich scattering, the capacity is indeed increased significantly. In contrast to this, a radio channel with only few propagation paths will offer almost no improvement compared to a single antenna system.

Simulations of communication systems are of crucial importance to evaluate the design and implementation of new systems. In such simulations the relevant radio channel properties need to be modeled realistically and an adequate statistical model for the essential properties of this channel need to be found. Unfortunately, simple multi-antenna radio channel models will predict the increased MIMO capacity to be available in all circumstances, which will result in too optimistic simulation results.

In this thesis, a new multi-antenna radio channel model will be developed that characterizes the relevant properties of the channel but is still easily configurable. The relevant parameters of a MIMO radio channel model are explained and lead to the newly introduced MIMO-WSSUS (Wide Sense Stationary Uncorrelated Scattering) radio channel model. This approach promises to represent the MIMO-related channel properties realistically enough, so that MIMO techniques can now be evaluated by simulations which give realistic performance results.

Subsequently, this thesis introduces several basic MIMO techniques:

- *Receiver Diversity* where multiple receiving antennas for combining several independent copies of the received signal are used.

- *Transmit Diversity* to send one data stream in precoded form over multiple transmit antennas simultaneously, which will be re-assembled in the receiver.

- *Spatial Multiplexing* to transmit multiple data streams in parallel, which can be distinguished in the receiver as long as the radio channel has rich enough scattering.

These techniques are evaluated by simulations in the context of high data rates and different radio channel conditions. Simulations are carried out both in a simple radio channel model and the newly proposed MIMO-WSSUS model.

Additionally, a linear precoding technique with variable amount of feedback from [Tau05] is explained and improved. This technique calculates a matrix factorization of the optimum precoding matrix into unitary product matrices, some or all of which can be used for the approximation of the optimum precoding matrix. All or only a subset of the factorization matrices can be fed back to the transmitter to reduce the required feedback data rate. This enables a trade-off between the amount of feedback information and system performance. In this thesis, an improvement to the matrix parameterization is introduced, which shows a performance gain over the original parameterization.

For all techniques, the performance will be evaluated and the dependency on the radio channel model and its chosen parameters will be shown. It is expected that in a rich scattering channel even the simple Spatial Multiplexing techniques with linear receiver will strongly increase the available data rate when increasing the number of transmit and receive antennas. However, in a more unfriendly radio channel with little scattering as modeled with the new MIMO-WSSUS model, it is expected that Spatial Multiplexing techniques perform not as good anymore.

It can be concluded that MIMO performance simulations must use a MIMO radio channel model which adequately describes the radio channel conditions even with little scattering. Otherwise unrealistically optimistic performance results will occur. The introduced MIMO-WSSUS radio channel model is a simple approach that represents these statistical properties accurately enough and is still easily configurable.

The thesis is divided as follows:

The general properties of radio channels are introduced in chapter 2 for single-antenna communication.

Chapter 3 explains the OFDM transmission technique as an effective way of broad-band communication.

In chapter 4, a new multi-antenna radio channel model is being developed in logic continuation to the single-antenna radio channel WSSUS model, but with adequately representing the important multi-antenna correlation. This introduces the new MIMO-WSSUS radio channel model.

Several basic MIMO techniques will be introduced in chapters 5 through 7. Each of the described MIMO techniques are evaluated both in simple MIMO radio channels and in the MIMO-WSSUS model, and in some cases this gives different results than what has been expected by previously proposed channel models.

To demonstrate the important influence of the MIMO radio channel model, eventually chapter 8 repeats some system evaluations but with different MIMO radio channel models as taken from literature. This will underline the importance of the radio channel model developed in this thesis and the required attention for the channel model when system performance is evaluated with simulations.

The thesis is finished by the conclusion and appendix.

2 Radio Channel Model

2.1 Introduction

The fundamental limitations of wireless data transmission are given by the properties of the radio channel. The first step in understanding the relevant performance parameters in every study is to characterize the radio channel and find suitable models for those effects that will actually appear in reality.

For a single radio communication link, three effects are most relevant for the digital communication and are considered in the following section:

- Path loss
- Shadowing
- Multi-path propagation

From the point of view of a mobile receiver, all these effects will influence the received signal after transmission through the channel. Eventually it will not be necessary to model each effect correctly individually, but instead to model the effect of the whole radio channel on the transmitted input signal. For this reason, the radio channel is modeled as a *Linear Time-Invariant (LTI) system*.

In multi-antenna (MIMO) radio communication, in addition the *dependency* or *correlation* properties between the multiple available radio channels are extremely relevant to the performance of a communication system, which will be discussed in chapter 4.

For any kind of proposed transmission system it is vital to demonstrate the actual benefit of one approach versus others. In order to show this comparison under controllable conditions, it is necessary to use a statistical radio channel model in which the algorithms and systems can be evaluated. The following section describes the relevant effects of the radio channel and the implications on radio channel models.

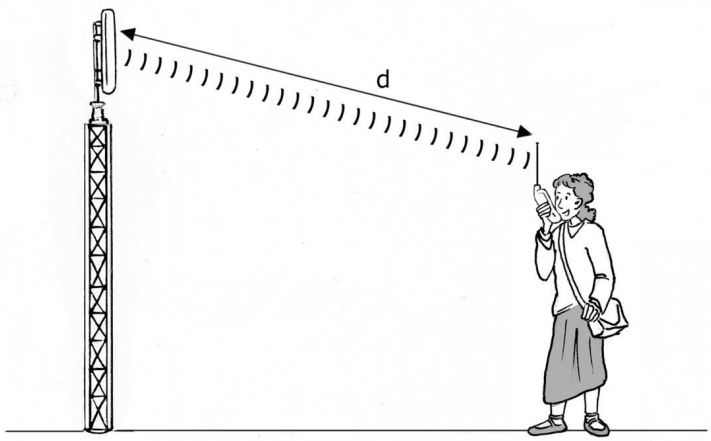

Figure 2.1: Path loss as a function of distance d

2.2 Path Loss

The signal power of a received radio signal decreases with increasing distance d between transmitter and receiver (figure 2.1). In free-space propagation, the received power $P(d)$ at distance d decreases according to

$$P(d) = \frac{P_t G_{tx} G_{rx} \lambda^2}{(4\pi d)^2} \tag{2.1}$$

where P_t is the transmitted power, G_{tx} and G_{rx} is the antenna gain of the transmit and receive antenna, respectively, and λ is the wave length of the transmission wave.

It is obvious from (2.1) that the received power decays with d^{-2} in free space propagation conditions. If the free space condition is not met and instead objects are placed in between the transmitter and receiver, the power decay will be even stronger, leading to a decay according to $d^{-\alpha}$ with the *path loss exponent* $\alpha > 2$.

The received signal power in free space propagation can be calculated deterministically. However, in realistic propagation conditions it is not possible to take into account all different objects that exists in the propagation region. Instead, some approximations from extensive measurements will be used to model the path loss as a function of distance. Examples of path loss approximations can be found in [OOKF68, Hat80, WB88, IYTU84].

In this work, the decay of the received power is approximated by the model of a deterministic function that decreases with the distance d. Two different path gain models will be considered: Single-slope exponential decay, and dual-slope exponential decay.

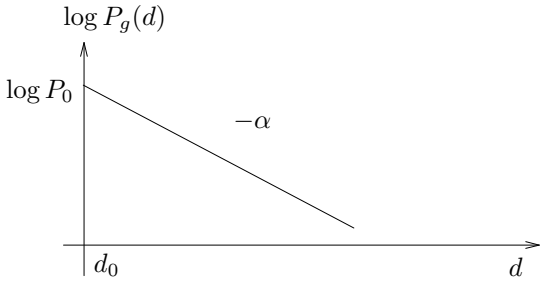

Figure 2.2: Single-slope radio channel model ($P(d)$ plotted in logarithmic scale)

2.2.1 Single-slope path loss model

The first path gain model in this work is assumed to follow a single slope exponential decay (figure 2.2), so that the received power after path gain $P_g(d)$ at a distance d from the transmitting antenna is approximated by

$$P_g(d) = P_0 \left(\frac{d}{d_0}\right)^{-\alpha} \tag{2.2}$$

where P_0 is the reference received power at some reference distance d_0, and α is the *path loss exponent* and the equation can also be given in dB, as follows:

$$P_g(d)_{[dB]} = P_{0[dB]} - \alpha \cdot 10 \log(\frac{d}{d_0}) \tag{2.3}$$

Common choices for the path loss exponent α are in the range $2 \ldots 4$. In this work, a value of $\alpha = 3.0$ [SCR05] is being used.

The constants P_0 and d_0 are a simplification from (2.1) that take into account the transmit power, both antenna gains, and the additional constants. This simplification is especially useful because in this work, only relative power levels are of importance instead of absolute ones.

2.2.2 Dual-slope path loss model

As an alternative radio propagation model, a *dual-slope* exponential decay could be considered as well (figure 2.3). The received power after path gain $P_g(d)$ at a distance d from the transmitting antenna is then approximated by

$$P_g(d) = \begin{cases} P_0 \left(\frac{d}{d_0}\right)^{-\alpha_1} & \text{for } d \leq D_t \\ P_0 \left(\frac{D_t}{d_0}\right)^{-\alpha_1} \left(\frac{d}{D_t}\right)^{-\alpha_2} & \text{for } d > D_t \end{cases} \tag{2.4}$$

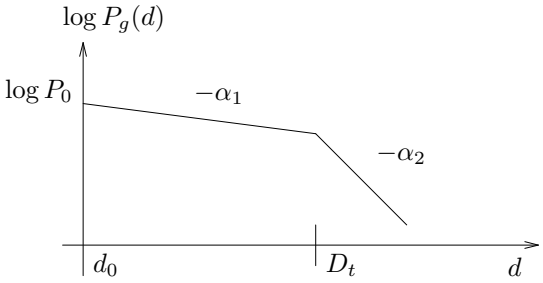

Figure 2.3: Dual-slope radio channel model ($P(d)$ plotted in logarithmic scale)

The dual-slope model has two different path loss exponents, where the exponent of the smaller distances α_1 is chosen smaller than the exponent α_2 of the larger distances. This model should take into account the change in propagation conditions of dense urban areas, where there is a different path loss between the base station and the first row of buildings compared to the second and further row of buildings.

The threshold distance D_t is defined in terms of the cell radius R of a cellular system as

$$D_t = \delta_t R \tag{2.5}$$

where δ_t denotes the *relative threshold distance*. Possible values for the relative threshold distance in the following are $\delta_t = 1$, 1.2, 1.5, or 2, i.e. the threshold distance is on the order of the cell radius or slightly larger.

One common choice for the path loss exponents is $\alpha_1 = 2, \alpha_2 = 4$. For the relative threshold distance a value $\delta_t = 1.2$ would result for a particular cell radius $R = 250m$ and a threshold distance $D_t = 300m$, resulting in the abovementioned relative threshold distance [WDM05].

The constants P_0 and d_0 do not need to be fixed here because only the *SIR* expressions are of interest below and these constants will cancel out anyway.

2.3 Shadowing

The path-loss at a particular location depends not only deterministically on the distance to the base station, but also randomly on particular terrain features such as obstructions in the radio channel propagation, or additional reflections from neighboring buildings, or diffraction from vegetation, see figure 2.4. These influences are called *shadowing* [Rap01]. Although each of these effects are well known, in general it is not possible to calculate the resulting received power exactly because of the large number of input parameters. Therefore in radio communications the effect of shadowing is commonly summarized by a stochastic

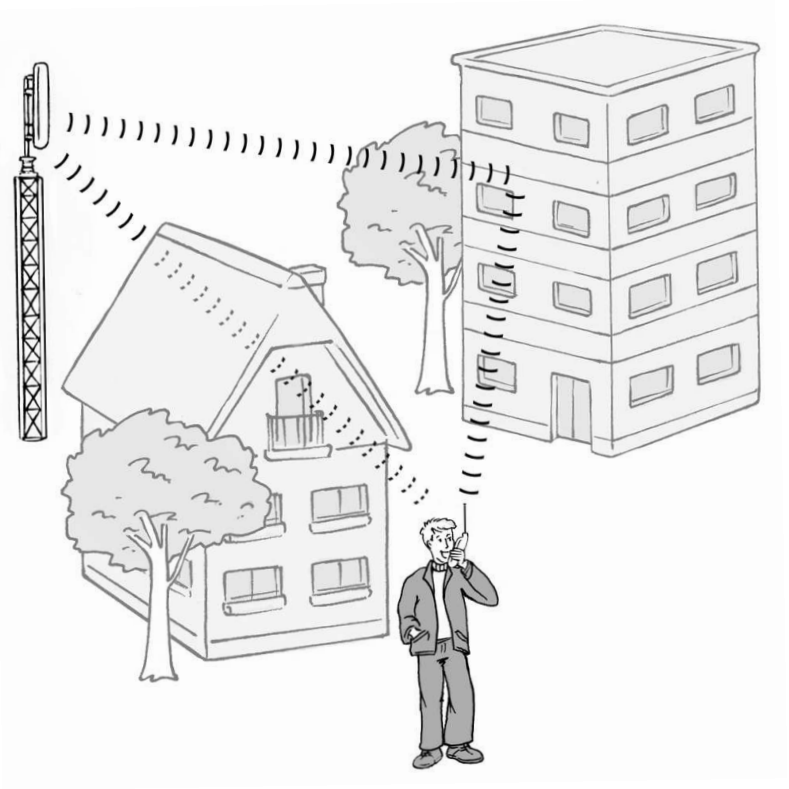

Figure 2.4: Obstructed and reflected radio propagation: Shadowing

model as an additional *random variable* X_σ with *log-normal* distribution. The received power including path gain and shadowing $P_s(d)$ is then

$$P_s(d) = P_g(d) \cdot X_\sigma \tag{2.6}$$

where $P_g(d)$ is the path gain from (2.2) or (2.4).

On a linear scale, the shadowing is a multiplicative random variable X_σ with log-normal distribution. A random variable with log-normal probability distribution is one whose logarithm is normally (GAUSSIAN) distributed, and the probability density function (figure 2.5) is

$$f_{X_\sigma}(x; \mu, \sigma) = \frac{1}{x\sigma\sqrt{2\pi}} \exp\left(-\frac{(\ln x - \mu)^2}{2\sigma^2}\right) \tag{2.7}$$

for $x > 0$, where μ and σ are the mean and standard deviation of the variable's logarithm $\ln x$. The expectation is $E(X) = e^{\mu+\sigma^2/2}$ and the variance is $var(X) = (e^{\sigma^2} - 1)e^{2\mu+\sigma^2}$. This distribution is suitable for this problem because it models the multiplicative product of many small independent factors, which model the multiplicative changes to the path loss by many different objects involved in the propagation path.

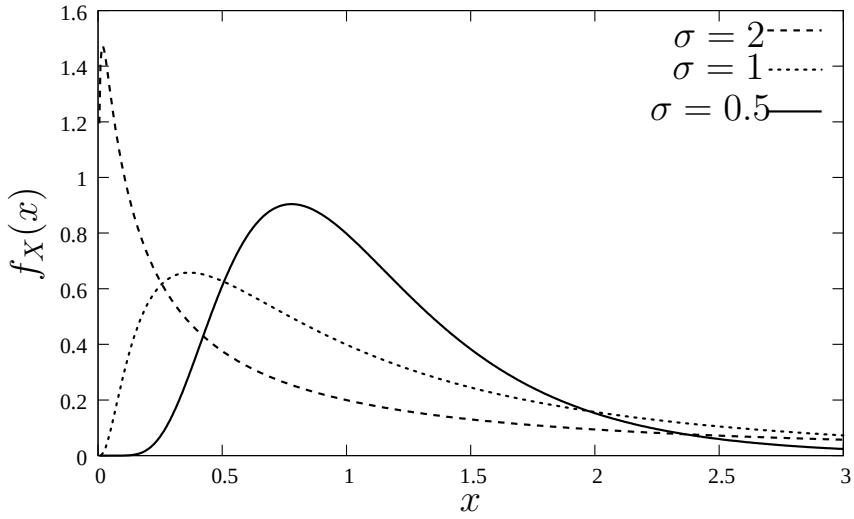

Figure 2.5: Log-normal Probability Density Function, linear scale

If the path loss is described on a logarithmic scale (in dB), then the shadowing $X_{\sigma[dB]}$ is modeled by an additive random variable with GAUSSIAN distribution, standard deviation σ and zero mean. The received power after path gain in dB (2.3) and shadowing is then given by:

$$P_s(d)_{dB} = P_{0[dB]} - \alpha \cdot 10 \log(\frac{d}{d_0}) + X_{\sigma[dB]} \tag{2.8}$$

Since the shadowing has a normal distribution in dB, so has the received power $P_r(d) = P_s(d)$. The probability that the received power will exceed a particular level x is obtained from the Q-function[1] as:

$$Prob[P_r(d) > x] = Q\left(\frac{x - \bar{P_r}(d)}{\sigma}\right) \tag{2.9}$$

Typical values of the standard deviation σ for the lognormal distribution of the shadowing are around 7-9 dB for a transmission at 1-3 GHz and outdoor environments and 1-16 dB for indoor applications [Rap01]. Values of σ between 1-6 dB and 1-4 dB are reported from indoor measurements at 2 GHz [PL95].

2.4 Multi-Path Propagation

The third – and for digital communication most significant – effect of the radio channel on the transmitted signal is the reception of a superposition of multiple

[1]The Q-Function is defined as a normalized form of the cumulative GAUSSIAN probability density function, $Q(x) = \frac{1}{\sqrt{2\pi}} \int_0^x e^{-t^2/2} dt = \frac{1}{2}\left[1 - erf(\frac{x}{\sqrt{2}})\right]$

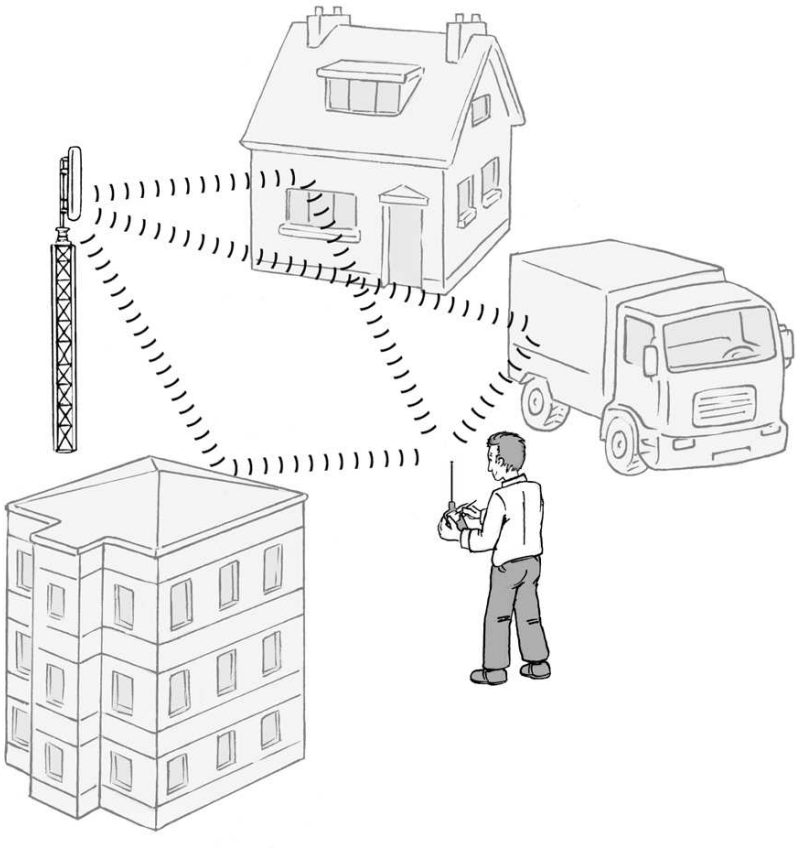

Figure 2.6: Superposition of multiple radio propagation paths: Multi-Path

propagation paths (figure 2.6). These effects are modeled by describing the radio channel as a LTI system, which is fully characterized by its the *impulse response* $h(\tau)$ or the *transfer function* $H(f)$. The path gain and shadowing from before will be multiplied to calculate the actual channel impulse response

$$h_g(\tau, d) = P_s(d) \cdot h(\tau) \tag{2.10}$$

For brevity, the factor $P_s(d)$ will be neglected in the rest of this section and only $h(\tau)$ will be considered.

2.4.1 Multiple reflectors

The most important property of the radio channel is the propagation over multiple paths, which are all attenuated and delayed differently (figure 2.7). Each of these K paths (figure 2.7) has different delay τ_k, phase shift θ_k, and attenuation $\alpha_k > 0$. For a single-antenna system, this results in the following channel impulse response:

$$h(\tau) = \sum_{k=1}^{K} \delta(\tau - \tau_k)\alpha_k e^{j\theta_k} \tag{2.11}$$

The Fourier transform of the channel impulse response is called the *channel transfer function* $H(f)$. It is calculated from $h(\tau)$ by the Fourier transform which is

$$H(f) = \int_{-\infty}^{\infty} h(\tau) \cdot e^{-j2\pi\tau f}\, d\tau \tag{2.12}$$

The channel transfer function for a multi-path radio channel shows a characteristic behavior which is called *frequency selectivity*.

This model (2.11) describes well the situation of a large number of propagation paths that have an attenuation of approximately the same order of magnitude. This corresponds to the physical situation where no direct line-of-sight propagation path exists (figure 2.4), which is also called a *non line-of-sight* (NLOS) radio channel. The opposite case would be the existence of a *line-of-sight* (LOS) propagation path, but this case is not considered in this thesis.

2.5 Statistical channel model

From the mobile receiver point of view, all these effects will influence the received signal after transmission through the channel. It is therefore no longer

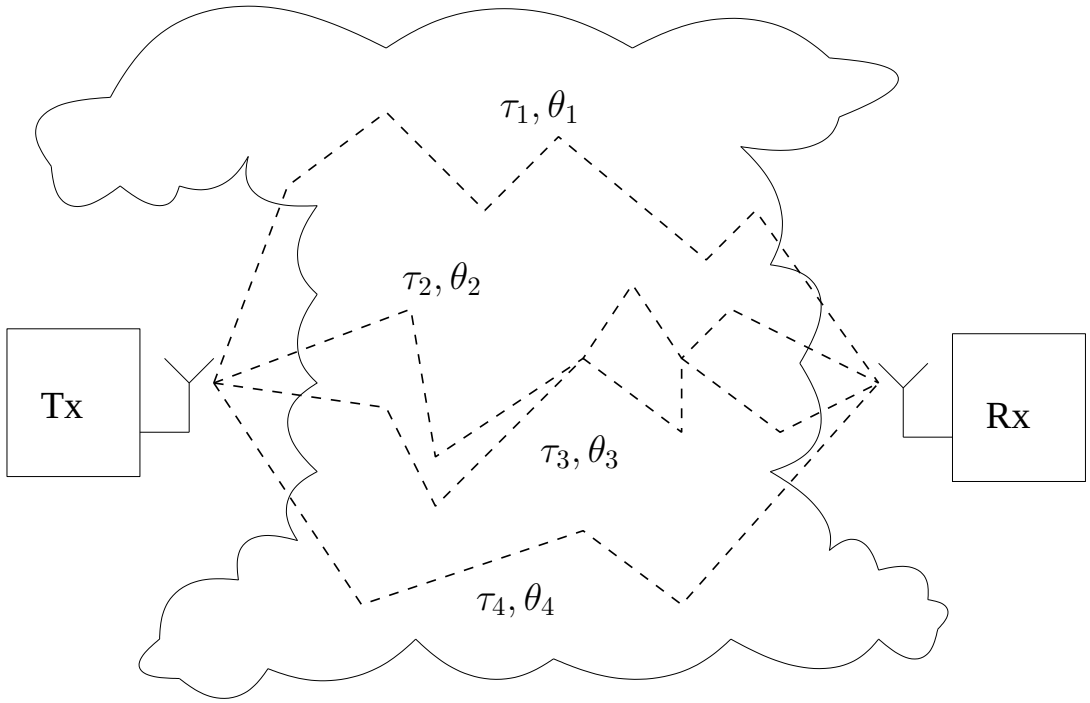

Figure 2.7: Single-Antenna (SISO) radio channel model with multiple paths: Delays τ_k, Phases θ_k

necessary to model each effect individually, but instead the effect of the whole radio channel on the transmitted input signal needs to be modeled in terms of the impulse response $h(\tau)$.

In the rest of this work, a statistical channel model needs be used of which many realizations can be computer-generated to evaluate the system performance under many different channel situations. For this reason, the equivalent base-band impulse response of the radio channel is considered. Also, for a communication system with bandwidth W and sampling time $T = 1/W$ only the discrete-time impulse response of the channel is of interest.

2.5.1 Broad-band and Narrow-band radio channel

A communication system will communicate over a radio channel at a symbol clock with symbol duration T and an occupied system bandwidth $W = 1/T$. A radio channel's impulse response $h(\tau)$ can have its delay times spread over a time interval that is either large or small compared to the symbol duration. An important characterization of the channel impulse response is this time interval in which most of the delayed propagation paths are located.

This time interval is denoted as *maximum delay*[2] $\tau_{\max}$ and is defined to be the interval of all impulse response contributions whose magnitude has not yet decreased to a level lower than e.g. $-30dB$ compared to the maximum magnitude.

Equivalently, in the frequency domain the *coherence bandwidth* W_C is defined as the bandwidth in which the channel "does not change too much", and the coherence bandwidth is proportional[3] to the inverse of the maximum delay as $W_C \sim 1/\tau_{\max}$.

Depending on the relation between symbol duration and maximum delay of the radio channel, the complete communication system is said to be

- Narrow-band if $T \gg \tau_{\max}$ and $W \ll W_C$, or
- Broad-band if $T \ll \tau_{\max}$ and $W \gg W_C$.

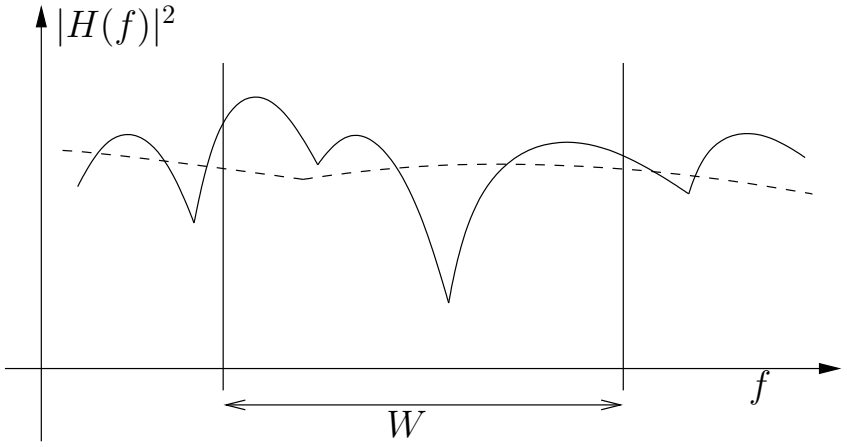

Figure 2.8: Transfer function of broad-band (solid) and narrow-band (dashed) communication system in bandwidth W

The channel transfer functions in the relevant bandwidth of a broad-band and a narrow-band communication system can be distinguished very easily, figure 2.8: In a broad-band system, the transfer function is varying (figure 2.8, solid), whereas in a narrow-band system it is approximately constant (figure 2.8, dashed). For a narrow-band communication system, the channel transfer function can therefore be approximated by one complex-valued constant H_0:

$$H(f) \approx H_0 \quad \text{if } T \gg \tau_{\max} \tag{2.13}$$

[2] Also called *maximum excess delay*

[3] The exact relation depends, among others, on the actual shape of $h(\tau)$. For an exponentially decreasing impulse response, $W_C = 3\sqrt{3}\ln(10)/(\pi\tau_{\max})$ (from [Gal06])

In a narrow-band communication system, the influence of the channel is fully described by this simple complex-valued number H_0 which is called *channel transfer factor*.

2.5.2 Narrow-band statistical models

For the narrow-band communication system, the channel transfer factor H_0 is modeled as a random variable with certain probability distributions.

Complex Gaussian distribution

In a NLOS situation the real part and the imaginary part of H_0 are the sum of a large number of small independent real random variables each. Due to the central limit theorem, it follows that both the real and imaginary part of H_0 can be modeled as an independent zero-mean GAUSSIAN random variable with variance $\sigma/2$, denoted as $\mathcal{N}(0, \sigma^2/2)$ each. The channel factor H_0 is then a circularly symmetric[4] complex Gaussian random variable with variance σ^2, denoted by $\mathcal{CN}(0, \sigma^2)$.

σ^2 is also the power of that channel transfer factor. Its magnitude $|H_0|$ has RAYLEIGH distribution and its phase[5] $\arg H_0$ has uniform distribution in $[0, 2\pi]$.

Rayleigh distribution

The Rayleigh distribution has the probability density function (PDF)

$$p_{Rayleigh}(r) = \frac{2r}{\sigma^2} \exp\left(-\frac{r^2}{\sigma^2}\right) \tag{2.14}$$

with mean $\sigma\sqrt{\pi}/2$ and variance $(1 - \pi/4)\sigma^2$, where σ^2 is the power of the underlying complex Gaussian and $\sigma^2/2$ the variance of its real part and imaginary part, respectively[6].

[4] $\boldsymbol{x}$ is circularly symmetric if $e^{j\theta}\boldsymbol{x}$ has the same distribution of $\boldsymbol{x}$ for any θ [TV05].

[5] The operator $\arg r \cdot e^{j\phi}$ is defined as the argument ϕ of the complex number.

[6] Note: In some textbooks [Pro00] the variance of the real and imaginary part is defined as σ^2, but here it is defined as $\sigma^2/2$ [TV05].

2.5.3 Time-invariant WSSUS model

Each of the propagation paths in multi-path propagation is characterized by a slightly different propagation delay. Hence, the impulse response of the superposition of all paths has a certain *maximum delay* in time direction. Additionally, due to different propagation distances and potentially different reflections, all paths have experienced a different phase shift and potentially a different attenuation. And finally, in multi-antenna (MIMO) communication, each propagation path has a different angle of arrival/departure at the receiving/transmitting antenna array.

All these effects are modeled by a *WSSUS* channel model (Wide-Sense Stationary Uncorrelated Scattering) [Bel63]. This WSSUS model in the single-antenna case is described in the following.

For the usual single-antenna WSSUS channel model (Single-Input Single-Output, SISO), a number of *propagation paths* K are considered (figure 2.7), and for each path the delay τ_k, the phase shift θ_k, and the attenuation $\alpha_k > 0$ are chosen randomly from some given distribution (e.g. exponential delays, uniform phases, Rayleigh attenuations). For a single-antenna system, this results in the channel impulse response

$$h(\tau) = \sum_{k=1}^{K} \delta(\tau - \tau_k)\alpha_k e^{j\theta_k} \,. \tag{2.15}$$

If the number of paths K is large enough (e.g. $K \geq 30$), then the amplitude can even be modeled as fixed ($\alpha_k = 1 \; \forall k$), since the sum over a large number of paths with random phases is a good approximation for a complex-valued Gaussian random variable (with Rayleigh fading amplitude). For the sake of brevity, $\alpha_k = 1$ will be assumed in the rest of this work.

As an additional impairment in *mobile* data communication, the radio channel in reality changes over time. This is caused by movements of the transmitter, the receiver, or the reflecting objects. However, these radio channel variations are not considered in this thesis. Instead, only *time-invariant* radio channels will be considered in the following.

3 OFDM Transmission Technique

3.1 OFDM System Model

The principle of multicarrier modulation is to map a serial high rate source stream onto multiple parallel low rate substreams and to modulate each substream on another subcarrier. Since the symbol rate on each subcarrier is much less than the serial source symbol rate, the effects of delay spread significantly decrease, reducing the complexity of the equalizer a lot. The N_c subcarriers are chosen such that each subchannel ideally appears frequency-nonselective. The data symbol rate per subcarrier is reduced by a factor of N_c and with that, the Inter-Symbol Interference (ISI) is reduced. The ISI can even be avoided totally by using a guard time as described below.

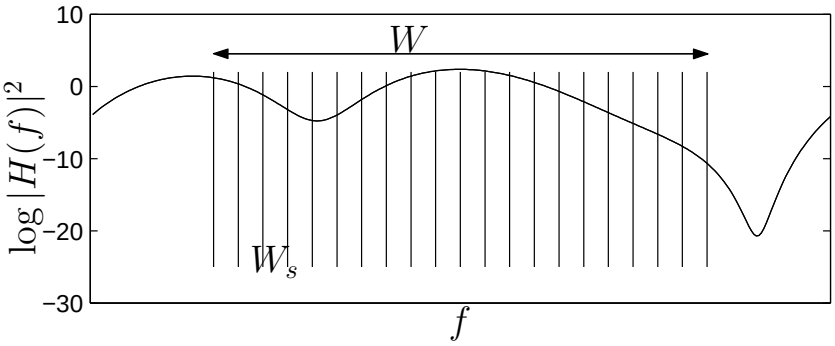

Figure 3.1: Bandwidth divided into multiple subcarriers

A common realization of multicarrier communications is conventional frequency division multiplexing where the subbands are completely separated in the frequency domain. However, due to finite steepness of the filter roll-offs, the subchannel spacing has to be greater than the Nyquist bandwidth to avoid inter-subchannel interference (ICI). This inefficient use of the available spectrum can be overcome by permitting spectral overlap between adjacent subchannels. In that case, ICI can be avoided by guaranteeing orthogonality between the signals on the subcarriers. With rectangular pulse shaping, orthogonality between

the signals is obtained by choosing a subcarrier spacing equal to the inverse symbol duration per subcarrier T_s. This technique is referred to as *Orthogonal Frequency Division Multiplexing* (OFDM). [WE71, Cim85]

One of the main design goals for a multicarrier transmission scheme based on OFDM in a mobile radio channel is that the channel can be considered as time-invariant during one OFDM symbol and that the fading per subcarrier can be considered as flat. Thus, the OFDM symbol duration should be smaller than the coherence time $(\Delta t)_c$ of the channel and the subcarrier spacing should be smaller than the coherence bandwidth W_C of the channel. By fulfilling these conditions, the realization of low-complex receivers is possible.

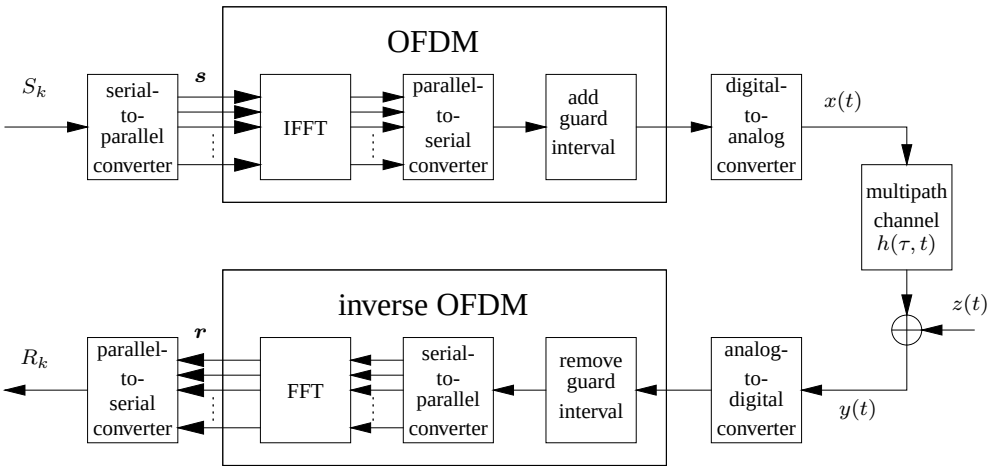

Figure 3.2: Multi-Carrier transmission with OFDM

System structure

In the following, the basic setup of an OFDM system is described, see Figure 3.2. The multicarrier modulator maps a sequence S_k of N_c serial source symbols of rate $1/T$ onto N_c parallel substreams, where k is the time index. The symbol rate per substream $1/T_s$ reduces to

$$\frac{1}{T_s} = \frac{1}{N_c T} \tag{3.1}$$

According to OFDM, the N_c substreams are modulated on subcarriers with a spacing of

$$W_s = \frac{1}{T_s} \tag{3.2}$$

to achieve orthogonality between the signals on the N_c subcarriers, presuming a rectangular pulse shaping. The N_c in parallel modulated source symbols $S_k,\ k = 0, \ldots, N_c - 1$ are referred to as an OFDM symbol of duration T_s.

3.1.1 Transmission Signal

A key advantage of using OFDM is that the multicarrier modulation can be implemented in the discrete domain by using an Inverse Discrete Fourier Transform (IDFT), or a computationally much more efficient IFFT [WE71]. The sequence of transmission samples $x(\nu)$ is calculated by taking the IDFT of the sequence S_k as

$$x(\nu) = \frac{1}{\sqrt{N_c}} \sum_{k=0}^{N_c-1} S_k e^{j2\pi k\nu/N_c}, \quad \nu = 0, \ldots, N_c - 1 \tag{3.3}$$

and the transmission symbol rate is N_c/T_s. The block diagram of an multicarrier modulator based on an IFFT and the respective demodulator employing inverse OFDM based on a FFT is illustrated in Figure 3.2.

When the number of subcarriers increases, the OFDM symbol duration T_s becomes large compared to the duration of the channel impulse response $\tau_{\max}$ and the amount of ISI reduces. However, to completely avoid the effect of ISI and, thus, to maintain the orthogonality between the signals on the N_c subcarriers and avoid ICI, a *guard interval* of duration

$$T_g \geq \tau_{\max} \tag{3.4}$$

has to be inserted between adjacent OFDM symbols [Pro00]. The guard interval is a cyclic prefix added to each OFDM symbol which is obtained by extending the duration of an OFDM symbol to

$$T_s' = T_g + T_s \tag{3.5}$$

The discrete length of the guard interval has to be

$$L_g \geq \left\lceil \frac{\tau_{max} N_c}{T_s} \right\rceil \tag{3.6}$$

samples to prevent ISI.

Time-continuous signal

For the actual transmission, the sampled sequence $x(\nu),\ \nu = -L_g, \ldots, N_c - 1$ is passed through a digital-to-analog converter to get the continuous-time signal $x(t)$. This signal is then transmitted through the channel. The continuous-time output signal of the channel is obtained from convolution of $x(t)$ with the channel impulse response and addition of a noise signal $z(t)$,

$$y(t) = \int_0^{\tau_{\max}} x(t-\tau)h(\tau,t)d\tau + z(t) \tag{3.7}$$

The output of the receiver's analog-to-digital converter is a sequence $y(\nu)$, which is the received signal sampled at rate N_c/T_s. Since ISI is only present in the first L_g samples of the received sequence, these L_g samples are removed before demodulation. The ISI-free part of $y(\nu)$ is demodulated by inverse OFDM using a DFT or FFT. The output of the FFT is the sequence R_k consisting of N_c complex-valued symbols

$$R_k = \frac{1}{\sqrt{N_c}} \sum_{\nu=0}^{N_c-1} y(\nu)e^{-j2\pi k\nu/N_c}, \quad k = 0, \ldots, N_c - 1 \tag{3.8}$$

Since ICI does not exist due to the assumption of a stationary channel, and ISI can be avoided due to the guard interval, each subchannel can be considered separately. When, furthermore, assuming that the fading on each subchannel is flat and ISI is removed, a received symbol R_k at the output of the FFT is obtained from the frequency domain representation according to

$$R_k = H_k S_k + Z_k, \quad k = 0, \ldots, N_c - 1 \tag{3.9}$$

where H_k is the channel transfer factor of the kth subcarrier and Z_k represents the AWGN of the kth subcarrier. The flat fading factor H_k is the sample of the channel transfer function $H(k,i)$ at the kth subcarrier, where the time index i has been dropped for notational convenience due to the stationarity assumption of the channel. With this equation, the OFDM transmission system can be viewed as a discrete-time and discrete-frequency transmission system with a set of N_c parallel Gaussian channels with different complex-valued attenuation.

Matrix-Vector Notation

In some cases, a matrix-vector description of the OFDM system is more suited for the calculations to follow. In a matrix-vector notation, the sequence S_k of

source symbols transmitted in one OFDM symbol is represented by the vector

$$\boldsymbol{s} = (S_0, S_1, \ldots, S_{N_c-1})^T \tag{3.10}$$

The respective receiver sequence $R_k,\ k = 0, \ldots, N_c - 1$ is given by the vector

$$\boldsymbol{r} = (R_0, R_1, \ldots, R_{N_c-1})^T \tag{3.11}$$

The received vector r is obtained from

$$\boldsymbol{r} = \boldsymbol{H} \cdot \boldsymbol{s} + \boldsymbol{z} \tag{3.12}$$

see also figure 3.3. The $N_c \times N_c$ channel matrix

$$\boldsymbol{H} = \begin{pmatrix} H_0 & 0 & \ldots & 0 \\ 0 & H_1 & & 0 \\ \vdots & & \ddots & \vdots \\ 0 & 0 & \cdots & H_{N_c-1} \end{pmatrix} \tag{3.13}$$

is a diagonal matrix due to the absence of ICI. The diagonal components of $\boldsymbol{H}$ are the complex-valued flat fading coefficients H_k. The vector

$$\boldsymbol{z} = (Z_0, Z_1, \ldots, Z_{N_c-1})^T \tag{3.14}$$

represents the additive white Gaussian noise on the N_c subcarriers.

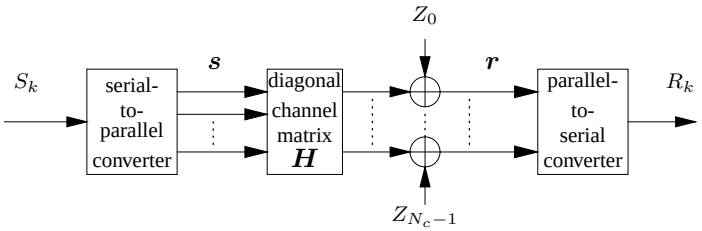

Figure 3.3: Simplified OFDM transmission

Advantages of OFDM

With these assumptions, the necessary equalization on the receiver side can simply be realized by one complex-valued multiplication per subcarrier. This is a significant simplification because otherwise, the equalizer needs to take into account all intersymbol-interference over the whole length N_g of the channel

impulse response. The algorithmic complexity of such an equalizer grows with $O(N_g^3)$ [Pro00] due the necessary convolution operation, which is too large in most broad-band systems. But OFDM is an effective technique to avoid such complexities.

In addition to the simplified equalization process, the structure of an OFDM system also provides the flexibility to apply numerous different schemes for adaptive modulation. [RGG01, GBR01] This is especially important since future radio systems will require much higher flexibility in the air interface for each user and also for multiple access schemes. [CGR02, RG05]

3.2 Channel Capacity

The capacity of an individual AWGN channel was given by Shannon in his ground-breaking 1948 paper [Sha48]. He showed that there is a maximum data rate, called the *channel capacity*, for which one can communicate with as small an error probability as desired, given sufficiently intelligent coding of the information.

This capacity of a continuous-time AWGN channel (normalized by the channel bandwidth) is

$$C = \log_2\left(1 + \frac{P|H|^2}{N_0}\right) \quad \text{bits/s/Hz} \tag{3.15}$$

where P is the transmit power, H is the channel transfer factor, and N_0 the noise power density in the bandwidth of interest[1]. The logarithm is taken to the basis 2 in order to obtain the capacity in *bits* per second per Hertz.

The right-side expression in the logarithm of (3.15) is frequently summarized as the Signal-to-Noise ratio at the receiver, $SNR = P|H|^2/N_0$. Figure 3.4 shows the capacity as a function of this *SNR*, given in dB.

This capacity of the AWGN channel gives an *upper bound* to actual data rates that can be achieved with non-ideal channel coding and practical modulation schemes. In contrast to this, the *actual* data rate is described by a different measure, the bandwidth efficiency.

[1] In [Sha48] and when considering a channel with concrete bandwidth, the capacity is given as $W \log_2 1 + \frac{P|H|^2}{N_0}$ bits/s, i. e. proportional to the channel bandwidth. However, here and in the rest of this thesis the capacity is always normalized by the channel bandwidth, as the considerations in this thesis are independent of the actual bandwidth. For the sake of brevity the capacity will be used in normalized form with the unit [bits/s/Hz], similar to [Tel99, TV05] and many other literature.

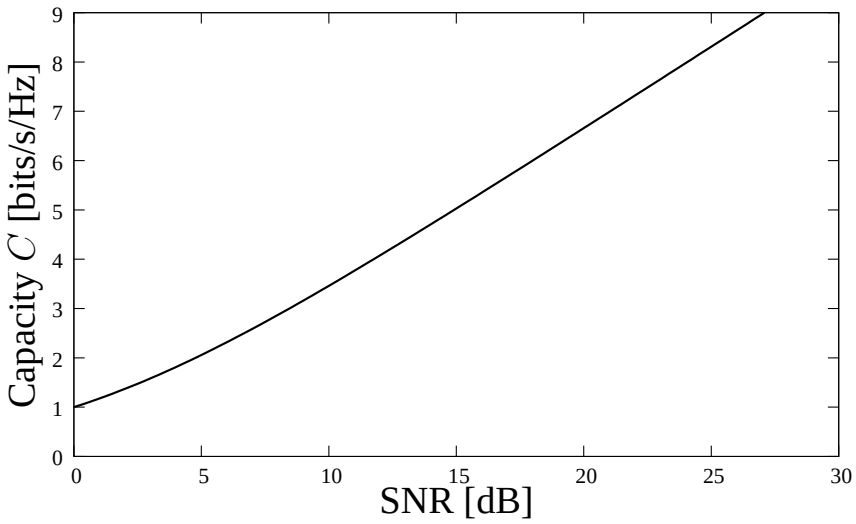

Figure 3.4: Capacity (3.15) of a continuous-time AWGN channel

3.2.1 Bandwidth Efficiency

Any concrete communication system needs to choose a specific modulation scheme and channel coding rate (see next section). This choice sets a specific data rate that is transmitted over the channel. Depending on the SNR and radio channel conditions, the resulting bit error rate of that communication system is sufficient for normal usage. This data rate, normalized by the system bandwidth, will be called the *bandwidth efficiency* E (also known as *spectral efficiency* or *spectrum efficiency*). The bandwidth efficiency specifies the amount of information that can be transmitted over the given bandwidth in a specific communication system, measured in bits per second per Hertz.

In this work, the bandwidth efficiency of a combination of modulation and coding that can be communicated with a bit error rate less than a threshold of, say, 10^{-4}, is used as a comparison criterion of different transmission techniques.

By definition, the bandwidth efficiency will always be lesser than or equal to the channel capacity. Hence, this quantity describes “how close to the capacity” an actual system is being realized. For this reason, the bandwidth efficiency and (as its upper bound) the corresponding channel capacity will be used as a comparison criterion for the performance of the systems in the rest of this thesis.

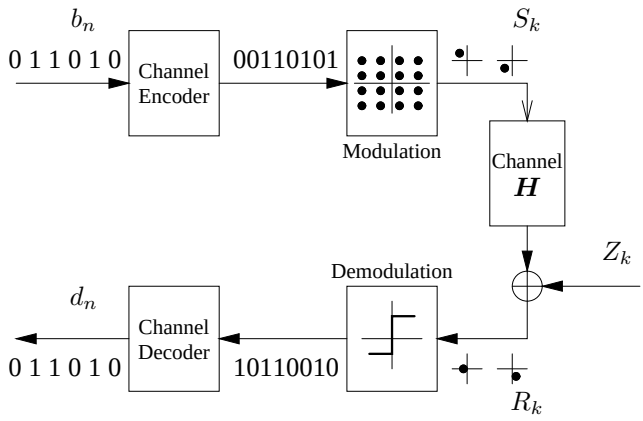

Figure 3.5: OFDM system with channel coding and modulation

3.2.2 OFDM Capacity

In the frequency selective radio channel of an OFDM system, the capacity can be calculated by recognizing each subcarrier as one of many parallel AWGN channels. With an arbitrary transmit power allocation, the bandwidth efficiency of an OFDM system is the sum of the bandwidth efficiencies of all subcarriers, given by

$$E_{OFDM} = \sum_{k=0}^{N_c-1} \log_2 \left(1 + \frac{P_k |H_k|^2}{N_0}\right) \text{ bits/s/Hz,} \tag{3.16}$$

where the P_k and H_k are the transmit powers and channel transfer factors on each subcarrier k, respectively. The resulting bandwidth efficiency E_{OFDM} depends not only on the statistics of the noise, but now additionally on the statistics of the channel transfer factors $|H_k|^2$ and also on the chosen transmit power allocation P_k. The efficiency E_{OFDM} is maximized by optimizing the transmit power allocations, explained in section 3.3.3 below. This optimized E_{OFDM} is the capacity of the OFDM channel.

3.3 Modulation

The above OFDM system of figure 3.2 just assumed that the source bits b_n were modulated on complex modulation symbols S_k according to some modulation scheme. In a realistic OFDM system, the source bits b_n will be coded by a *channel code* with an additional bit interleaving before the modulation as shown in figure 3.5.

In this thesis, both modulation and channel coding is not investigated in de-

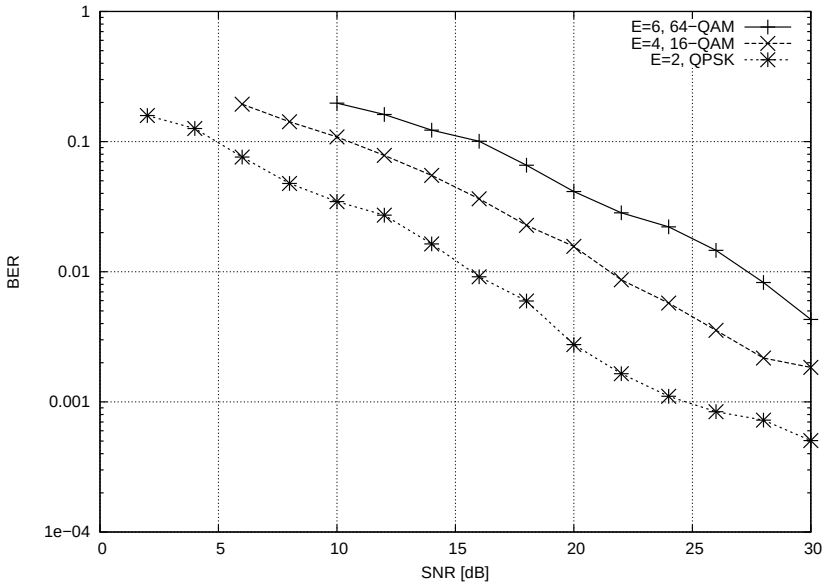

Figure 3.6: Bit Error Rate of uncoded OFDM and three modulation schemes, Rayleigh Fading channel, simulation parameters of table 3.2

tail. Several modulation schemes are explained in the next sections. In terms of channel coding, a well-known convolutional code with Viterbi decoding is being used as explained in section 3.3.2 below.

3.3.1 Fixed Modulation

In general, a modulation scheme is a mapping of M bits to one complex value out of a modulation alphabet $\{C_1, C_2, \ldots, C_{2^M}\}$, where the modulation alphabet has 2^M elements. The modulation scheme is the most relevant system component to decide upon the number of bits that are transmitted per OFDM symbol. The resulting bandwidth efficiency of a modulation scheme is directly given by the number of bits per symbol, $E = M$ bits/s/Hz.

As a first approach, all subcarriers will utilize the same modulation scheme. This single modulation scheme is called the *PHY mode*. The PHY mode can be chosen independently of the current radio channel situation, in which case it would have to be chosen according to the expected worst case of the radio channel. This usually means a very bad performance on average. Instead, the PHY mode is chosen according to some criterion that depends on the current radio channel. Under the title *Link Adaptation* many different techniques have been proposed to choose one single PHY mode and modulation scheme for all subcarriers together, see [Lam04].

One straightforward modulation scheme is the Quadrature Amplitude Modulation (QAM) where the symbols are placed on a regular rectangular grid in the constellation diagram [Pro00]. This scheme is denoted as e.g. QPSK (4-QAM), 16-QAM, or 64-QAM, where the number refers to the alphabet size 2^M and M bits are mapped to each symbol. The resulting bandwidth efficiency is then $E = M$ bits/s/Hz.

When using such a QAM modulation scheme, an uncoded bit error rate (BER) as shown in figure 3.6 can be achieved in a fading channel (Broad-band Rayleigh fading channel, see section 2.5.1). In this case the BER is limited by the probability that a few of the subcarriers are in a deep fading situation (figure 3.1). This fading probability leads to a characteristic *error floor* in uncoded OFDM transmission, as can be observed in figure 3.6 for all modulation schemes shown.

In practical systems, the circumvention for this is to apply *channel coding*, described in the next section.

3.3.2 Channel Coding

Channel coding is a practical means to provide *forward error correction*. Extra bits are added to the input bit stream so to add redundancy to the transmitted bit sequence. This will make the transmission of data more robust to disturbances encountered in the radio channel.

Many different channel codes exist. In this work simply a convolutional code [Pro00] will be considered with memory length 6 as used in the WLAN standards IEEE 802.11a and HiperLAN/2. The generator polynomial in octal notation is $171\ 133$ and puncturing is used when code rates larger than $1/2$ are needed.

When applying channel coding, the bit error curves in OFDM will improve significantly as shown in figure 3.7. To achieve a given bandwidth efficiency E, various combinations of modulation scheme (bits per symbol) and code rate can be considered. In general, it is not known in advance which combination of modulation and rate (the so-called *PHY mode*) will give optimal results. In the above figure only the best PHY mode for this radio channel model is shown. The chosen PHY mode combinations in the single-antenna system are summarized in table 3.1.

In order to compare the bandwidth efficiency of these transmission schemes with the channel capacity (3.15), a threshold on the BER curves is considered as “close enough to error-free”. In particular, the intersection point of the BER

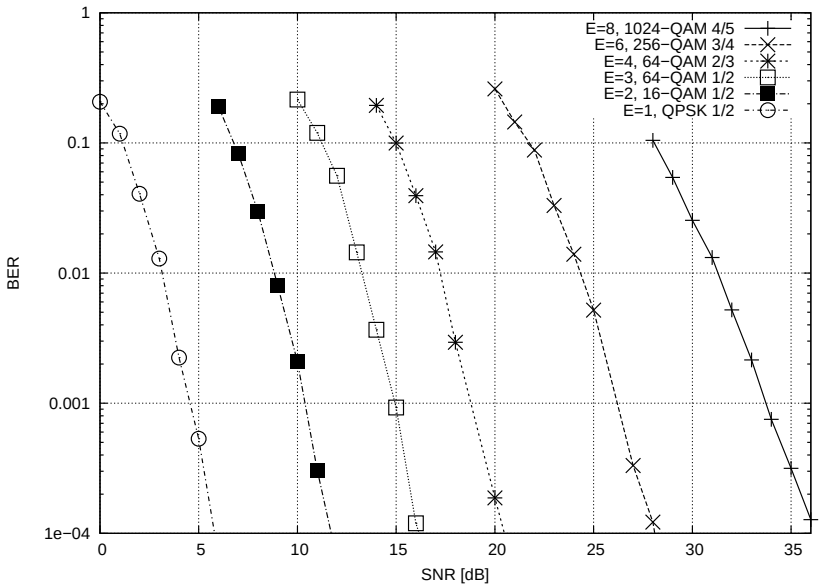

Figure 3.7: Bit error rate of OFDM with channel coding in Rayleigh Fading channel; PHY modes from table 3.1

E	Modulation	Code Rate
1	QPSK	1/2
2	16-QAM	1/2
3	64-QAM	1/2
4	64-QAM	2/3
6	256-QAM	3/4
8	1024-QAM	4/5

Table 3.1: Chosen modulation scheme and code rate (PHY Mode) for each bandwidth efficiency E

curve with 10^{-4} is considered almost error-free, and the bandwidth efficiency at that SNR is plotted in figure 3.8. The channel capacity of an AWGN channel[2] according to Shannon's formula (3.15) is shown as a comparison as well.

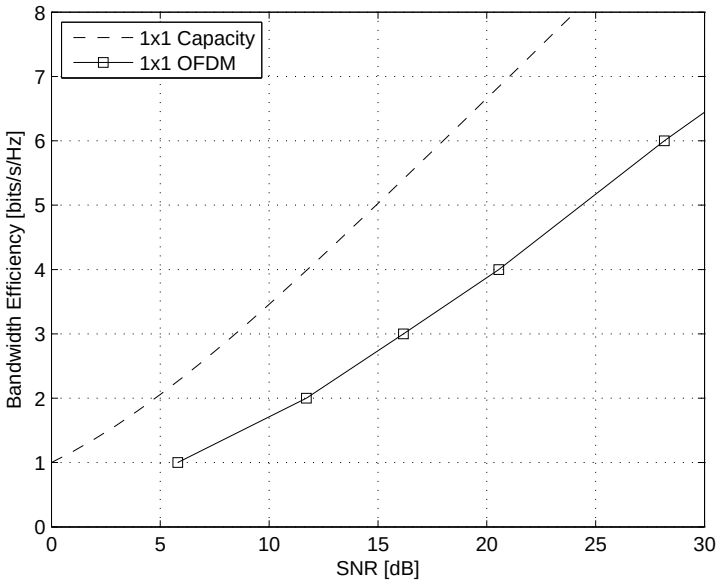

Figure 3.8: Bandwidth Efficiency of PHY modes from table 3.1 at BER=10^{-4} in Rayleigh Fading channel (coded); AWGN capacity

One can observe in figure 3.8 that all simulated bandwidth efficiencies clearly achieve less data rate than the predicted upper bound of the capacity. Hence, the interesting question is *how close to the capacity can each actual system perform?* In the following, each investigated transmission technique will be compared with this AWGN capacity.

Up to now all subcarriers were modulated with the same modulation schemes. The OFDM transmission technique would alternatively offer the possibility to modulate each subcarrier with a different individual modulation scheme. This is explained in the next section.

3.3.3 Adaptive Modulation

In the OFDM technique, the multicarrier approach offers the advantageous degree of flexibility as different modulation schemes can be used on differ-

[2]The capacity of a Rayleigh Fading channel (which is used for BER simulations) is not identical to the one of the AWGN channel. However, in the SNR region of interest the difference is rather small (less than 1 bit/s/Hz [TV05]) and for this reason the AWGN capacity is still used as a comparison here and in the rest of this thesis.

ent subcarriers. With a frequency-selective radio channel, the individual subcarriers encounter different transfer factors H_k and thus offer different individual channel capacities. Selecting the modulation scheme for each subcarrier with respect to the current transfer factor is called *Adaptive Modulation*. [Grü00, Lam04, Gie06, Gal06]

Water Pouring

The capacity C is defined as the maximum bandwidth efficiency E_{OFDM} (3.16) that can be transmitted over the channel, optimized over all possible transmit symbols. In the OFDM system, this can be varied according to the different transmit power allocations P_k over the different subcarriers. Hence, the maximum efficiency must be calculated by solving the optimization problem for the transmit powers P_k subject to a fixed overall transmit power $N_c\bar{P}$.

This is an optimization problem with the objective

$$C = \max_{P_k} \sum_{k=0}^{N_C-1} \log\left(1 + \frac{P_k|H_k|^2}{N_0}\right) \tag{3.17}$$

subject to

$$\sum_{k=0}^{N_c-1} P_k = N_c\bar{P} \tag{3.18}$$

The solution is calculated by introducing a Lagrange multiplier β and considering the objective function

$$f(\beta, P_0, \ldots, P_{N_c-1}) = \sum_{k=0}^{N_C-1} \log\left(1 + \frac{P_k|H_k|^2}{N_0}\right) - \beta \sum_{k=0}^{N_c-1} P_k \tag{3.19}$$

The solution, i. e. the optimum power allocations $\hat{P}_k$, must satisfy the Kuhn-Tucker conditions

$$\frac{\partial f}{\partial P_k} = \begin{cases} = 0 & \text{for } P_k > 0 \\ \leq 0 & \text{for } P_k = 0 \end{cases} \tag{3.20}$$

These conditions are fulfilled by the power allocation

$$\hat{P}_k = \max\left(0, \frac{1}{\beta} - \frac{N_0}{|H_k|^2}\right) \tag{3.21}$$

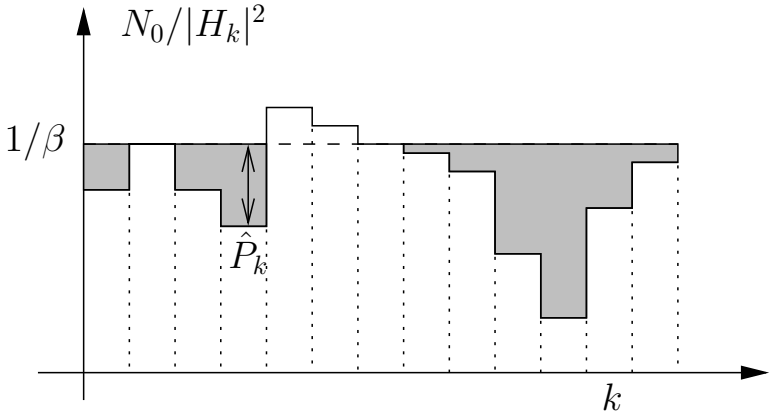

Figure 3.9: Water pouring solution

where the constant β is chosen to satisfy the power constraint

$$\sum_{k}^{N_c-1} \max\left(0, \frac{1}{\beta} - \frac{N_0}{|H_k|^2}\right) = N_c\bar{P} \tag{3.22}$$

Figure 3.9 explains this result. The values $N_0/|H_k|^2$, i. e. the inverse SNRs of the subcarriers, can be viewed as the bottom of a vessel. If $N_c\bar{P}$ units of water are filled in this vessel, the depth of the water at sub-carrier k is the power allocated to this particular subcarrier, and $1/\beta$ is the overall height of the surface. Hence, this optimal solution is called the *water pouring* or *water filling* solution. [Pro00, TV05]

With this solution, some subcarriers might actually have a value $N_0/|H_k|^2$ above the water level. In these subcarriers, the radio channel is too bad for any communication and no power at all is allocated to them. Instead, this strategy rather allocates more power to the stronger subcarriers in order to take advantage of the better channel conditions.

Power Loading

An OFDM system with *fixed* modulation schemes can use the power allocation of (3.21) to adapt the transmit power to the channel conditions. This adaptation strategy is called *power loading* and its particular advantage is that no signaling of the allocated powers has to be done.

However, the different capacities of each subcarrier are not at all exploited as long as the modulation scheme and data rate are chosen identical for all subcarriers. For this reason, as was shown in [Gie06], adapting only the power allocations will degrade the performance of the overall OFDM system.

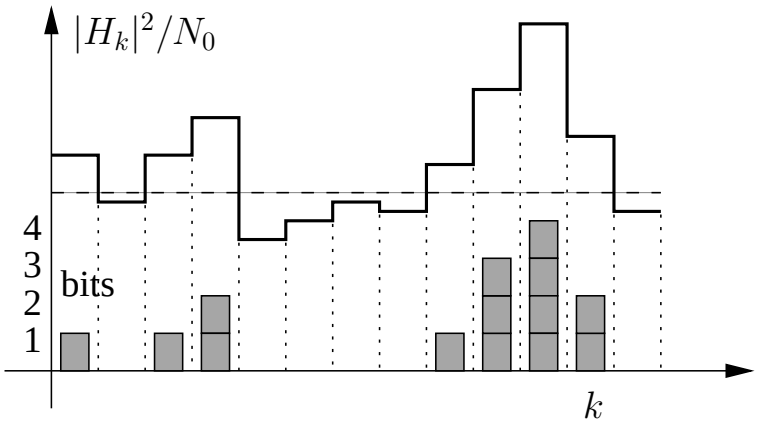

Figure 3.10: Different bit allocations on each subcarrier by Adaptive Modulation

Instead, any adaptive modulation in OFDM must adapt the data rates as well. This is described in the next section.

Bit and power loading

In contrast to allocating only different power levels, the modulation schemes should be adapted on a per-subcarrier basis as well [Gie06]. For each subcarrier, the optimum power allocation is calculated from (3.21). In a second step, for each subcarrier the modulation scheme for each subcarrier is chosen as a function of the receiver SNR $P_k|H_k|^2/N_0$. This process is called *bit loading*.

Various algorithms for bit loading have been proposed, e. g. [HH87, FH96, GBR01, Grü00, Gie06]. One principal problem here is that modulation schemes exist only for some discrete data rates, but the solution of the capacities are continuous values. Each different loading algorithm has different approaches to deal with the impreciseness that arises from this discrete values.

In general, all loading algorithms achieve a comparable performance.

Bit Loading

Although the optimum solution is obtained by modifying both the power levels and the modulation schemes, practical systems might require a fixed power level on each subcarrier. For these cases, changing the modulation schemes only is a viable solution. As was shown in [Gie06], in the usual case the performance with bit loading only but no power loading is not too different from loading both.

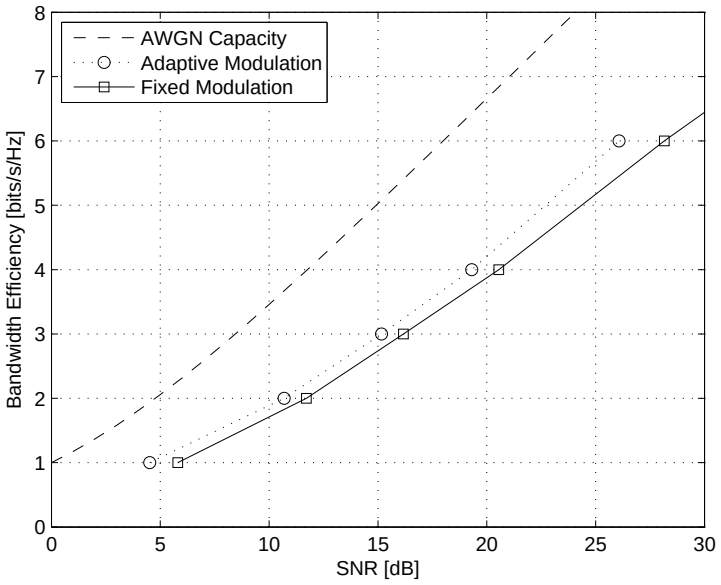

Figure 3.11: Bandwidth Efficiency (at BER=10^{-4}) in Rayleigh Fading channel (coded); AWGN capacity

Performance

The actual BER performance with subcarrier-specific bit loading is improved compared to the uniform modulation scheme. In both cases only the system with channel coding is interesting. The resulting bandwidth efficiencies are shown in figure 3.11. Again, the different available PHY modes are taken from table 3.1 and the AWGN capacity[3] is shown as a comparison.

It can be concluded that bit loading is an efficient strategy for OFDM in frequency selective radio channels. However, in systems with interleaved and coded transmission, the additional gain by subcarrier-specific modulation turns out to be rather small. For that reason it can be concluded that a uniform PHY mode combined with a strong channel code is more efficient in a single-user transmission system.

3.4 Simulation Parameters

The OFDM simulations in this thesis are being conducted with the parameters as shown in table 3.2. The transmission system will be simulated in time do-

[3] Again, even though the capacity of a Rayleigh Fading channel is different from the one of the AWGN channel, this difference is small enough to be neglected here, see explanation at figure 3.8.

OFDM Transmission	
Number of subcarriers	$N_c = 64$
System bandwidth	$W = 20$ MHz
Subcarrier spacing	$W_s = W/N_c = 312.5$ kHz
Useful symbol length	$T_s = 1/W_s = 3.2$ μs
Guard interval length	$T_g = 0.8$ μs
Total symbol length	$T'_s = 4$ μs
Channel coding	
Generator polynomials of $r = 1/2$ code	$[131]_8$,$[177]_8$
Memory length	6
Puncturing, Modulation	see table 3.1
Radio channel model	
Delay power spectral density	negative exponential
Maximum excess delay (-30 dB)	$\tau_{\max} = 0.8$ μs
Doppler frequency	0 (no time-variance)

Table 3.2: OFDM parameters

main, so that the radio channel influence is calculated by the convolution of the OFDM time signal with the channel's impulse response. The physical parameters of this system are chosen to match those of the WLAN standards IEEE 802.11a and HiperLAN/2, as those are intended for high data rate communication already.

4 Multi-Antenna Radio Channel Models

4.1 Introduction

In multi-antenna (MIMO) communications, the decisive difference to single-antenna communications is the availability of multiple radio channels. Between each available transmit and receive antenna (figure 4.1) there is a different radio channel impulse response. Each of these impulse responses can be modeled according to (2.15) individually, but the interesting question now is: In which way are the impulse responses related or correlated to each other? In other words, what is an adequate MIMO radio channel model that captures all performance-relevant relations between the different channels, yet is simple enough to be understandable?

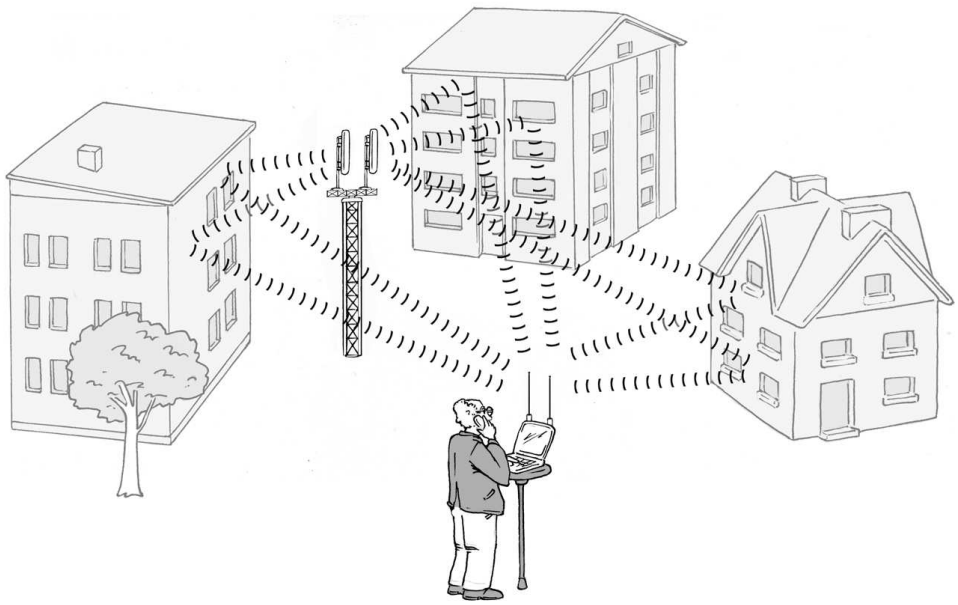

Figure 4.1: Multi-path propagation and multiple antennas

It is an open question how the effects of the MIMO radio channel (figures

4.1, 4.2) can adequately be modeled in a baseband simulation system [DM03, GC02, TV05].

There are very simple MIMO channel models available, the "i.i.d. Gaussian" being the most prominent. But, as information theory has shown [DM05], this is already the upper bound for performance measures such as the capacity of the channel, and many realistic channel conditions will exhibit much worse performance for communication. Some of the MIMO techniques described in later chapters will show radically different performance depending on the radio channel model used. In those cases, performance simulations are much too optimistic and meaningless as long as their radio channel model does not represent the reality in the most performance-relevant aspects.

This section will describe the simple channel models and the newly proposed modeling approach of this thesis. The new multi-antenna radio channel model will be developed that characterizes the relevant properties of the channel but is still easily configurable. The relevant parameters of a MIMO radio channel model are explained and lead to the newly introduced MIMO-WSSUS (Wide Sense Stationary Uncorrelated Scattering) radio channel model. This approach promises to represent the MIMO-related channel properties realistically enough, so that MIMO techniques can now be evaluated by simulations which give realistic performance results.

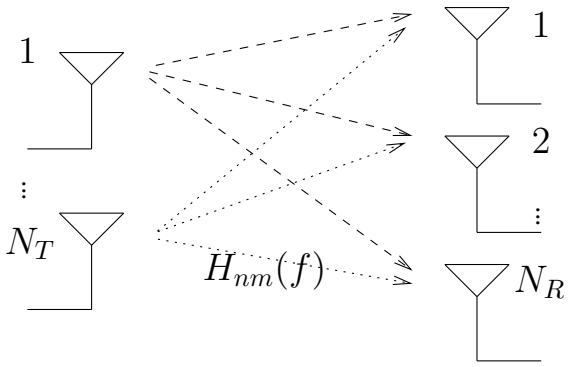

Figure 4.2: MIMO channel representation

4.2 MIMO Channel Representation

As shown in figure 4.2, the multi-antenna (MIMO) radio channel is described as follows: Let N_T be the number of transmit antennas, N_R the number of receive antennas. The impulse response of antenna n to m is denoted as $h_{mn}(\tau)$. The transfer function from antenna n to m is denoted as $H_{mn}(f)$.

All $m \cdot n$ transfer functions together can be written as a matrix-valued transfer function $\boldsymbol{H}(f)$ as follows

$$\boldsymbol{H}(f) = \begin{pmatrix} H_{11}(f) & \cdots & H_{1N}(f) \\ & \ddots & \\ H_{M1}(f) & \cdots & H_{MN}(f) \end{pmatrix} \tag{4.1}$$

In an OFDM system, this frequency selective transfer function is turned into a set of parallel flat fading subcarriers, each of which is described by one complex-valued constant $H_{mn}(p)$ per subcarrier p,

$$H_{mn}(p) \approx H_{mn}(f) \tag{4.2}$$

In the following, only one single subcarrier will be considered. For the sake of brevity the subcarrier index p will be dropped from the notation.

All MIMO radio channels on this subcarrier can now be described by the complex-valued *MIMO channel matrix*

$$\boldsymbol{H} = \begin{pmatrix} H_{11} & \cdots & H_{1N} \\ & \ddots & \\ H_{M1} & \cdots & H_{MN} \end{pmatrix} . \tag{4.3}$$

To explain the benefit of this matrix notation, consider one subcarrier of an OFDM communication system in this time-invariant channel. Let the transmitted symbols at transmit antennas 1 through N_T on this subcarrier be given as $s_1 \ldots s_{N_T}$. Let the received symbols at receive antennas 1 through N_R on this subcarrier be given as $r_1 \ldots r_{N_R}$.

Due to the superposition of all transmitted signals on each receive antenna, the received symbol at antenna m is

$$r_m = \sum_{n=1}^{N_T} H_{mn} \cdot s_n + z_m \tag{4.4}$$

where z_m is some additive noise at receive antenna m. With $\boldsymbol{s} = (s_1, \ldots, s_{N_T})^T$ and $\boldsymbol{r} = (r_1, \ldots, r_{N_R})^T$, the vector of *all* received symbols can be written in vector-matrix notation as

$$\boldsymbol{r} = \boldsymbol{H} \cdot \boldsymbol{s} + \boldsymbol{z} \tag{4.5}$$

For an OFDM communication system, the question of MIMO channel modeling is summarized by the question how to model the channel matrix $\boldsymbol{H}$ in (4.5). The easiest model is to assume each entry of the channel matrix to be an independent identically distributed random variable, which is described in the next section.

4.3 I.i.d. Gaussian Radio Channel Model

The easiest radio channel model for MIMO-OFDM applications is to assume uncorrelated subcarriers, and on each subcarrier the vector of received symbols is given by

$$\boldsymbol{r} = \frac{1}{\sqrt{N_T}} \boldsymbol{H}\boldsymbol{s} + \boldsymbol{z}\,. \tag{4.6}$$

The matrix $\boldsymbol{H}$ is constructed from $N_R \cdot N_T$ *independent and identically distributed* (i.i.d.) complex Gaussian random variables with unit variance $\sigma_H^2 = 1$. The normalization factor $1/\sqrt{N_T}$ is introduced to account for the fixed total transmit power constraint: When more transmit antennas are added, the transmit power at each single antenna is reduced by $1/\sqrt{N_T}$ so that the sum transmit power of the full antenna array is constant. In this model, for simplicity the transmit power constraint is expressed by this additional factor so that σ_H^2 and $|s_n|^2$ can be chosen independently from the actual number of transmit antennas.

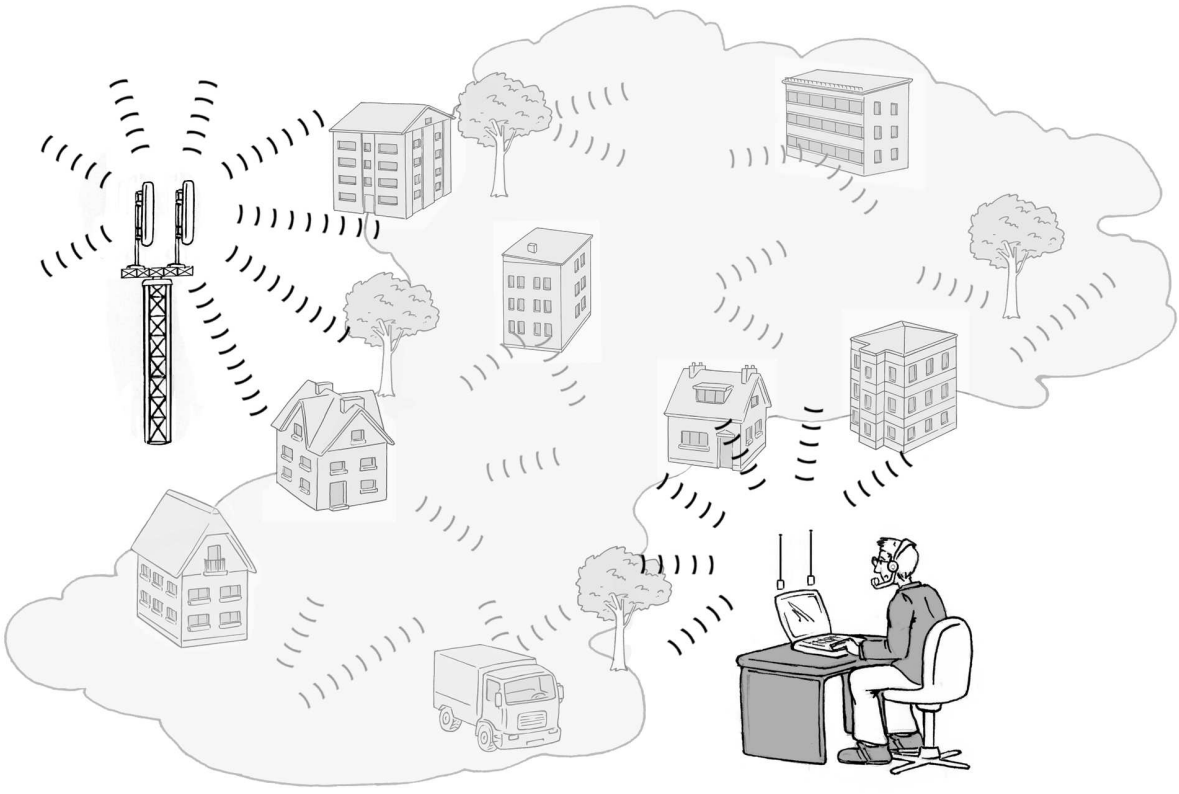

Figure 4.3: MIMO radio channel with a lot of scattering as assumed in the i.i.d. Gaussian channel model

From information theory [DM05], a MIMO channel with this statistical behavior was shown to have *maximum capacity*. This represents a physical situ-

ation where the propagation at each antenna array proceeds by a huge number of scattering propagation paths, visualized in figure 4.3. This large number of scattering paths will result in independent radio channels for each pair of transmit and receive antennas, hence the matrix coefficient will be uncorrelated.

However, in reality the coefficients of the matrix $\boldsymbol{H}$ are not independent but instead have non-negligible correlation. The assumption of the existence of a huge number of scattering paths does not hold in reality most of the time, and this results in a significant correlation between the radio channels and in turn the matrix coefficients. This also results generally in lower MIMO capacity. Therefore some extensions of the radio channel model are needed which describe the physical situation more precisely.

In any case this i.i.d. Gaussian channel model will always be the model with optimum capacity, which means it can be used as a reference case with optimum performance for any communication technique.

In order to characterize the different radio channel models more easily, some measures for predicting the expected MIMO performance need to be found. The actual MIMO techniques will use the $\boldsymbol{H}$ matrix directly for their algorithms and no additional specific knowledge about the radio channel. Hence, characterizations of the stochastic and algebraic properties of this matrix are needed for the MIMO techniques. Those are being investigated in the following sections.

A stochastic measure of the $\boldsymbol{H}$ properties is the pair-wise correlation between all entries of the channel matrix. However, in some channel models this correlation will unexpectedly show no relation to the resulting MIMO performance at all. Nevertheless the correlation and its behavior will be discussed for each radio channel model. This is followed by the algebraic characterization of the $\boldsymbol{H}$ matrix through its singular value decomposition, which will turn out to be a useful measure for all radio channel models.

4.3.1 Correlation

The correlation of all entries of $\boldsymbol{H}$ is a first measure to characterize the statistical properties of the MIMO channel matrix, even though its result will be of limited value.

In the i.i.d. Gaussian model, the matrix entries are assumed to consist of independent random variables. In this case the covariance (and due to this also the correlation coefficient) between each pair of matrix entries will be zero by

definition:

$$Cov\{H_{ij}, H_{k\ell}\} = \begin{cases} \sigma_H^2 & \text{if } ij = k\ell \\ 0 & \text{else} \end{cases} \tag{4.7}$$

This result is a first hint with which one can expect a good performance for each MIMO technique that assumes a "high independence", i.e. zero correlation between the different radio channels of the MIMO antenna arrays.

However, some radio channel models with non-zero correlation between the antenna elements have the interesting property that this correlation is a fixed value, independent of the actual MIMO technique's performance (see section 4.4.5). For this reason, another evaluation criterion has to be considered, and the chosen criterion is the behavior of the singular value decomposition of the $\boldsymbol{H}$ matrix. This is described in the next section.

4.3.2 Singular Value Decomposition

The Singular Value Decomposition (SVD) of any matrix $\boldsymbol{H} \in \mathcal{C}^{N_R,N_T}$ is defined as

$$\boldsymbol{H} = \boldsymbol{U}^H \boldsymbol{\Sigma} \boldsymbol{V} \tag{4.8}$$

where[1] $\boldsymbol{U} \in \mathcal{C}^{N_R,N_R}$ and $\boldsymbol{V} \in \mathcal{C}^{N_T,N_T}$ are unitary matrices, and $\boldsymbol{\Sigma} \in \mathcal{R}^{N_R,N_T}$ is a rectangular matrix with non-negative real numbers on the diagonal and zeros elsewhere. The values on the diagonal of $\boldsymbol{\Sigma} = \mathrm{diag}(\sigma_1, \sigma_2, \ldots, \sigma_K)$ are called *singular values* and are sorted by value, $\sigma_1 \geq \sigma_2 \geq \ldots \sigma_K$

This implies that the squared singular values σ_j^2 are the Eigenvalues of the matrix $\boldsymbol{H}\boldsymbol{H}^H$ and also of $\boldsymbol{H}^H\boldsymbol{H}$. There are at most $K = \min(N_R, N_T)$ singular values. The number of non-zero singular values $k \leq K$ is the rank of the matrix $\boldsymbol{H}$.

Singular Values in Gaussian Channel Model

If the channel matrix $\boldsymbol{H}$ consists of random variables, the singular values of that matrix will be random variables as well. To investigate the properties of the singular values it is desirable to find out their PDF or joint distribution.

The joint distribution of the singular values of $\boldsymbol{H}$ with i.i.d Gaussians has been solved before [Ede88], but is a complicated expression. In this work, the resulting PDF is simply shown graphically as obtained by numerical experiments: A large sample of random channel matrices was used to calculate a

[1] By $\boldsymbol{U}^H$ the Hermitian of $\boldsymbol{U}$ is denoted, i.e. the transposed and complex conjugate matrix.

histogram of the respective random variables, which is a good enough approximation of the actual PDF.

The resulting PDF for all four singular values of a 4x4 MIMO channel matrix is shown in figure 4.4. It can be seen that each of the four expected singular values have a bell-shaped distribution around some mean value. This mean value and the whole bell shape is decreasing for the smaller singular values.

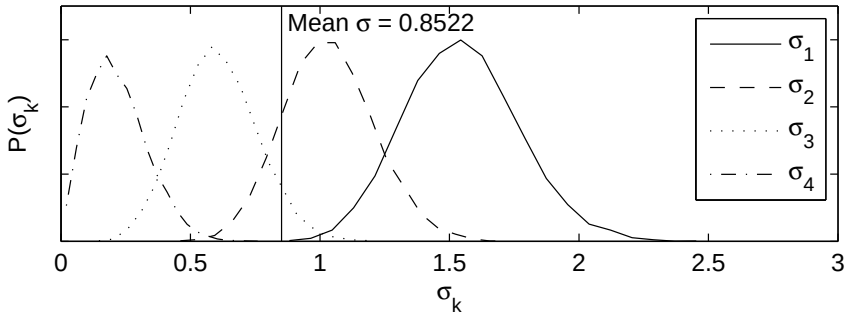

Figure 4.4: PDF of the four singular values of an i.i.d. Gaussian $\boldsymbol{H}$ in a 4x4 channel

The important result is that all four singular values and even the smallest σ_4 are non-zero with very high probability. This means MIMO techniques which assume the existence of many non-zero singular values can be expected to show very good performance in this channel model. And indeed, the spatial multiplexing techniques explained below will demonstrate a very good performance in such radio channels.

But such radio channels cannot be expected to appear in reality in all cases. Instead, a different channel model has to be considered that models the changing radio channel properties in a better way than the Gaussian model. This is explained in the next section.

4.4 MIMO-WSSUS Radio Channel Model

Multi-antenna radio channels are characterized by the spatial relations of the different propagation regions or paths, and a channel model should capture this relations that exist in space. Fortunately, the Wide Sense Stationary Uncorrelated Scattering (WSSUS) channel model for time-variant frequency-selective single antenna channels [Bel63, Pät02] from section 2.4 already included the spatial propagation path characteristics in its modeling approach. This can readily be extended to MIMO situations in a straightforward way.

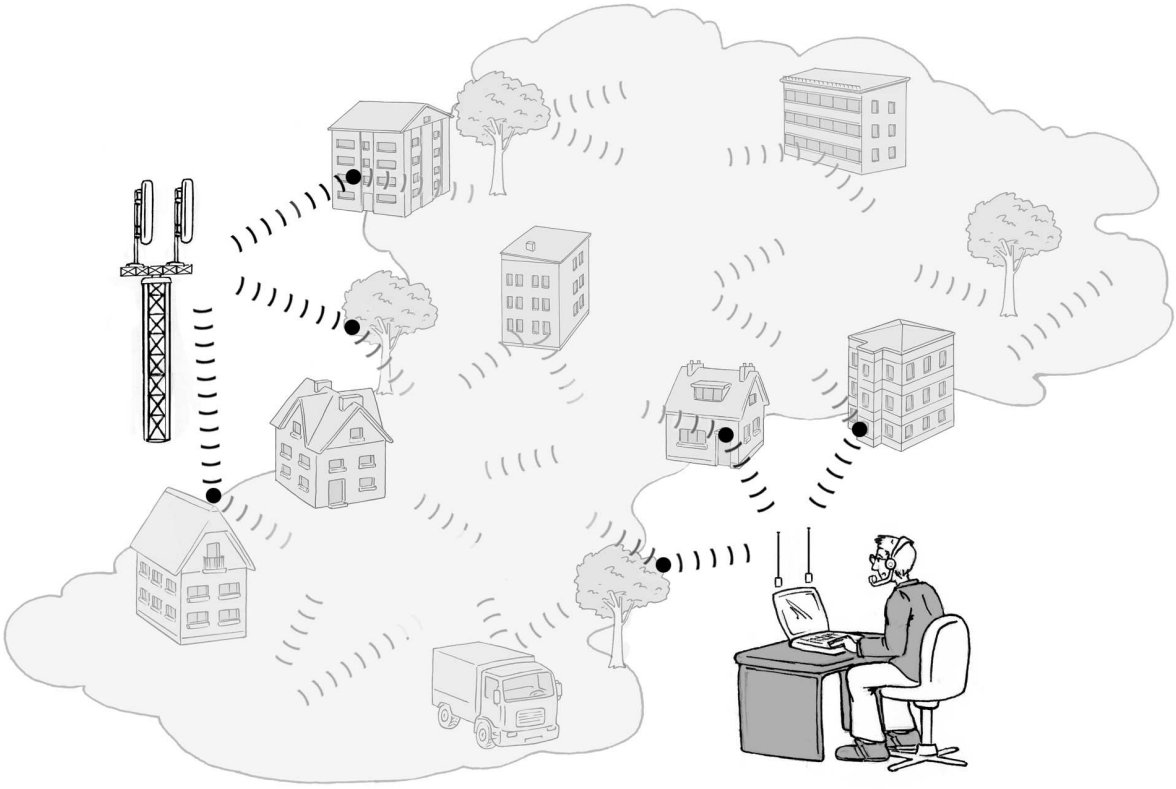

Figure 4.5: MIMO radio channel with a small number of scatterers (here $L = 3$) as assumed in the MIMO-WSSUS channel model

In the multi-antenna case, it is necessary to rethink the different spatial propagation properties of all the simulated WSSUS paths. The WSSUS model only assumes the fact that "much scattering is taking place all over the whole radio channel" (figure 4.3), but for MIMO it is necessary to model this scattering in a slightly more detailed way. Namely, the scattering reflection that determines the *angle of arrival* (and departure) has to be modeled.

Measurements have shown [DM03] that the number of these "scatterers closely located to the antennas" L is surprisingly small and in the range of $L = 5, 6, 7$. Therefore this number of *transmit scatterers* L_T and *receive scatterers* L_R are introduced as two new parameters in the MIMO-WSSUS model, visualized in figure 4.5. For the propagation between one transmit scatter and one receive scatterer, K propagation paths are assumed, so that the total number of paths now is $K \cdot L_T \cdot L_R$. Similar to the single-antenna WSSUS model, each propagation path is characterized by a set of parameters as described in the next section.

4.4.1 Scatterers

For each of these scatterers, the Angle of Arrival (AoA) of the arriving wave at the receiver is denoted by ψ_i. As explained below (section 4.4.3), this parameter can either be chosen as a uniformly distributed random variable, or it can be set to the fixed Fourier angles to simplify the correlation analysis.

Similarly, the Angle of Departure (AoD) at the transmitter is denoted by β_j. For each pair of scatterers i and j, the K different propagation paths linking these two scatterers have a random delay τ_{ijk} and phase θ_{ijk} which are numbered by the three-fold index i, j, and k. These parameters are shown in figure 4.6.

Additionally the actual geometry of the antenna arrays at the transmitter and receiver need to be known (e.g. uniform linear with spacing $\lambda/2$). Depending on this geometry of the antenna arrays, one can calculate different phase shifts for each antenna as a function of β_k and ψ_k by determining the phase shift $\phi_m(\beta_k)$ of path k at antenna m as a function of ψ_k at the receiver and as a function of β_k at the transmitter.

4.4.2 Antenna Array geometries

The phase shifts $\phi_m(\psi)$ on each antenna as a function of the angle of arrival/departure is calculated from the geometry of the antenna array [CKBS04].

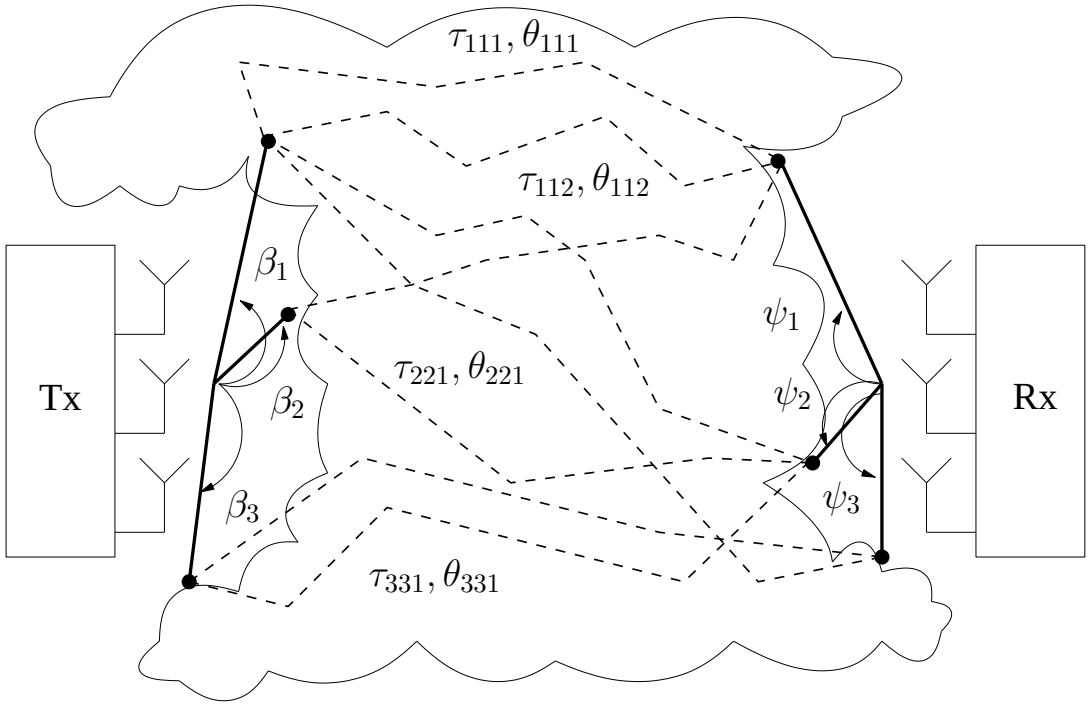

Figure 4.6: Parameters of MIMO-WSSUS radio channel model: AoA ψ_i, AoD β_j, Delays τ_{ijk}, Phase shifts θ_{ijk}

In this thesis, a *Uniform Linear Array* with antenna spacing $d = \lambda/2$ and random orientation is assumed, as shown in figure 4.7. The radiation pattern of each single antenna is assumed to be omnidirectional in the horizontal plane, which could be implemented in reality by e.g. a vertically oriented dipole antenna.

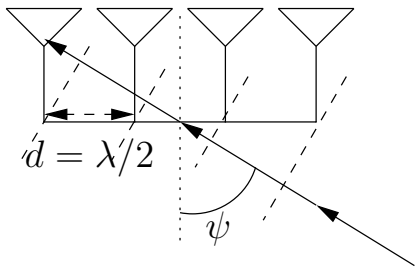

Figure 4.7: Uniform linear antenna array with impinging wave and wave fronts

This results in the following phase shifts at antenna element number m for an incoming angle ψ and wave length λ:

$$\phi_m(\psi) = m\frac{2\pi}{\lambda}d\sin(\psi) = m\pi\sin(\psi) \tag{4.9}$$

4.4.3 Random Angles vs. Fourier Angles

An antenna array can distinguish between only a limited number of directions from which an impinging wave is arriving. This limit also describes the granularity by which different angles can be resolved i.e. distinguished, or can not be resolved any longer. An array with N antennas can only resolve up to N different angles or directions. The maximum number of resolvable directions can be seen by the *beam forming pattern* of the antenna array.

Beam Forming Pattern

The beam forming pattern of a Uniform Linear Array (ULA) with four antennas is shown in figure 4.8. This pattern is always symmetric with respect to the array line so that each beam occurs both to the front and the back of the array.

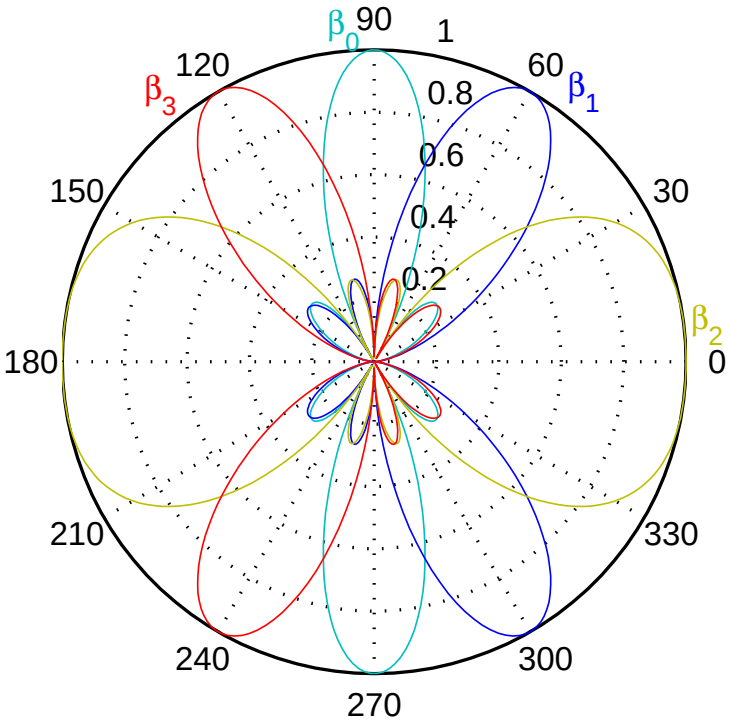

Figure 4.8: Beam forming pattern of $N = 4$ Uniform Linear Array with element spacing $\lambda/2$

In any case, with four antennas only four directions can be resolved, denoted as $\beta_0, \ldots, \beta_3$ in figure 4.8. If arriving propagation paths occur from more than those four directions, the received signal vector will contain the energy from the non-resolved signal components spread out over the resolvable beams.

This "angular sampling" is the same situation as the time sampling when trying to resolve multipath components in time. The multiple paths can only be resolved up to the sampling time, but not finer than that. This very same sampling theorem applies for the angles here as well.

Fourier Angles

The N angle directions of the ULA beams are given by

$$\sin(\beta_p) = \frac{2p}{N} \quad \text{for any integer } p \text{ with } -N < 2p \leq N \tag{4.10}$$

These angles are also the coefficients of a Fourier series, and for this reason the directions of the beam forming pattern are also called *Fourier directions*.

Figure 4.9 demonstrates those discrete angles for the case $N = 4$. The Fourier angles are those radian measures whose sine (the projection on the y-axis) is an integer multiple of $2/N$, which is $2/4 = 1/2$ in the example of figure 4.9. Hence, the four Fourier angles are those with a sine value of $-1/2$, 0, $1/2$, and 1.

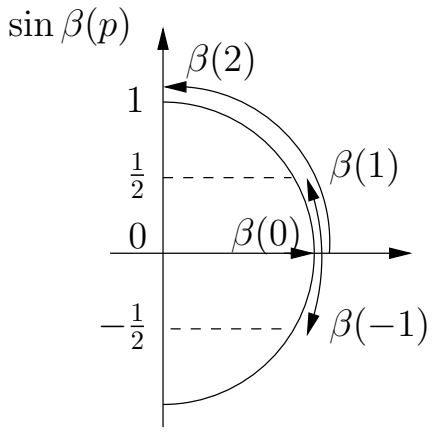

Figure 4.9: The four Fourier angles for $N = 4$ and $p = \{-1, 0, 1, 2\}$

Inserting this set of Fourier angles into the phase shift expression (4.9) gives the following set of phase shifts

$$\phi_m(\beta) = m\pi \sin(\beta) = \frac{m\pi 2p}{N} \quad \text{for any integer } p \text{ with } -N < 2p \leq N \tag{4.11}$$

The proposed MIMO-WSSUS model assumes the path angles β_k, ψ_k as uniform random variables, which is how the physical propagation properties can be represented. However, for the correlation analysis of the resulting $\boldsymbol{H}$ matrix,

it is useful to choose the path angles β_k as the fixed Fourier directions instead. This will be picked up in the correlation and singular value discussion below, but the model itself assumes random path angles instead.

4.4.4 Wide-band MIMO channel impulse response

The wide-band MIMO channel impulse response from antenna n to antenna m is then given by

$$h_{mn}(\tau) = \sum_{i=1}^{L_R} e^{j\phi_m(\psi_i)} \cdot \sum_{j=1}^{L_T} e^{j\phi_n(\beta_j)} \cdot \sum_{k=1}^{K} \delta(\tau - \tau_{ijk}) e^{j\theta_{ijk}} \,. \tag{4.12}$$

It is important to emphasize that no further assumption about the actual propagation geometry is made, except for the known angles. There is no further assumption about the distances, or about the space in between the transmit scatterers and receive scatterers. These parts of the radio channel are still assumed to be unknown, similar to the original assumptions of WSSUS, where only the facts of wide-sense stationarity of the impulse response ("WSS") and of uncorrelated scattering ("US") is assumed but nothing more.

The sums over the different scatterers in equation (4.12) can also be written as a vector-matrix equation

$$h_{mn}(\tau) = \boldsymbol{\psi}_m \cdot \boldsymbol{\Theta}(\tau) \cdot \boldsymbol{\beta}_n \,, \tag{4.13}$$

where the *steering vectors* with all the phase shifts at the receive antenna $\boldsymbol{\psi}_m$ and transmit antenna $\boldsymbol{\beta}_n$ are defined as

$$\boldsymbol{\psi}_n = \begin{pmatrix} e^{j\phi_n(\psi_1)} \\ \vdots \\ e^{j\phi_n(\psi_{L_T})} \end{pmatrix} \,, \tag{4.14}$$

$$\boldsymbol{\beta}_m = \begin{pmatrix} e^{j\phi_m(\beta_1)} & \dots & e^{j\phi_m(\beta_{L_R})} \end{pmatrix} \,. \tag{4.15}$$

The *scatterer linking matrix* $\boldsymbol{\Theta}$ describes the sum of propagation paths from one transmit scatterer j to one receive scatterer i. Its entries for one pair of scatterers are

$$\boldsymbol{\Theta}_{ij}(\tau) = \sum_{k=1}^{K} \delta(\tau - \tau_{ijk}) e^{j\theta_{ijk}} \,. \tag{4.16}$$

Now, writing the propagation path sums for all scatterer pairs into one matrix gives the following full scatterer linking matrix

$$\boldsymbol{\Theta}(\tau) = \begin{pmatrix} \sum_{k=1}^{K} \delta(\tau - \tau_{11k}) e^{j\theta_{11k}} & \cdots & \sum_{k=1}^{K} \delta(\tau - \tau_{1L_Tk}) e^{j\theta_{1L_Tk}} \\ \vdots & \ddots & \vdots \\ \sum_{k=1}^{K} \delta(\tau - \tau_{L_R1k}) e^{j\theta_{L_R1k}} & \cdots & \sum_{k=1}^{K} \delta(\tau - \tau_{L_RL_Tk}) e^{j\theta_{L_RL_Tk}} \end{pmatrix} . \tag{4.17}$$

The steering vectors $\boldsymbol{\beta}_m$ and $\boldsymbol{\psi}_n$ for all transmit and receive antennas can be written into one matrix each, which will result in the matrix-valued broadband MIMO impulse response

$$\boldsymbol{H}(\tau) = \underbrace{\boldsymbol{\Psi}}_{\text{Receiver Steering}} \cdot \underbrace{\boldsymbol{\Theta}(\tau)}_{\text{Scatterer Linking}} \cdot \underbrace{\boldsymbol{\Phi}}_{\text{Transmitter Steering}} . \tag{4.18}$$

This is the matrix-valued MIMO impulse response which can be used to simulate a wide-band transmission system in time domain.

Wide-band MIMO channel transfer function

Alternatively, the impulse response can be transformed into frequency domain to obtain the matrix-valued MIMO transfer function $\boldsymbol{H}(f)$. This is achieved by calculating the Fourier transforms of the entries (4.16) of the scatter linking matrix as

$$\boldsymbol{\Theta}_{ij}(f) = \sum_{k=1}^{K} e^{j(\theta_{ijk} - 2\pi f \tau_{ijk})} . \tag{4.19}$$

Inserting this into (4.18) gives the matrix-valued MIMO transfer function $\boldsymbol{H}(f)$ for simulations in the frequency domain

$$\boldsymbol{H}(f) = \underbrace{\boldsymbol{\Psi}}_{\text{Receiver Steering}} \cdot \underbrace{\boldsymbol{\Theta}(f)}_{\text{Scatterer Linking}} \cdot \underbrace{\boldsymbol{\Phi}}_{\text{Transmitter Steering}} . \tag{4.20}$$

Fourier directions

If the Angles of Departure or Arrival (AoD, AoA) β_i are chosen from the fixed Fourier directions, the phase shifts due to the antenna array are no longer random variables and even the steering vectors and matrices are no longer random. Inserting the phase shifts for the Fourier angles (4.11) into the steering vector (4.15) gives

$$\boldsymbol{\beta}_m = \begin{pmatrix} e^{-j2\pi m 0/L_R} & \dots & e^{-j2\pi m(L_R-1)/L_R} \end{pmatrix} \tag{4.21}$$

and the full steering matrix

$$\mathbf{\Phi} = \begin{pmatrix} e^{-j2\pi 0 \cdot 0/L_R} & \dots & e^{-j2\pi 0(L_R-1)/L_R} \\ & \ddots & \\ e^{-j2\pi(N_R-1)\cdot 0/L_R} & \dots & e^{-j2\pi(N_R-1)(L_R-1)/L_R} \end{pmatrix} . \tag{4.22}$$

For $L_R = N_R$ this result is identical to the inverse Discrete Fourier Transform (DFT) matrix. As the DFT matrix is a unitary matrix, this means the statistical properties of the scatterer linking matrix $\mathbf{\Theta}$ will be preserved after multiplication with the steering matrices in the Fourier direction case.

4.4.5 Correlation

In order to get insight into the statistical properties of the resulting MIMO-WSSUS radio channel matrices, the correlation coefficients between its matrix entries will be investigated. First, the fixed path angles from the Fourier directions will be considered, where a nice relation between correlation and resulting MIMO performance exists. Second, the random path angles will be considered, where unexpectedly no relation to the resulting MIMO performance is found at all. Nevertheless the correlation and its behavior will be discussed. This is followed by the algebraic characterization of the $\boldsymbol{H}$ matrix through its singular value decomposition in the next section, which will turn out to be a useful measure for all radio channel models.

Fourier directions

As there are only up to N_T and N_R Fourier directions on each side, the number of scatterers with Fourier directions is limited by $L_T \leq N_T$ and $L_R \leq N_R$. In this case, the scatterer linking matrix will contain nonzero entries up to the number of scatterers, and zeros for the rest[2]. The steering matrices on each side are simply an inverse DFT matrix, and the statistical properties of the $\boldsymbol{H}$ matrix is determined from the scatter linking matrix $\mathbf{\Theta}$.

For the maximum number of Fourier direction scatterers $L_T = N_T, L_R = N_R$ this results in a scatter linking matrix with $N_T \times N_R$ Gaussian entries, multiplied by the unitary steering matrices. The resulting $\boldsymbol{H}$ is then Gaussian i.i.d. as well and this is identical to an i.i.d. Gaussian radio channel model.

[2] In [TV05], this matrix configuration is given for the angular representation of the channel, which is denoted $\boldsymbol{H}^a$, sec. 7.3.4.

For smaller number of scatterers $L_T < N_T, L_R < N_R$, there will be a non-zero correlation between at least some of the matrix elements. An example of this is visualized by the grey-scale image in figure 4.10 and following. First, the 4x4 system with $L_T = L_R = 2$ instead of 4 Fourier directions is shown:

The larger boxes are arranged like the full matrix entries. Each 4x4 square visualizes the correlation of one matrix entry (the black-most square) to all other matrix entries, calculated by the Monte-Carlo method. The correlation of the matrix entry with itself is always one. All other correlations are smaller than that and visualized by different shades of grey, up to zero correlation which is visualized by white. The entries which are "further away" obviously have smaller correlation, visualized by a white or light grey entry. The neighboring entries have the highest correlation coefficient, visualized by a dark grey entry.

The resulting correlation pattern corresponds to an *over-sampling* of the L_R random variables in the scatterer linking matrix into the received signal vector of size $N_R > L_R$.

The actual values of the correlation coefficients can be calculated analytically for each combination of N_T, N_R, L_T, L_R and each pair of $\boldsymbol{H}$ matrix entries. In all cases the covariance expression between the matrix elements reduces to the variance of some of the Gaussian random variables, multiplied with powers of the coefficients from the DFT matrix.

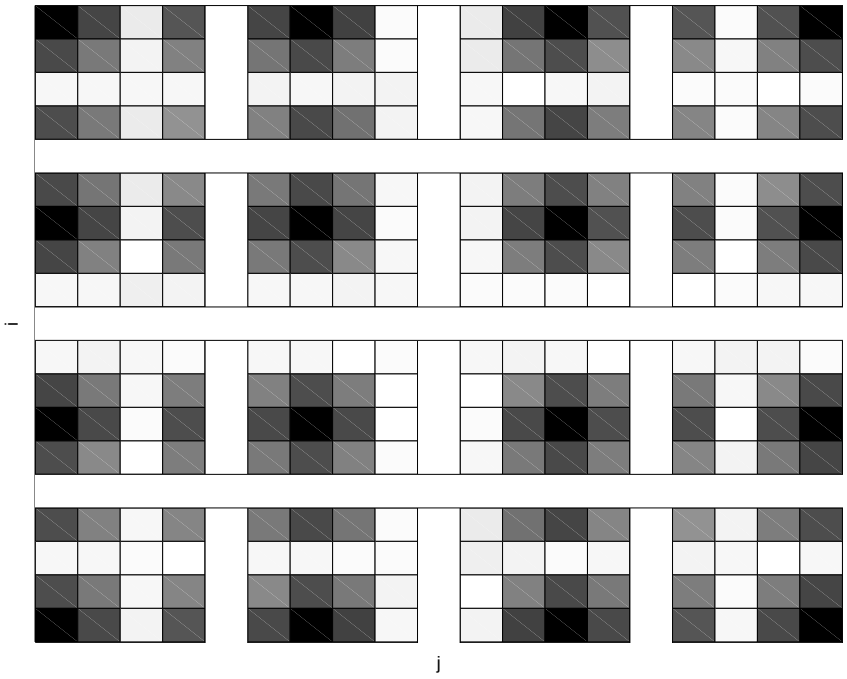

Figure 4.10: Correlation coefficients between matrix elements, Fourier directions, $L = 2$ scatterers, 4x4 ULA. Mean correlation 0.37

In figure 4.10 which visualizes the correlation with $L = 2$ scatterers one can observe the high correlation of neighboring matrix entries, but no correlation to the "far end" of the matrix. When more scatterers are available with $L = 3$ in figure 4.11, the pattern changes and the mean correlation coefficient (as denoted in the figure caption and also in table 4.1) reduces.

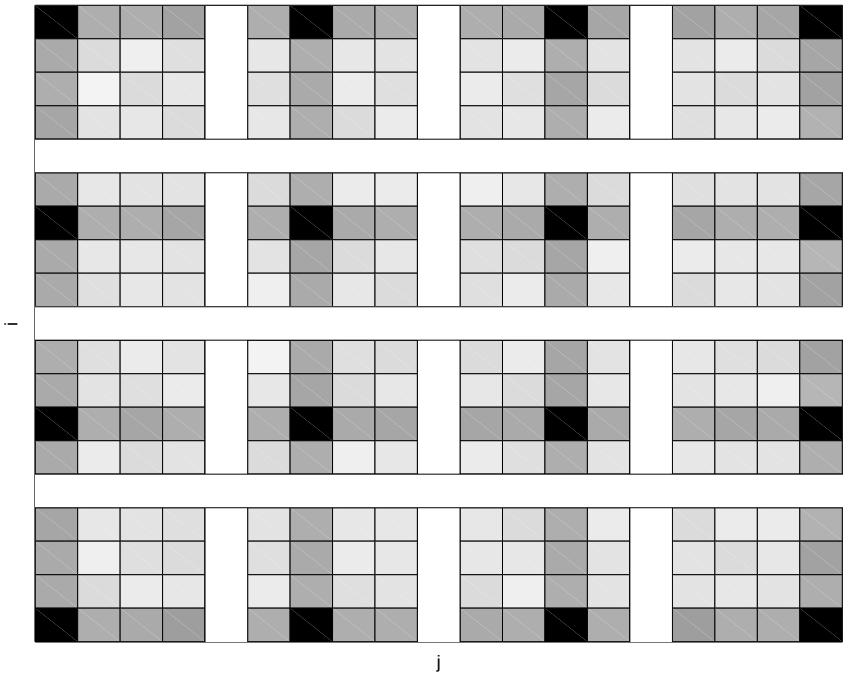

Figure 4.11: Correlation coefficients between matrix elements, Fourier directions, $L = 3$ scatterers, 4x4 ULA. Mean correlation 0.25

With $L = 4$ scatterers in the Fourier direction case, the resulting $\boldsymbol{H}$ entries are completely independent again, which results in the rather boring pattern of figure 4.12.

In order to give one single classification number, the *mean correlation coefficient* is also calculated. This is basically the mean of all numbers in figure e.g. 4.10. This mean will always be non-zero because by taking the mean between all pairs, the covariance of each random variable with itself will also be taken into account, which is simply the variance (which is 1 by definition here). Hence, in the 2x2 case with 2 Fourier directions the covariance between each of the four different channel matrix entries is zero, but out of the 16 different covariances 4 will unity because they are the variances itself. The *mean* correlation coefficient in this case is $4/16 = 0.25$.

The mean correlation coefficient for several antenna configurations and scatterer numbers is shown in table 4.1.

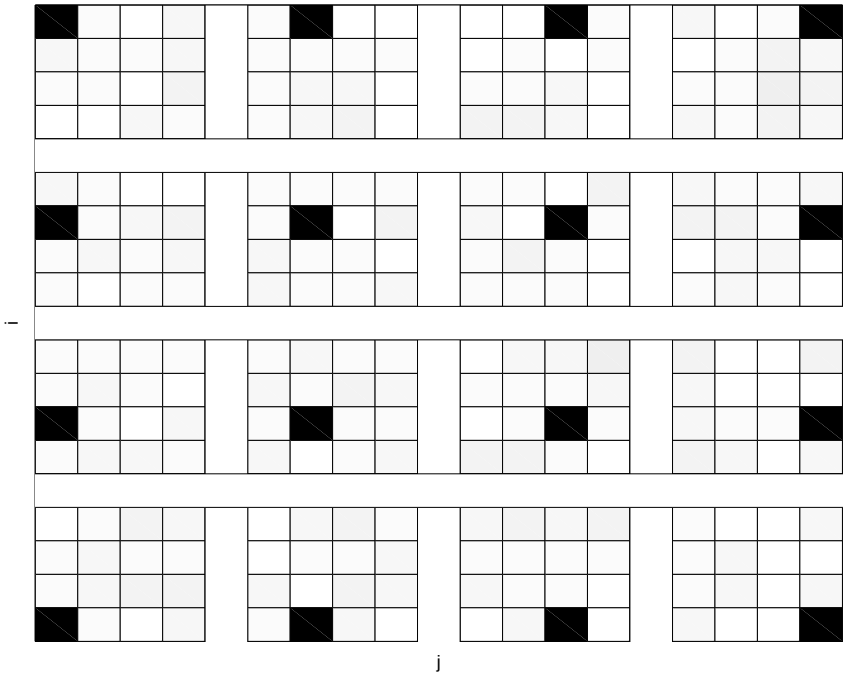

Figure 4.12: Correlation coefficients between matrix elements, Fourier directions, $L = 4$ scatterers, 4x4 ULA. Mean correlation 0.07

Antennas	Scatterers	Mean correlation
2x2	1	1
	2	0.25
4x4	1	1
	2	0.37
	3	0.25
	4	0.07

Table 4.1: Mean correlation coefficient, Fourier directions

Random directions

With random paths angles β_i, ψ_j, the correlation shows an unexpected and interesting property: The correlations between the $\boldsymbol{H}$ entries turn out to be independent of the number of scatterers! This means even though the correlation can be calculated, it is not a useful measure for predicting the MIMO performance. Instead, the algebraic characterization of the channel matrix by the singular value decomposition has to be used for predicting the MIMO performance, which will be considered in the next section.

The reason for the fixed correlation is as follows: Each covariance expression can be factored into the product of independent expectations. Due to the independence of the scatterer linking matrix $\boldsymbol{\Theta}$ and the random path angles, the covariance will always end up as the product of the variance of one Gaussian random variable, multiplied with the mean value of the phase shift random variable.

This is shown as an example with a 3x1 system and one scatterer:

$$\boldsymbol{H} = \begin{pmatrix} e^{-j\pi 0 \sin\beta_1} \\ e^{-j\pi 1 \sin\beta_1} \\ e^{-j\pi 2 \sin\beta_1} \end{pmatrix} \begin{pmatrix} X_1 \end{pmatrix} \begin{pmatrix} 1 \end{pmatrix} = \begin{pmatrix} X_1 \\ X_1 \cdot e^{-j\pi \sin\beta_1} \\ X_1 \cdot e^{-j\pi 2 \sin\beta_1} \end{pmatrix} \tag{4.23}$$

In contrast to the MIMO-WSSUS definition, the entries of the scatter linking matrix (here: only X_1) are here assumed to be Gaussian random variables, with zero mean and variance σ_H^2. In the MIMO-WSSUS definition (4.16), these were a sum of random phase rotations, but that in turn is rather an approximation for a Gaussian random variable. That approximation is valid as long as the sum is large, which was assumed to be the case. In any case for this analysis Gaussian random variables are used for simplicity.

The covariance of, say, the first two entries of (4.23), H_{11} and H_{21}, is

$$Cov\{H_{11}, H_{21}\} = E\{[H_{11} - \overline{H_{11}}][H_{21} - \overline{H_{21}}]^*\} \tag{4.24}$$

Both matrix entries have zero mean. For H_{11} this follows from the definition of X_1. For H_{21} due to the independence of X_1 and β_1 this follows also from the definition of X_1. The covariance simplifies to

$$Cov\{H_{11}, H_{21}\} = E\{[H_{11}][H_{21}]^*\} = E\{X_1 \cdot X_1^* \cdot e^{j\pi \sin\beta_1}\} \tag{4.25}$$

Due to the independence of X_1 and the random phase shift angle β_1, this is

$$Cov\{H_{11}, H_{21}\} = \sigma_H^2 \cdot E\{e^{j\pi \sin\beta_1}\} \tag{4.26}$$

As a result, the covariance is just the X_1 variance multiplied by the expected value of the random phase shift. In appendix A.1, the PDF and the expected value for the random phase shift is derived; the result is

$$E\{e^{jn\pi \sin \beta_1}\} = J_0(n\pi) \tag{4.27}$$

where $J_0(\cdot)$ is the Bessel function of the first kind of order zero.

If the channel matrix $\boldsymbol{H}$ is calculated from a larger sum of scatters and not only one as in this example, due to the linearity of the expectation in (4.25) and the independence of multiple X_i and multiple random phases, the expression will turn out as a sum of multiple results of form (4.27). Eventually, even with a larger sum of scatterer paths, the resulting covariance between entries of $\boldsymbol{H}$ is still one of the fixed values $J_0(n\pi)$ of (4.27), independent of the number of paths.

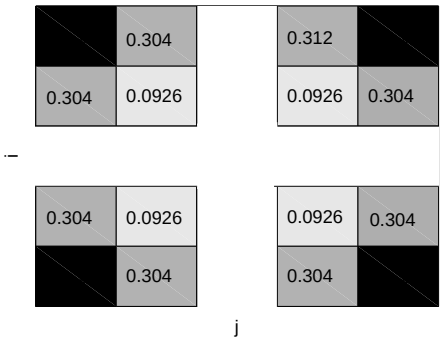

Figure 4.13: Correlation coefficients between matrix elements, Random directions, 2x2 ULA. Mean correlation 0.4253

This is shown for a 2x2 system in figure 4.13, a 3x3 system in figure 4.14, and a 4x4 system in figure 4.15, all calculated from (4.27).

However, even though the correlation in the resulting $\boldsymbol{H}$ is independent of the number of paths, the performance of MIMO techniques is not. For this reason, another evaluation criterion has to be considered. As explained in the previous section, the more interesting evaluation criterion is the behavior of the singular value decomposition of the $\boldsymbol{H}$ matrix. This is described in the next section.

4.4.6 Singular Values

Similar to the evaluation of the $\boldsymbol{H}$ matrix in the Gaussian model (section 4.3.2), the singular values of the channel matrix are evaluated in the MIMO-WSSUS

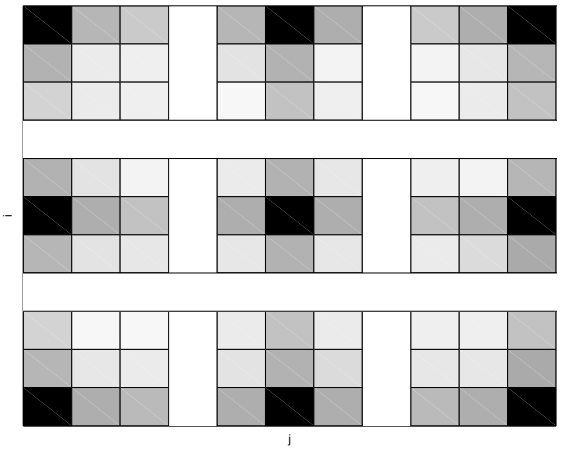

Figure 4.14: Correlation coefficients between matrix elements, Random directions, 3x3 ULA. Mean correlation 0.2678

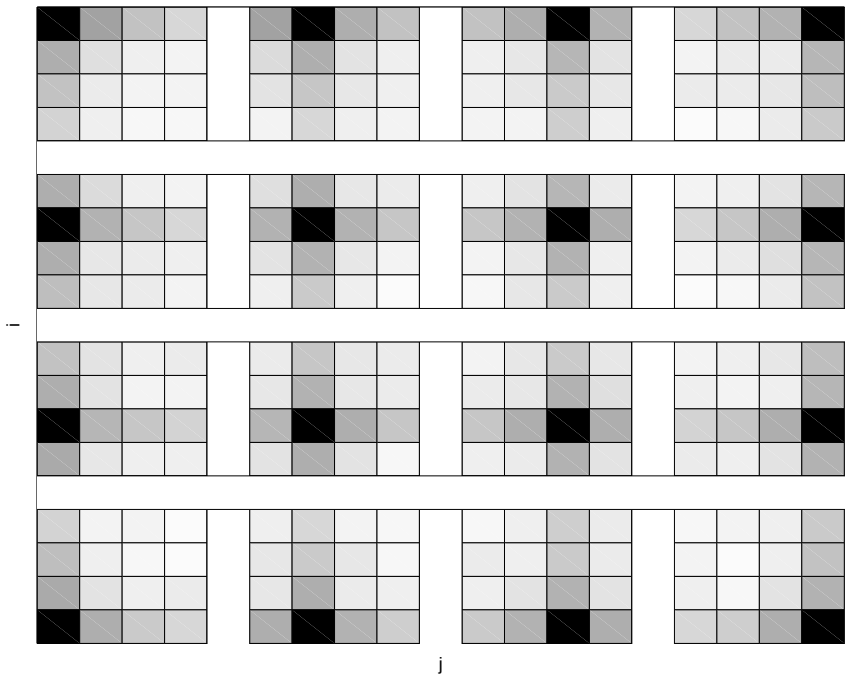

Figure 4.15: Correlation coefficients between matrix elements, Random directions, 4x4 ULA. Mean correlation 0.1948

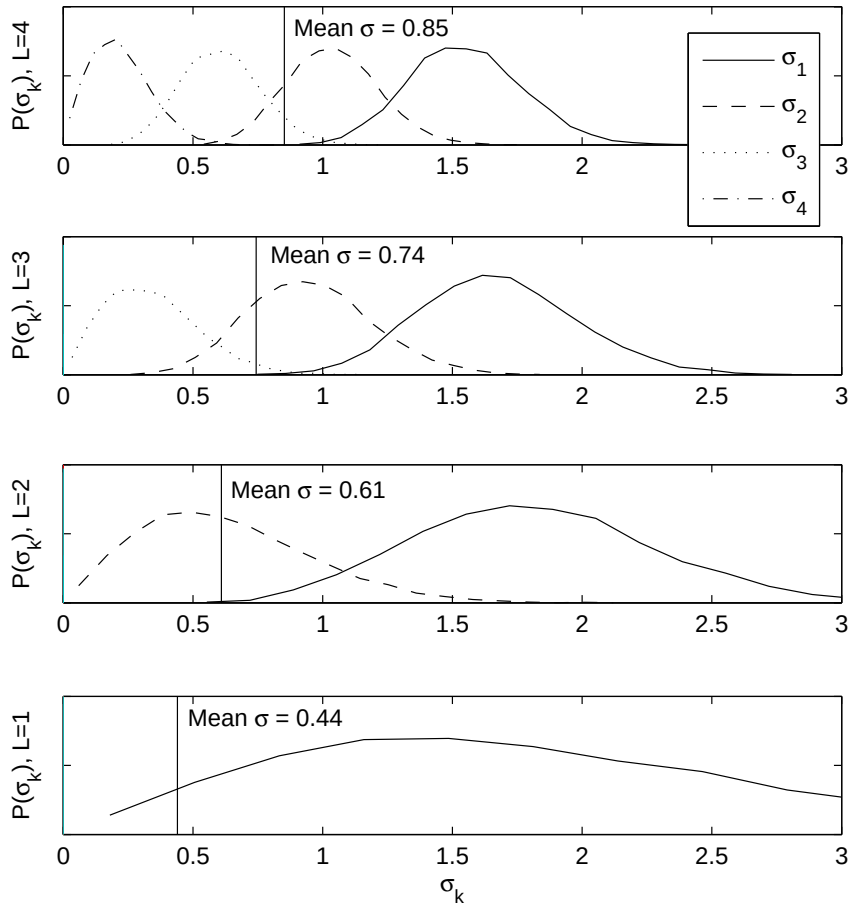

Figure 4.16: PDF of the singular values in a 4x4 MIMO-WSSUS model with Fourier directions and different numbers of scatterers

model as well. First the singular values in MIMO-WSSUS with fixed Fourier directions are evaluated, then the singular values with random directions.

The PDF of the singular values of the 4x4 matrix $\boldsymbol{H}$ of the MIMO-WSSUS model with Fourier directions are shown in figure 4.16, calculated by the Monte-Carlo method. In case of all four Fourier directions (top plot), the PDF are identical to the Gaussian case by definition. In case of less than four Fourier directions, the PDF changes: The smallest singular values will now disappear as they are zero, and the larger singular values have a broader PDF so that they are of smaller value with higher probability than before.

This behavior of the singular values nicely demonstrates how MIMO techniques using multiple singular values will degrade their performance if a lower number of scatterers is present in the radio channel.

The MIMO-WSSUS model with random directions shows exactly the same behavior, see figure 4.17, except that the number of scatterers can now go up to infinity instead of the fixed number of Fourier directions.

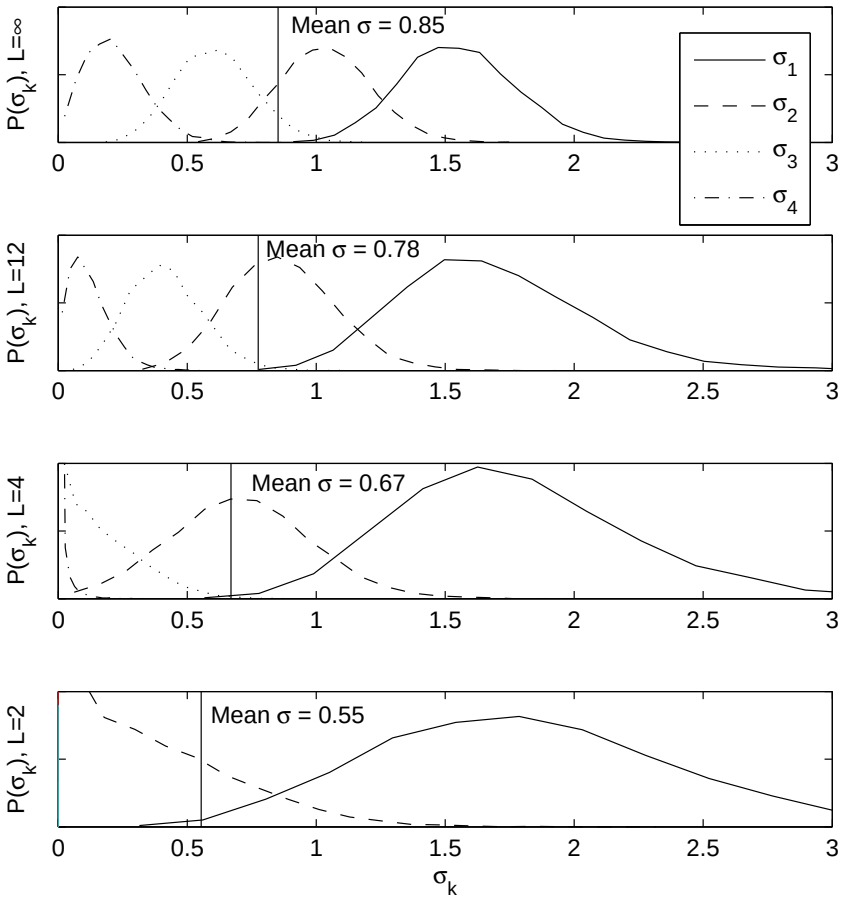

Figure 4.17: PDF of the singular values in a 4x4 MIMO-WSSUS model with random directions and different numbers of scatterers

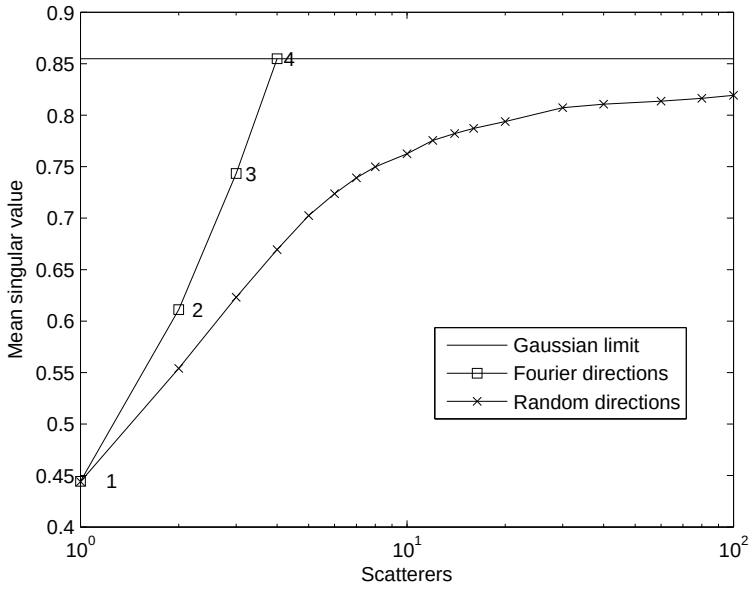

Figure 4.18: Mean singular value in a 4x4 MIMO-WSSUS $\boldsymbol{H}$ as a function of the number of scatterers (logarithmic scale) with Fourier and Random directions

With random directions, the limiting case of an infinite number of scatterers is the i.i.d. Gaussian model by definition, which is why the SVD PDF of the Gaussian matrix is shown at the top of figure 4.17. When a finite number of scatterers exists, the PDF of the smaller singular values shifts towards zero or disappears completely, but in a smoother transition as compared to the Fourier direction picture.

To summarize, the *mean value of all singular values* is shown in figure 4.18 over the number of MIMO-WSSUS scatterers. The i.i.d. Gaussian model shows the largest mean value, which confirms this model to be the optimum radio channel situation. The MIMO-WSSUS model with Fourier directions nicely shows the increasing mean singular value with increasing number of Fourier directions, up to the size of the matrix at which the mean value of the Gaussian model is met. The MIMO-WSSUS model with random directions shows the same trend, except that the upper limit of the Gaussian model will be met asymptotically at an infinite number of scatterers. With a finite number of scatterers the mean singular value is less than the Gaussian upper limit, but increases monotonically with increasing scatterers.

4.5 Other MIMO Channel Models

In the previous section, a MIMO-WSSUS radio channel model was introduced. This model will be compared with some other radio channel models in terms of the BER performance of actual MIMO techniques in chapter 8, after the MIMO techniques have been introduced. Those models are briefly described in the following.

In [DM03, DM05], a different channel model is derived on the basis of maximizing the entropy that is represented by the model. The resulting construction of the channel matrix $\boldsymbol{H}$ is very similar to the one introduced in the MIMO-WSSUS model, see section 8.3.

In [GC02, GC04], another MIMO channel model is proposed based on an exact geometrical description of the area used for transmission. The MIMO channel matrix $\boldsymbol{H}$ will be calculated through ray-tracing simulations inside a two-dimensional plane. This construction of the channel matrix is very different from the one presented here, but the resulting system performance can still be characterized by only one parameter, similar to the MIMO-WSSUS approach. This will be shown in section 8.4.

Other MIMO radio channel models are being proposed and used in [RC98, GBGP02], but those were not considered in this thesis.

One interesting relation to another well-explained proposal should be noted: In [TV05] an angular domain approach to MIMO channel modeling is introduced. The significant influence of “close scatterers” in this thesis is modeled as a transformation from physical to angular domain in [TV05]. A high-capacity MIMO channel would be characterized by a dense angular domain channel matrix instead of a sparse one in that model. Hence, the MIMO-WSSUS steering and scatter linking matrices can be viewed as transformation and angular domain channel matrices, respectively, where the MIMO-WSSUS path angles are chosen as Fourier directions. In effect, the resulting construction of $\boldsymbol{H}$ is very similar to the one in this thesis. The performance characterization through the number of close scatterers is similarly available by the number of nonzero elements in the angular domain channel matrix. Thus, the comparison of chapter 8 is valid for that channel model as well, but the model will not be considered any further in this thesis.

4.6 Channel Normalization

For some applications it is useful to normalize the channel. This is done to reduce the random effects that influence the performance. For example, the *average power* of a realization of $H(f)$ can be normalized to a certain constant (figure 4.19), so that the performance depends only on the frequency selectivity but not on the fluctuation of the total power.

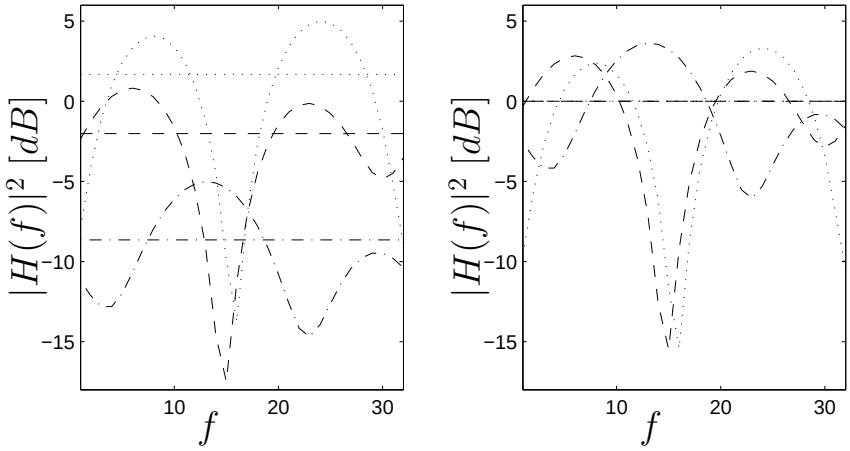

Figure 4.19: Three channel transfer functions and their average power without (left) and with (right) normalization

A time-invariant radio channel model is usually being normalized *in frequency* with a normalization factor γ so that the integral over the transfer function $H'(f) = \gamma H(f)$ of bandwidth W is unity:

$$\frac{1}{W}\int_{W} \gamma |H(f)|^2 df = 1 \tag{4.28}$$

This way, the fluctuations of the average power is eliminated and only the effects of the frequency selective fading is being investigated. This is useful if and only if the investigated techniques should combat the frequency selectivity, and other techniques for compensating the changing average power are proposed and investigated separately.

This normalization does not make sense anymore for a time-variant radio channel model, because in that case the fluctuations of the average power is a fundamental outcome of the time variant model and techniques for its compensation must be included in the system model. Thus this discussion is restricted to the time-invariant case.

In MIMO, there is an additional degree of freedom. One not only has to choose whether to normalize in frequency or in time, but also *in space*. In MIMO simulations one is interested in the fading between the different MIMO subchannels, i.e. the variations of the channel between the different antennas. Our main interest is not the fast fading of the overall channel, i.e. the variation in time from sample to sample that is common for all MIMO subchannels. A straightforward extension of the above normalization in frequency would be to normalize *in space*:

$$\frac{1}{W}\int_{W} \gamma \|\boldsymbol{H}(f)\|^2 df = 1 \tag{4.29}$$

The matrix norm $\|\boldsymbol{H}\|$ can be chosen as e.g. the FROBENIUS norm, $\|\boldsymbol{H}\|_F^2 = \sum_n \sum_m |H_{nm}|^2$, but other matrix norms can be used as well. The actual choice has no noticeable impact on the resulting simulated radio channels.

In the rest of this thesis, such normalized channels will be considered according to (4.29) unless otherwise noted.

4.7 Conclusion

The behavior and performance of a MIMO communication system needs to be confirmed by quantitative simulation results. It is important to use a radio channel model in these simulations that will capture as much realistic circumstances as possible, but without distracting from the relevant results by offering too many parameters.

The characterization of MIMO radio channels was shown by construction of the channel matrix $\boldsymbol{H}$ and also by two derived measures, the pair-wise correlation of the $\boldsymbol{H}$ elements, and by the singular values of $\boldsymbol{H}$. In some cases, the correlation between the matrix elements turned out to have no relation to the relevant MIMO parameters, which means this measure is not useful as a prediction of the MIMO performance. In contrast to this, the algebraic characterization of the $\boldsymbol{H}$ matrix by its singular values were shown to be a useful measure for all radio channel models.

In simulations of communication systems the relevant radio channel properties need to be described realistically and an adequate statistical model for the essential properties of this channel need to be found. Unfortunately, simple multi-antenna radio channel models will predict the increased MIMO capacity to be available in all circumstances, which gives much too optimistic simulation results.

A new MIMO-WSSUS radio channel model was introduced. This model promises to represent the MIMO-related channel properties realistically enough, so that MIMO techniques can now be evaluated by simulations which give realistic performance results. It enables the simulation of different MIMO-OFDM systems with *only two additional parameters*, the number of transmit and receive scatterers. The relevance of this parameter will also be verified in chapter 8 by comparing different radio channel model approaches, leading to the same MIMO-OFDM system performance results.

One additional benefit of the MIMO-WSSUS channel modeling approach is that the statistics of the WSSUS approach are clearly preserved for any single radio channel in the model. The radio link between any transmit-receive antenna pair viewed in isolation will clearly be modeled according to the WSSUS channel impulse response. This serves as a strong indication that the frequency selectivity statistics will still be modeled in accordance with the conventional single-antenna broad-band research.

As a conclusion, the MIMO-WSSUS radio channel model and its comparison with the i.i.d. Gaussian model will be used for the rest of this work.

5 MIMO Techniques

Transmission techniques for multiple transmit and receive antennas (MIMO techniques) are able to increase the link reliability and data rate. This chapter explains the basic MIMO techniques in conjuction with broad-band OFDM transmission, so that these techniques can be evaluated both in a simple radio channel model and the newly proposed MIMO-WSSUS model. This thesis considers MIMO techniques only in the context of a single user, figure 5.1.

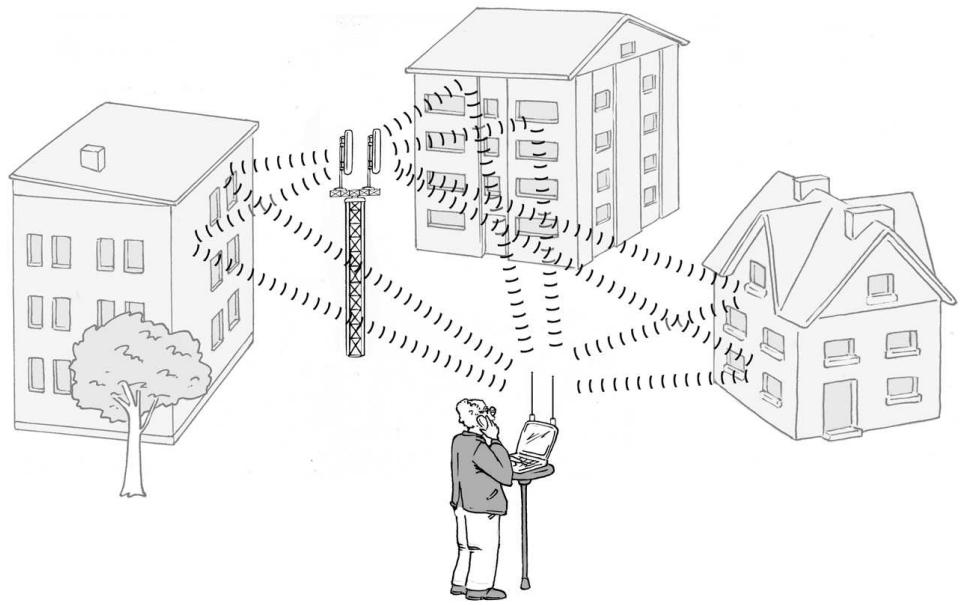

Figure 5.1: Single-user MIMO communication

5.1 MIMO-OFDM Structure

As mentioned earlier, most MIMO techniques have been proposed for a flat-fading radio channel. This assumption is unrealistic for future high data rate systems. High data rate demands will require using a bandwidth that is much greater than the coherence bandwidth of the radio channel. But by using OFDM,

each subcarrier can be seen as such a flat-fading channel, where any of the proposed MIMO techniques can be applied directly. This would lead to a system structure as shown in figure 5.2. This MIMO-OFDM system uses N_T transmission antennas, N_R receiver antennas, and N_c subcarriers as described in the previous section.

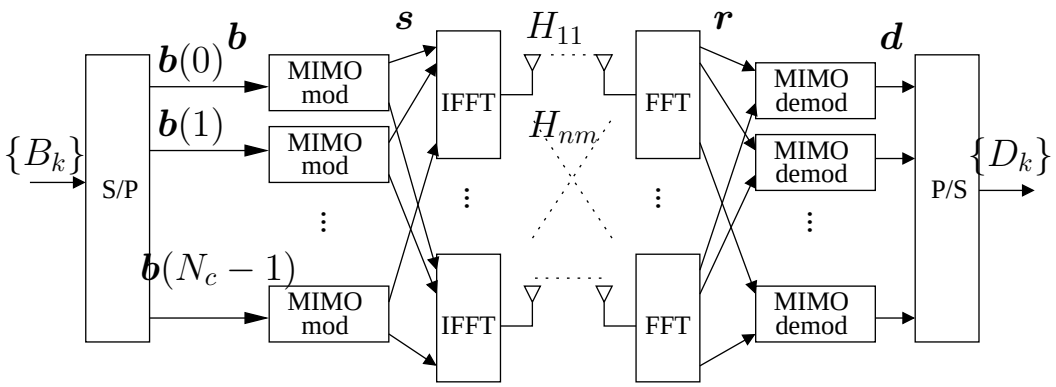

Figure 5.2: Subcarrier-specific MIMO in OFDM

In figure 5.2, the MIMO transmission system is presented as the following parts:

- The input to the MIMO modulation is the sequence of *modulation symbols* $\{B_k\}$, which may have been modulated just as in a normal SISO system.

- The output of the parallel per-subcarrier *MIMO modulation*, in turn, is a set of *MIMO transmission vectors*, one for each subcarrier.

- For OFDM processing, the IFFT is calculated for each antenna separately. Hence, all vector components that belong to the first antenna are processed by the first antenna's IFFT, all components belonging to the second are processed by the second IFFT, and so on. In the figure this is suggested by the re-ordering arrows.

- On the receiver side, the output of the OFDM processing's FFT is re-ordered into a set of *MIMO receive vectors*, one for each subcarrier.

- The parallel per-subcarrier *MIMO demodulation* will eventually calculate a sequence of receive symbols which are passed on to demodulation, just as in a normal SISO system.

The task of the "MIMO modulation" block, in general, is to modulate the sequence of complex input symbols into some "modulation" or "encoding scheme" that is suited to the MIMO transmission situation. The MIMO modulation can be either

- linear, or
- non-linear, but in this thesis, only linear MIMO modulation schemes are considered.

Additionally, potential MIMO modulation strategies are distinguished by the amount of required channel knowledge at the transmitter. The MIMO modulation can require

- full channel knowledge, i. e. H completely known but with a certain SNR_H, or
- partially known, e.g. only the magnitude of H might be known but not its phase, or
- no channel knowledge at the transmitter.

Examples for MIMO modulation strategies are:

- For an antenna selection technique (section 6.1.1), this means transmitting the input symbol on one antenna whereas the other antennas are kept silent.
- For a Space-Time Coding technique (section 6.2.1), this means mapping the input symbols on the codewords of the space-time code.
- For an SVD/Eigenbeamforming technique (section 7.1.1), this means multiplying the input symbols with the singular vectors of the radio channel.
- For a Space-Time layered architecture (e.g. BLAST, section 7.2), this means applying the layer-specific processing (e.g. channel coding) to each antenna layer.

More specifically, there is one MIMO modulator block per subcarrier, resulting in N_c MIMO modulator blocks. The sequence $\{B_k\}$, where k is the time index, holds the complex information symbols chosen from some constellation (e.g. QPSK). The bit stream that modulated these information symbols may

possibly have been processed by an outer channel code and interleaver (not shown), but as this is not directly MIMO-related, it will not be taken into account here. The serial-to-parallel converter routes the consecutive symbols of the input sequence into the subcarrier-specific processing chains.

Thus, the MIMO modulator at the nth subcarrier processes an input sequence $\{B_k(n)\}$ of complex scalars into an output vector sequence $\{\boldsymbol{s}_\ell(n)\}$ of dimension $N_T \times 1$ each, where ℓ is the time index (possibly but not necessarily different from k). Each component of those vectors is then modulated on a different antenna but on the same nth subcarrier. For a given time index ℓ, the time subscript is dropped and the output vectors of all MIMO modulators $\boldsymbol{s}(n),\ n = 0, \ldots, N_c - 1$ are written into one long vector $\boldsymbol{s}$ of dimension $N_T \cdot N_c \times 1$ as

$$\boldsymbol{s} = (\boldsymbol{s}(0)^T, \boldsymbol{s}(1)^T, \ldots, \boldsymbol{s}(N_c - 1)^T)^T \tag{5.1}$$

This vector is then OFDM modulated, i.e. each part corresponding to one antenna is IFFT processed, guard interval is added, D/A conversion is performed, and the signal is transmitted. It can easily be seen that several parts of the OFDM processing need to exist for each antenna separately. In particular, this applies to the IFFT/FFT and each processing step in between (not shown in Figure 5.2): Guard Interval introduction, D/A conversion, transmission circuitry, receiver circuitry, A/D conversion, and Guard Interval removal.

If this OFDM part of the system is designed according to the criteria mentioned in the previous section, then no ICI or ISI is present. Therefore on each subcarrier the channel transfer function for the transmission from antenna to another is again only one complex coefficient. Let $H_{ij}(n)$ denote this flat fading coefficient of the channel transfer function from antenna j to antenna i on subcarrier n. The matrix $\boldsymbol{H}(n)$ then holds all $N_R \times N_T$ channel coefficients on the nth subcarrier as

$$\boldsymbol{H}(n) = \begin{pmatrix} H_{11}(n) & \ldots & H_{1N_T}(n) \\ \vdots & & \vdots \\ H_{N_R1}(n) & \ldots & H_{N_RN_T}(n) \end{pmatrix} \tag{5.2}$$

The vector of received symbols on subcarrier n can be calculated as

$$\boldsymbol{r}(n) = \boldsymbol{H}(n)\boldsymbol{s}(n) + \boldsymbol{n}(n) \tag{5.3}$$

where $\boldsymbol{n}(n)$ is the noise vector containing the AWGN samples for each receiver antenna, and both $\boldsymbol{n}(n)$ and $\boldsymbol{r}(n)$ are of dimension $N_R \times 1$.

The basic assumption for this straightforward combination of MIMO in OFDM is that there is negligible correlation between neighboring subcarriers. This is

valid if there is sufficient interleaving among subcarriers, or if FDMA multi-user access is used so that each individual user is assigned a subset of subcarriers, where this subset can be chosen such that sufficiently spaced subcarriers are assigned for each user.

Alternatively, the MIMO modulation can be designed in frequency direction to exploit the available correlation in frequency. Example approaches for this are Space-Frequency Coding [BBP03]. However, this work only considers subcarrier-specific MIMO modulation in the following.

The MIMO-OFDM structure of figure 5.2 enables an efficient implementation of MIMO techniques in a broad-band radio channel [Ran08]. The intersymbol-interference which is introduced in the broad-band channel will be equalized by the frequency domain equalization of the OFDM technique. This simplified equalization is an important point because otherwise, the equalizer needs to take into account the whole length N_g of the channel impulse response for all MIMO radio channels in parallel. The algorithmic complexity of such an equalizer grows with $O(N_g^3)$ [Pro00] due the necessary convolution operation, which is too large in most broad-band systems. But OFDM is an effective technique to avoid such complexities, and in combination with MIMO even a large number of parallel radio channels can be processed with moderate implementation complexity.

6 Diversity

Diversity is the reception of one transmitted signal in several independently disturbed versions.

Under certain assumptions, different MIMO radio channels in a MIMO communication system will be changing independently from each other. Therefore these different MIMO channel can be considered as statistically independent and identically distributed random variables, and diversity techniques can be used to combat fading on these radio propagation paths.

It is known [ZT03] that if the fading is pairwise independent between antennas, an antenna array with N antennas can obtain a maximum *diversity gain* of N. This diversity gain is defined by observing that the average error probability can be made to decay like $1/SNR^N$ at high SNR, in contrast to the SNR^{-1} for the single antenna fading channel.

In the following analysis, the SNR distribution, the mean SNR, the analytically calculated BER and the simulated BER rates will be evaluated in order to verify this prediction for various diversity techniques. This evaluation is done in the i.i.d. Gaussian channel model first, and the additional degradation in a MIMO-WSSUS channel model is considered as a second step.

6.1 Receive Diversity

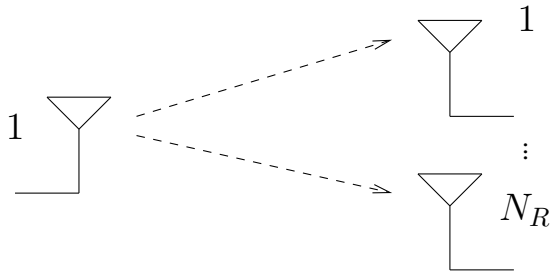

Figure 6.1: Receive diversity: Single transmit antenna, multiple receiver antennas

The easiest implementation of spatial diversity is *receive diversity*, where the

transmitter is using one antenna just as in conventional systems but the receiver is using multiple antennas (figure 6.1 and 6.2). This configuration is sometimes also called *SIMO (Single-Input Multiple-Output)*.

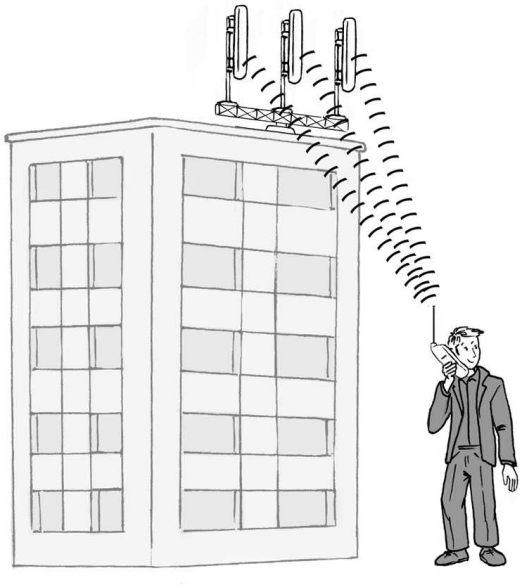

Figure 6.2: Communication link with antenna diversity on one end

6.1.1 Selection diversity

The easiest diversity technique is to select the best available version of the received signal and ignore the rest. This is commonly known as *selection diversity* and has been used for decades already [Pro00].

In a MIMO system, antenna selection can be employed both at the receiver or the transmitter. At the receiver, the signal from only one antenna is selected, and the receive signals of all other antennas on that subcarrier at this time are ignored. At the transmitter, the transmission signal is sent over one specific antenna, and all other antennas are inactive on this particular subcarrier at this time.

This selection can be done both at the receiver and transmitter, depending on the actual antenna configuration. For a transmitter-side antenna selection, the channel information about all magnitudes of $\|H\|$ would have to be available at the transmitter, which is rather uncommon but possible. For receiver-side antenna selection, that information would have to be available at the receiver, which is the case for almost any transmission system anyway. In any case, the analysis depends only on the number of available diversity branches, regardless

of where the selection from those diversity branches is made. Hence, the rest of this section considers N_R diversity branches to choose from.

PDF of selection diversity

In order to calculate the gain of selection diversity analytically, first the probability distribution of the resulting SNR is considered.

The error probability is always a function of the SNR$= |H|^2/N_0$. In a SISO random channel model with Rayleigh fading where the real and imaginary component are Gaussian, the SNR$\sim |H|^2$ is a random variable of Chi-square distribution with 2 degrees of freedom. With the variance of each component chosen as $\sigma^2 = 0.5$, the PDF of one channel is as simple as

$$f_{SNR,SISO}(x) = e^{-x} \,, \quad x \geq 0 \tag{6.1}$$

and has mean 1.

In selection diversity, one out of many such Rayleigh fading channels is selected, which means the resulting SNR is the *maximum* out of a set of random variables. By the help of *order statistics* [Pap84] the distribution of the maximum of N i.i.d. random variables is calculated from the individual distribution F and density f, which results in

$$f_{\max,N}(x) = N(F(x))^{N-1} f(x) \,. \tag{6.2}$$

Inserting the above Rayleigh channels (6.1) gives the following PDF for the resulting SNR after selection diversity

$$f_{SNR,sel}(x) = N(1 - e^{-x})^{N-1} e^{-x} \,, \quad x \geq 0 \tag{6.3}$$

which is shown in figure 6.3 for a few values of N.

The mean of this distribution is

$$\begin{aligned} \mu_{SNR,sel} &= N \sum_{k=0}^{N-1} \binom{N-1}{k} (-1)^k \int_0^\infty x e^{-(k-1)x} dx \\ &= N \sum_{k=0}^{N-1} \binom{N-1}{k} (-1)^k \frac{1}{(k+1)^2} \,. \end{aligned} \tag{6.4}$$

The first few values of this are shown in figure 6.4 for this technique and for the one in the next section. Clearly, the mean SNR increases with more diversity branches, but lesser than linearly and hence not optimal.

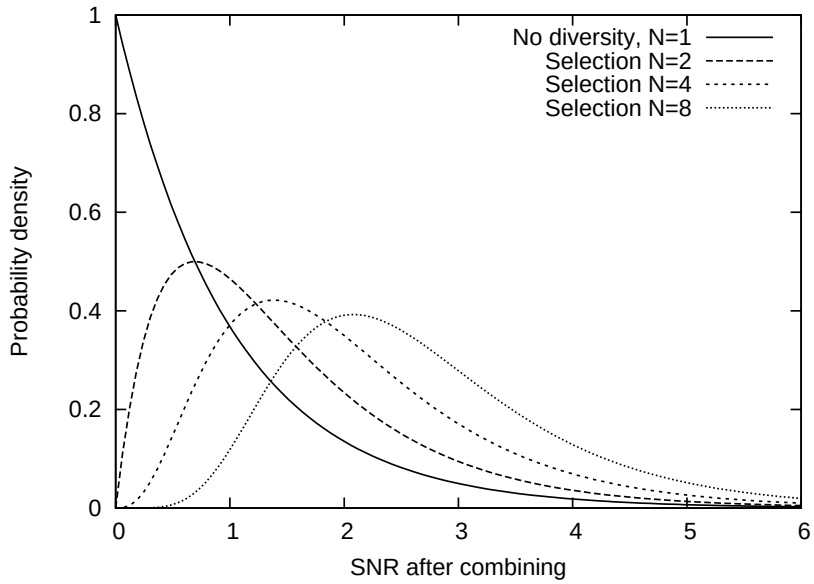

Figure 6.3: PDF of $|H|^2$ in Rayleigh fading, without and with selection diversity of degree $N = \{2, 4, 8\}$ ($\sigma = 1$)

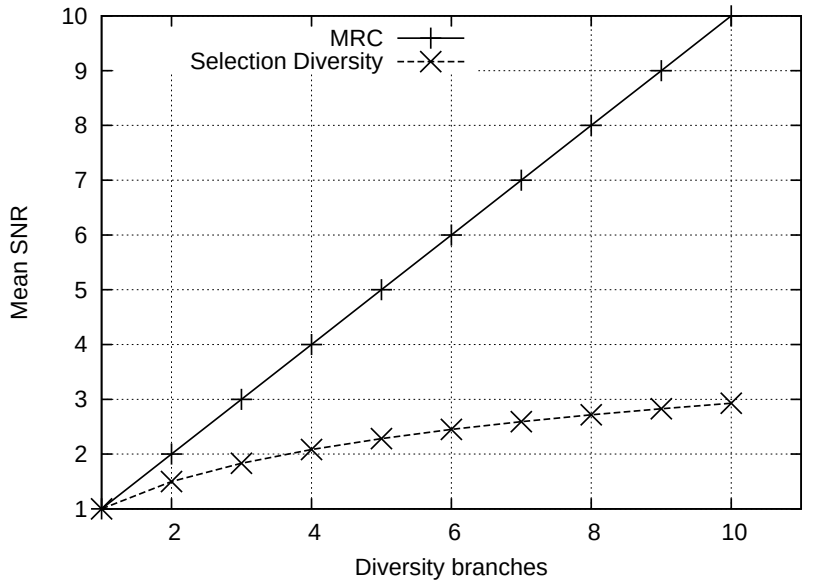

Figure 6.4: Mean SNR of Selection and MRC diversity

Analytical BER

However, the mean SNR is not the interesting criterion of evaluating the performance. Instead, the BER which depends on the full probability distribution is the interesting criterion. For that reason, a concrete modulation scheme is used as an example in the following. For BPSK modulation with constellation symbols $\{+a, -a\}$ the bit error rate can be calculated explicitly. The error probability, conditioned on a known channel $|h|^2$ after selection combining (6.3), is

$$Q(\sqrt{2|h|^2\rho}) \tag{6.5}$$

where $\rho = SNR = a^2/N_0$ is the average received signal to noise ratio per symbol, and $|h|^2\rho$ is the received SNR for the whole channel after selection combining. Now this expression is averaged over the distribution of $|h|^2$ to obtain the actual error probability. Again, independent Rayleigh fading with unit variance is assumed on each diversity branch. The corresponding PDF for $|h|^2$ was given in (6.3). Inserting this in (6.5) results in

$$p_{e,sel} = \frac{1}{2}\left[1 - \sum_{n=1}^{N} \binom{N}{n} (-1)^{n-1} \sqrt{\frac{\rho}{n+\rho}}\right] \tag{6.6}$$

[TV05]. This analytically calculated BER is shown in figure 6.5 together with simulation results which are consistent with the analytical ones.

To evaluate the asymptotic behavior at high SNR, a Taylor series expansion of the expression $\sqrt{\rho/(n+\rho)}$ is calculated in $1/\rho$ at $1/\rho \to 0$, as given by

$$\sqrt{\frac{\rho}{n+\rho}} = 1 - \frac{n}{2}\frac{1}{\rho} + \frac{3n^2}{2^2}\frac{1}{\rho^2} - \frac{3\cdot 5n^3}{2^3}\frac{1}{\rho^3} + \frac{3\cdot 5\cdot 7n^4}{2^4}\frac{1}{\rho^4} - \ldots \qquad \text{at } 1/\rho \to 0\,. \tag{6.7}$$

When inserting this into (6.6), it turns out all terms up to the Nth term will cancel out due to the to the binomial series and the factor n^k in the nominator of each Taylor term. Only the Nth term gives a nonzero contribution to the resulting p_e, which means

$$p_{e,sel} \sim \frac{1}{SNR^N}\,. \tag{6.8}$$

It can be concluded that selection diversity provides a diversity gain N.

Simulated BER

This analytically calculated BER of uncoded BPSK can also be observed in actual simulations, see figure 6.6 (right plot). However, even this uncoded BER

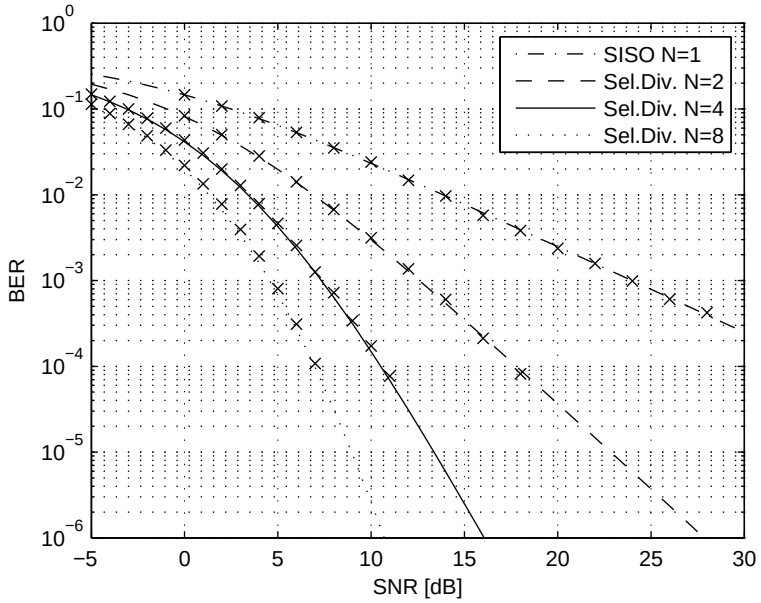

Figure 6.5: Analytically calculated BER of uncoded BPSK with selection diversity, $N = \{1, 2, 4, 8\}$ (markers: simulated values)

is not the final criterion of performance evaluation – the BER with channel coding is. Hence, figure 6.6 (left plot) shows the BER from simulations of a coded system. One can observe a significant performance increase due to the diversity. Each additional receive antenna gives an additional diversity branch and improves the uncoded and coded Bit Error Rate.

In an uncoded system, the achieved performance gain is very large because in the SISO system the BER is dominated by deep fades. Diversity is one means to combat this fading. Channel coding is another means, and extending channel coding by diversity will show smaller performance improvements. However, even in a coded system a noticeable increase of 3dB for the first and roughly 1dB for each additional diversity branch can be observed.

Finally, the achievable maximum bandwidth efficiency at a target BER is compared with the original channel capacity of a SISO channel, which was discussed in section 3.3.2. Figure 6.7 shows the capacity of a single-antenna Rayleigh fading channel and some achievable simulation results from figure 3.8. Additionally, the improved data rate through diversity is shown as well, which confirms nicely the performance gain through diversity.

However, this comparison neglects the fact that the theoretical capacity of a channel with diversity is much higher than the single-antenna capacity, which is the shown capacity. Nevertheless, it can be observed that the BER performance

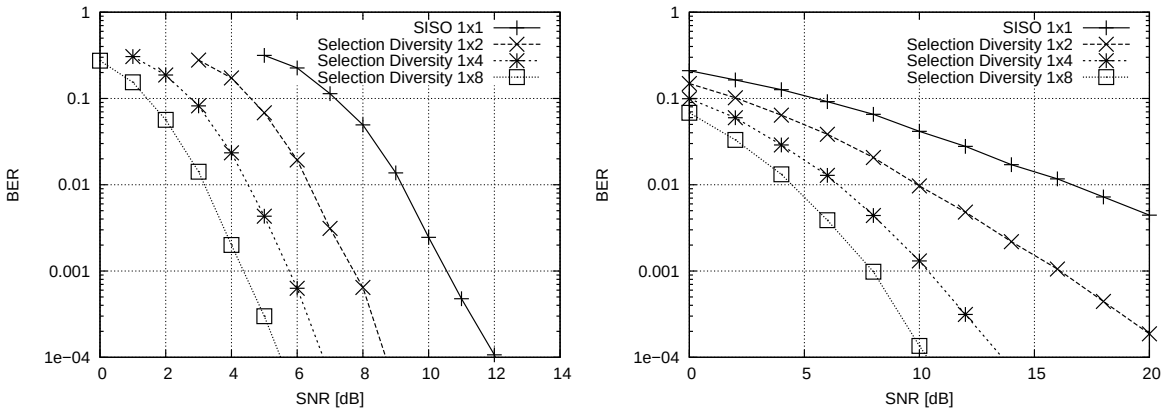

Figure 6.6: BER performance of antenna selection, coded and uncoded comparison, $E = 2$ bits/sec/Hz. (Left: 16QAM with code rate $r = 1/2$, Right: QPSK uncoded; Gaussian channel)

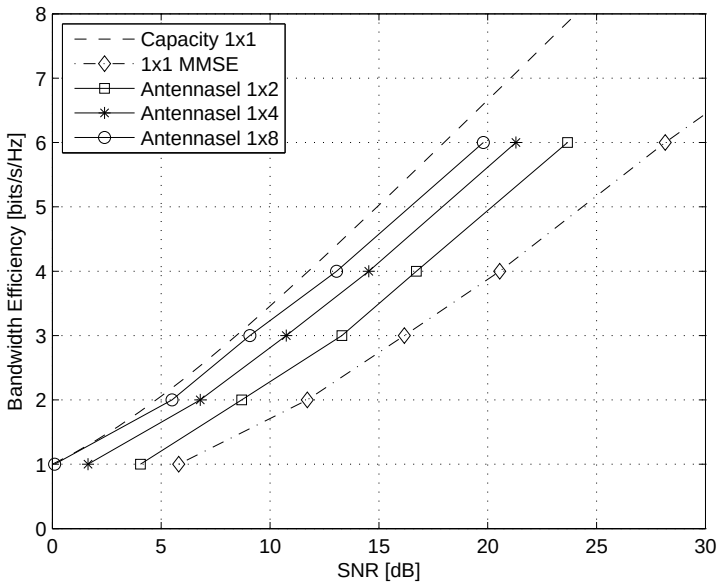

Figure 6.7: Bandwidth Efficiency (at BER=10^{-4}) of Antenna Selection (coded)

is significantly improved through the use of diversity, even with the simple but suboptimal selection diversity technique.

6.1.2 Maximum Ratio Combining

In the previous section, only one out of many available diversity branches was being used as the actual received signal. This approach can obviously be improved by using not only one diversity branch but instead using *all* branches by a suitable *combining* technique.

Maximizing the Signal-to-Noise Ratio

A combining technique is a function that maps all diversity branches r_i back to the one single desired signal $\tilde{s}$. Such a function is chosen according to a particular criterion. One common criterion is to maximize the resulting Signal-to-Noise Ratio. A combining technique that achieves this criterion is called *Maximum Ratio Combining* (MRC), also known as *matched filter* or *coherent combining*:

$$\tilde{s} = \sum_{i=1}^{N} h_i^* \cdot r_i \tag{6.9}$$

In order to evaluate the performance gain of MRC, the probability density of the SNR after MRC combining is considered. The PDF without diversity was e^{-x} with mean 1 (6.1). With MRC diversity, the SNR is the sum of $2N$ independent real-valued Gaussian random variables. Hence, its distribution is Chi-square with $2N$ instead of 2 degrees of freedom, which is

$$f_{2N}(x) = \frac{1}{(N-1)!} x^{N-1} e^{-x}, \quad x \geq 0\,, \tag{6.10}$$

which is shown for the first values of N in figure 6.8. The mean of (6.10) is simply N. Figure 6.4 nicely shows the performance advantage of MRC diversity compared to selection diversity, even when only paying respect to the mean SNR. The same result can be seen from comparing picture 6.8 to 6.3, which demonstrates the improved SNR by MRC.

Analytical BER

Again, the mean SNR is not the most interesting evaluation criterion, but the BER is. Therefore, a concrete modulation scheme is used to calculate the re-

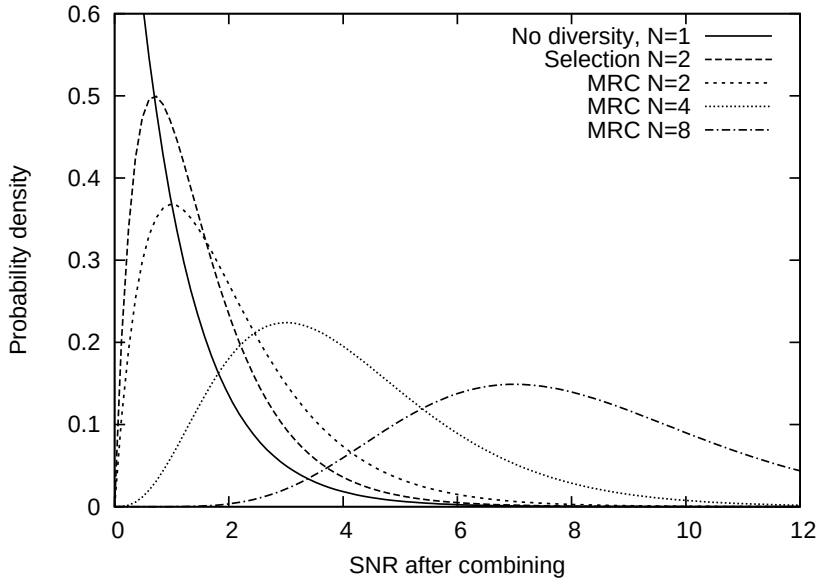

Figure 6.8: PDF of $|H|^2$ without diversity, selection diversity of degree 2, and with MRC diversity of degree $\{2, 4, 8\}$ ($\sigma = 1$)

sulting BER analytically. The error probability of BPSK with constellation symbols $\{+a, -a\}$, conditioned on the known channel realization $\boldsymbol{h}$ [TV05], is

$$Q(\sqrt{2\|\boldsymbol{h}\|^2 SNR}) \tag{6.11}$$

where $SNR = a^2/N_0$ is the average received signal to noise ratio per symbol, and $\|\boldsymbol{h}\|^2 SNR$ is the received SNR for the whole channel $\boldsymbol{h}$, almost similar to (6.5). This expression is averaged over the distribution of $\|\boldsymbol{h}\|^2$ to obtain the actual error probability.

The channel norm is distributed as Chi-square with $2N$ degrees of freedom, (6.10). With this density function, the resulting error probability of (6.11) can be computed analytically:

$$p_{e,mrc} = \frac{1}{2}\left[1 - \sqrt{\frac{SNR}{1+SNR}} \sum_{n=0}^{N-1} \binom{2n}{n} \frac{1}{4^n (1+SNR)^n}\right] \tag{6.12}$$

[TV05]. This bit error probability is shown in picture 6.9 for some $N = N_R$ together with simulation results which are consistent with the analytical results. Additionally, this figure shows the curves for selection diversity from figure 6.5. One can easily observe the better performance of MRC diversity.

Even more insight can be obtained from its approximation at large SNR using the Taylor series (6.7). In this case the linear term of the Taylor series is

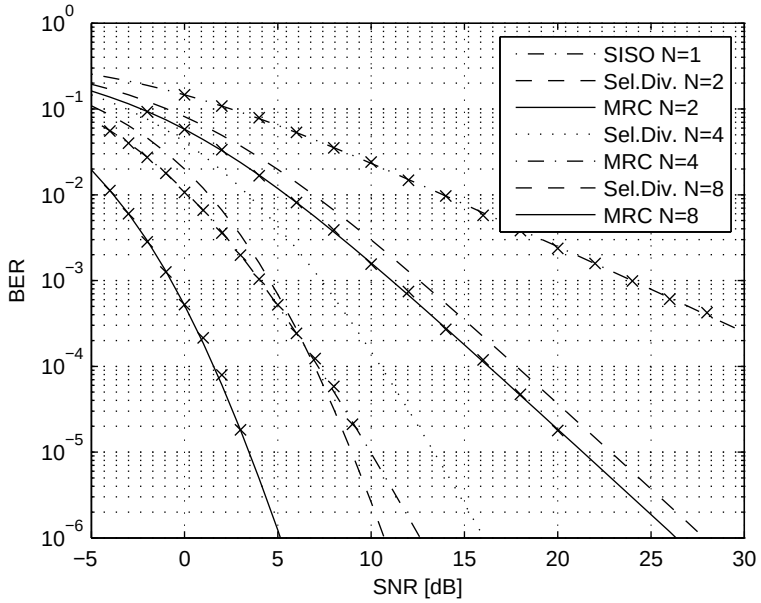

Figure 6.9: Analytically calculated BER of uncoded BPSK with MRC diversity (markers: simulated values) and selection diversity, $N_R = \{1, 2, 4, 8\}$

sufficient and this will result in a bit error probability at high SNR given by

$$p_{e,mrc} \approx \binom{2N-1}{N} \frac{1}{(4SNR)^N} \,. \tag{6.13}$$

This result shows that at high SNR, the error probability decreases with the Nth power of the SNR instead of the first power. Hence, MRC obtains a *diversity gain* of N, just as selection diversity does. In BER plots, this gain is visible as a faster decay of the error rate curves.

The previous technique, selection diversity, was shown to obtain a diversity gain of N as well. This can be seen by comparing the decent rate of both techniques in figure 6.9: Both techniques exhibit the same steepness, and MRC is only shifted to the left. This confirms as well that both techniques obtain the same diversity gain, although MRC additionally provides a performance gain on top of that.

Simulated MRC BER

The bit error rate of a MIMO transmission using MRC combining is shown in figure 6.10. Each additional receive antenna gives an additional diversity branch and improves the uncoded and coded Bit Error Rate.

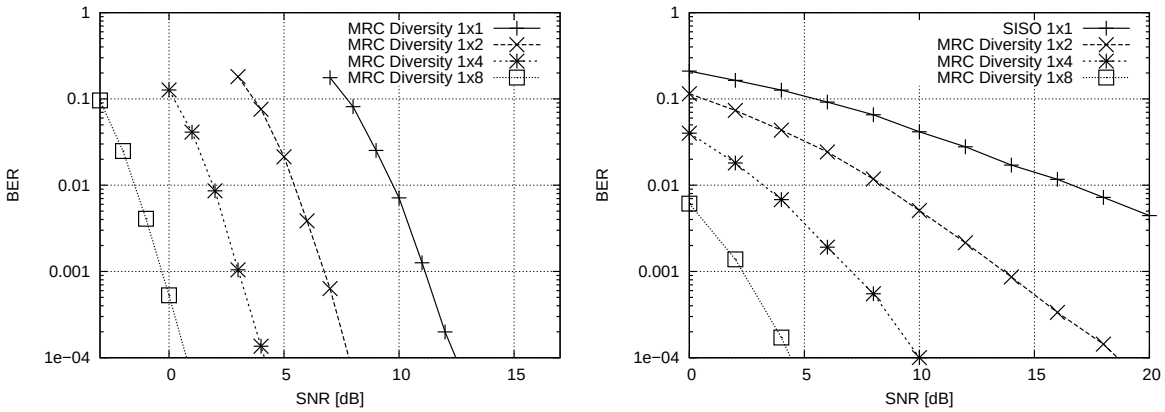

Figure 6.10: BER performance of Maximum Ratio Combining at the receiver, coded and uncoded comparison, $E = 2$ bits/sec/Hz. ($N_T = 1$, $N_R = \{1, 2, 4, 8\}$ Rx antennas. Left: 16QAM with code rate $r = 1/2$, Right: QPSK uncoded)

In theory this technique can be used not only for exploiting diversity but additionally in the context of spatial multiplexing for transmitting multiple data streams in parallel. However, in practice this is only usable if the error due to inter-stream interference is small compared to the noise. In other words, this would only be used at very high noise levels and low SNR, which is not the region of interest here. This section only considers the diversity benefits of MRC combining in the receiver.

Finally, the achievable maximum bandwidth efficiency at a target BER is compared with the original channel capacity of a SISO channel, which was discussed in section 3.3.2. Figure 6.11 shows the SISO capacity of a Rayleigh fading channel together with the improved data rate that can be achieved through MRC diversity.

6.1.3 Equal Gain Combining

As a simplification of MRC in terms of the computational complexity, *Equal Gain Combining* (EG) is a technique that corrects only the phase rotation of h_i but leaves the magnitude unchanged.

$$\tilde{s} = \sum_{i=1}^{N} \frac{h_i^*}{|h_i|} \cdot r_i \tag{6.14}$$

The simulated performance of Equal Gain combining in shown in figure 6.12 and 6.13, where the other diversity techniques are shown as well. Each addi-

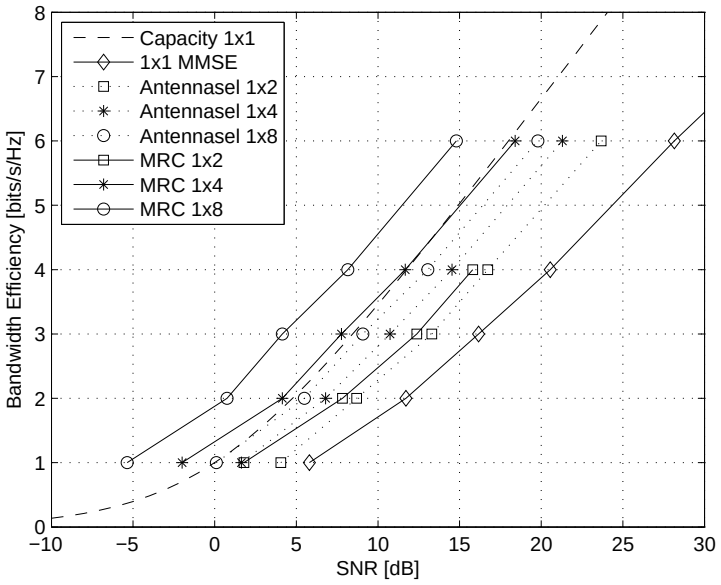

Figure 6.11: Bandwidth Efficiency of MRC Receive Diversity (coded)

tional diversity branch in EG increases the performance almost as much as with MRC combining.

The degradation compared to MRC combining is surprisingly small. Especially at low antenna numbers, there is almost no degradation compared to MRC combining. Even at higher antenna numbers the difference is small. The same comparison can be seen in the final bandwidth efficiency comparison of figure 6.14. It can be concluded that an equalization (6.14) is a useful simplification for the implementation complexity in the receiver hardware.

Comparison of Diversity Combining

	SNR increase diversity=2	SNR increase diversity=4	SNR increase diversity=8
Selection Div. Coded	3.3 dB	5.2 dB	6.5 dB
EG Coded	3.9 dB	7.4 dB	10.5 dB
MRC Coded	4.0 dB	7.7 dB	11.1 dB

Table 6.1: Resulting SNR increase at BER=10^{-4} compared to the SISO performance

As a comparison, some BER curves of the three considered diversity schemes

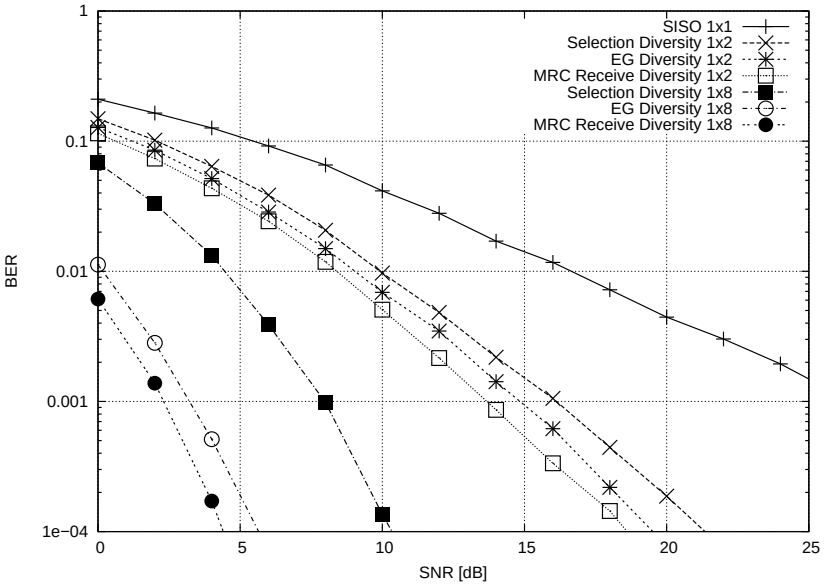

Figure 6.12: BER performance of different receive diversity schemes, uncoded QPSK, bandwidth efficiency $E = 2$ bits/sec/Hz.

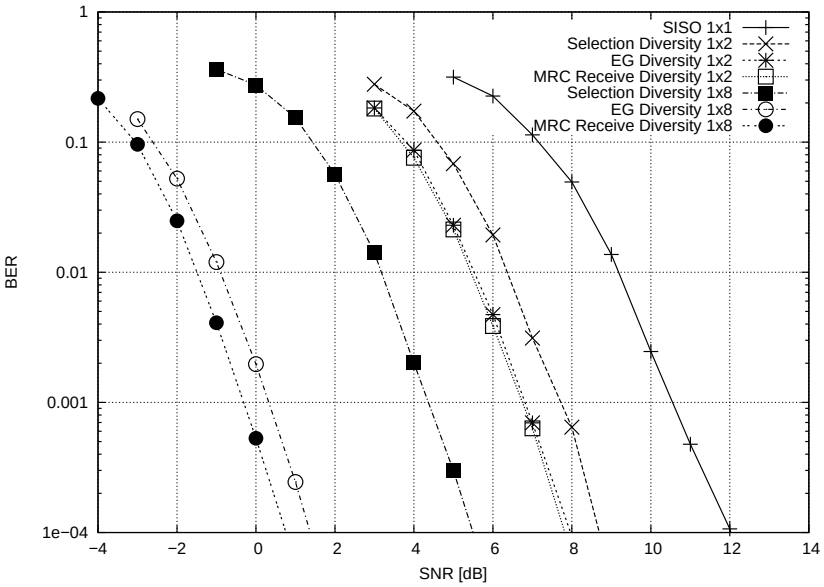

Figure 6.13: BER performance of different receive diversity schemes, coded (16QAM with $r = 1/2$ code), bandwidth efficiency $E = 2$ bits/sec/Hz.

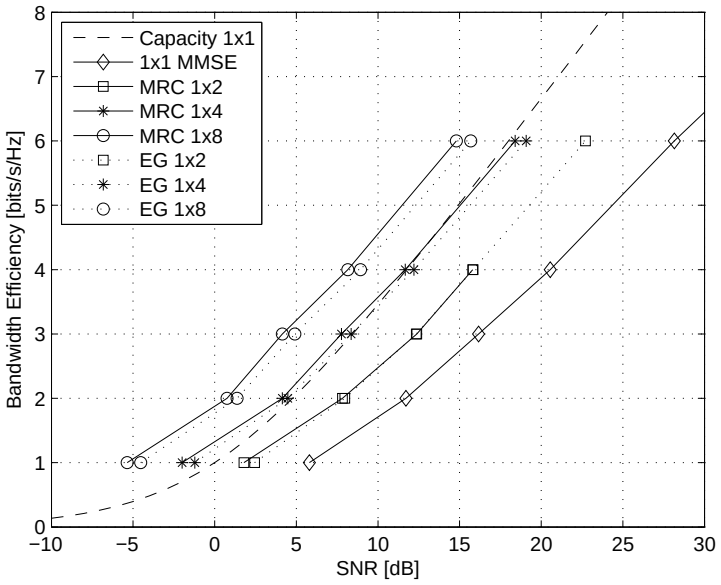

Figure 6.14: Bandwidth Efficiency of MRC and EG combining (coded, Gaussian channel)

are shown in figure 6.12 and 6.13, showing the performance at the same bandwidth efficiency. The performance gain in numbers is summarized in table 6.1.

Both the uncoded and coded simulations confirm any of the diversity techniques to be a good way of combating fading. Selection diversity is the easiest technique, but can provide only significantly less gain compared to MRC and EG. MRC diversity shows the best performance, which is being expected due to its construction criterion. Nevertheless the simpler EG diversity shows almost as much gain both in the uncoded and coded simulations.

The achievable bandwidth efficiency of the three diversity techniques is shown in figure 6.14, which confirms the observed improvement also for other bandwidth efficiencies in the i.i.d. Gaussian channel model.

In figure 6.15, the same improvement can be observed even in the MIMO-WSSUS channel model with $L_R = L_T = 6$ scatterers, even though the absolute bandwidth efficiency is slightly degraded compared to the i.i.d. Gaussian performance. Nevertheless, the performance increase by using receive diversity holds in both radio channel models alike.

Coherently combining schemes such as MRC and EG are significantly more efficient than simple selection diversity in both Gaussian and MIMO-WSSUS radio channels. It can be concluded that a large diversity gain is realized by coherently combining the different diversity branches. On the other hand, the EG simplification of neglecting the amplitude weighting does not degrade the

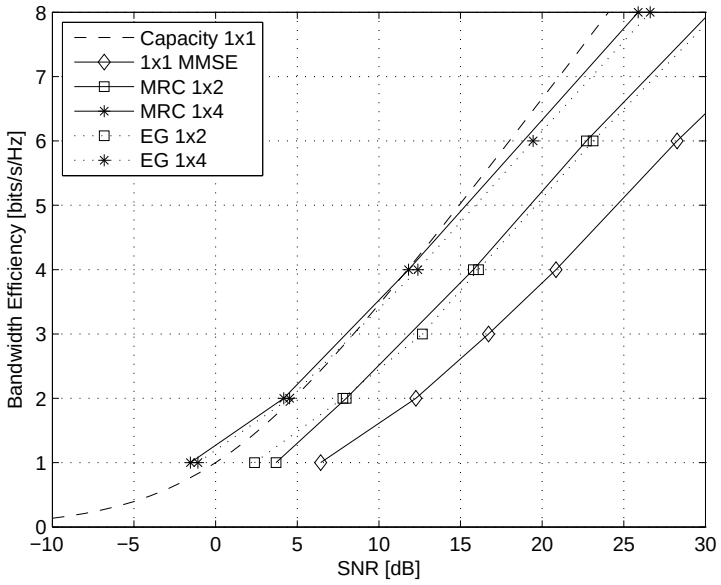

Figure 6.15: Bandwidth Efficiency of MRC and EG combining (coded, MIMO-WSSUS channel)

performance significantly. Hence, the additional weighting of the branches in MRC does not show a significant additional gain and can be skipped in order to decrease the computational complexity.

6.2 Transmit Diversity

As an alternative implementation of spatial diversity when it would be difficult to place multiple antennas at the receiver, *transmit diversity* can be used as well. In this case, the receiver is using one antenna just as in conventional systems, but the transmitter is using multiple antennas (figure 6.16). This configuration is sometimes also called *MISO (Multiple-Input Single-Output)*.

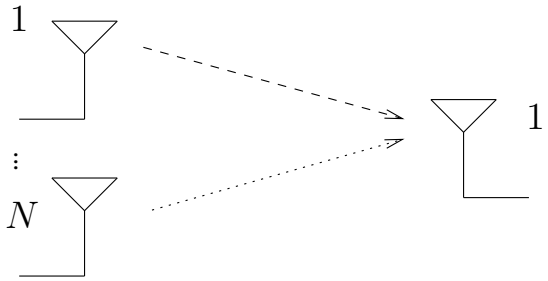

Figure 6.16: Transmit diversity: Multiple transmitter antennas, single receiver antenna

6.2.1 Space-Time Block Codes: Alamouti Scheme

A MIMO technique where a block of modulation symbols $\{B(k)\}$ are encoded to a block of transmission symbols $\{S(k)\}$ is called a *Space-Time Block Code*. A prominent example of this is the *Alamouti Scheme* [Ala98] which is a two-branch transmit diversity scheme.

For the Alamouti Scheme, a block of two modulation symbols $\{B(1), B(2)\}$ is considered in a system with two transmit and one receive antenna, $N_T = 2$, $N_R = 1$. The two modulation symbols are transmitted over the time duration of two time-steps, just as in a normal system without space-time coding. However, the symbols are not transmitted individually, but at each time-step both symbols are transmitted simultaneously, encoded in a special way.

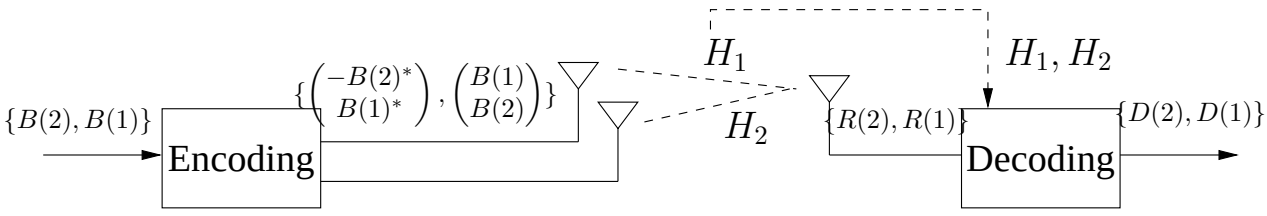

Figure 6.17: Alamouti Space-Time Block Code, $N_T = 2$, $N_R = 1$

This encoding is done as follows: At the first time-step $t = 1$, the transmit vector for the two transmit antennas is constructed as

$$\boldsymbol{s}(1) = \begin{pmatrix} B(1) \\ B(2) \end{pmatrix} . \tag{6.15}$$

At the next time-step $t = 2$, the transmit vector is constructed as

$$\boldsymbol{s}(2) = \begin{pmatrix} -B(2)^* \\ B(1)^* \end{pmatrix} . \tag{6.16}$$

The overall bandwidth efficiency is unchanged compared to a single antenna system, where two modulation symbols are transmitted in two time-steps as well. This Alamouti encoding scheme is depicted in figure 6.17.

At the receiver, the two receive symbols $\{R(1), R(2)\}$ of the two time-steps are used to recover an estimate $\{D(1), D(2)\}$ of the original modulation symbols by space-time decoding. This decoding requires the knowledge of the two channel transfer factors H_1, H_2 and these are assumed to be constant for the two time-steps in question. The decoding is done as follows:

$$\begin{aligned} D(1) &= H_1^* R(1) + H_2 R(2)^* && (6.17) \\ &= H_1^*(B(1)H_1 + B(2)H_2 + N(1)) + H_2(-B(2)^* H_1 + B(1)^* H_2 + N(2))^* \\ &= \underbrace{(|H_1|^2 + |H_2|^2)B(1)}_{Signal} + \underbrace{H_1^* N(1) + H_2 N(2)^*}_{Noise} . && (6.18) \end{aligned}$$

The decoding of the other symbol follows as $D(2) = H_2^* R(1) - H_1 R(2)^*$. If there were no noise, the original symbols are directly obtained, scaled by the channel power. In a realistic system with noise, the Signal-to-noise ratio is the interesting quantity.

The Signal-to-noise ratio of the decoded symbol results as

$$\begin{aligned} SNR &= E\{\frac{(|H_1|^2 + |H_2|^2)^2}{(H_1^* N(1) + H_2 N(2)^*)^2}\} = \frac{(\sigma_H^2 + \sigma_H^2)^2}{\sigma_H^2 \sigma_n^2 + \sigma_H^2 \sigma_n^2} \\ &= 2\frac{\sigma_H^2}{\sigma_n^2} , \end{aligned} \tag{6.19}$$

assuming unit power in the data symbol $B(k)$, σ_H^2 as the average channel power and σ_n^2 as the average noise power. This *SNR* is increased by a factor of 2 due to the increased diversity, compared to a single-antenna system.

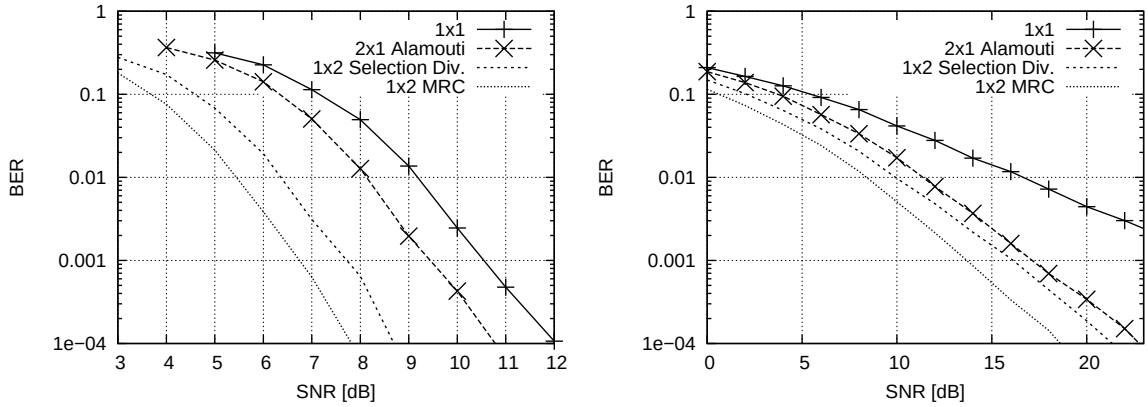

Figure 6.18: BER of Alamouti scheme and receive diversity (MRC and selection), coded and uncoded. (Left: 16QAM with code rate $r = 1/2$; Right: QPSK uncoded; Gaussian channel)

This result shows that the Alamouti Space-Time coding scheme increases the SNR by 3dB, which is just another way of saying that it achieves a diversity gain of 2. Also, the result after decoding is maximum-likelihood.

The Alamouti scheme [Ala98] is a simply way of exploiting diversity in a system with two transmit antennas. This can be generalized to multiple *receive* antennas, where the receiver uses maximum ratio combining on the receive symbol vector, although it has been shown that this scheme is no longer optimal [TV05]. For multiple *transmit* antennas, generalizations exist as well [TJC99], but all of them will incur a rate loss where the space-time encoded symbols need more time-steps to be transmitted compared to the original system without space-time code.

Performance

The bit error rate of the Alamouti scheme is shown in figure 6.18. This scheme offers a clear improvement over the SISO system by 1.3dB through exploiting Transmit Diversity. However, this does not quite meet the predicted 3dB of (6.19). This difference originates from the underlying OFDM transmission, which in turn limits the achievable BER because of the outage events due to channel fading.

The achievable bandwidth efficiency at various SNRs is summarized in figure 6.19. Using transmit diversity with the Alamouti schemes shows an improvement over using no diversity at all (the “1x1” curve). This is true for both i.i.d. Gaussian (figure 6.19) and MIMO-WSSUS radio channels (not shown here but in figure 7.18), as the diversity techniques show comparable perfor-

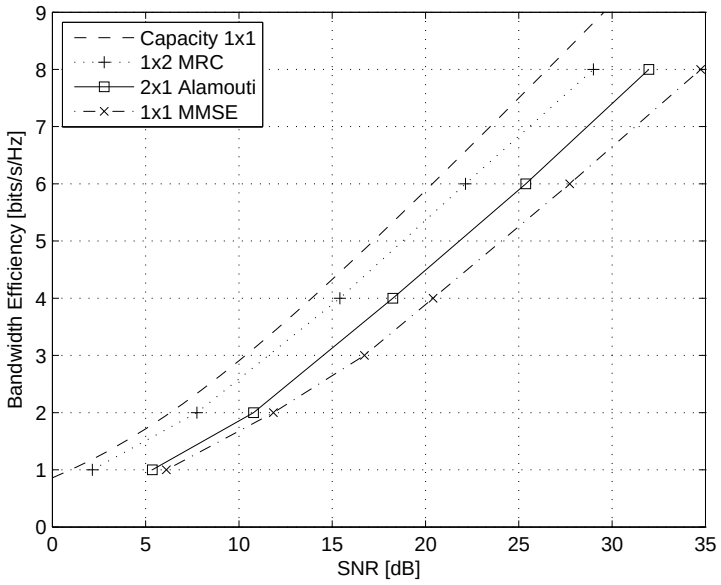

Figure 6.19: Bandwidth Efficiency (at BER=10^{-4}) of receive diversity (MRC) and transmit diversity (Alamouti), coded, Gaussian channel

mance improvements in both radio channel models alike.

Comparison of Receive and Transmit Diversity

The interesting question is how the performance of the Alamouti transmit diversity scheme compares to the receive diversity schemes discussed before. For this reason in figure 6.18 also two receive diversity schemes have been plotted.

Somewhat surprisingly it turns out even a simple antenna selection scheme offers significantly more improvement compared to Alamouti. The optimum receive diversity scheme with Maximum Ratio Combining shows an even larger improvement of 4.0dB over the SISO system, where Alamouti only shows 1.3dB as explained in the previous paragraph. This is true even for all bandwidth efficiencies shown in figure 6.19.

This difference between the Alamouti scheme and the other diversity schemes is a direct outcome of the fact that the other schemes exploit more knowledge about the MIMO radio channel. In the Alamouti scheme, the transmitter does not know the channel. The transmitter cannot assume any spatial structure of the channel and is unable to direct the transmit energy into specific channel directions, if there were any. On the other hand, the MRC scheme assumes channel knowledge at the receiver where the combining is done, which means the transmit energy can be collected from the specific channel directions.

For this reason, the Alamouti scheme shows less MIMO performance improvement than the other MIMO schemes that require and exploit more channel knowledge, see figure 6.19. If a system design faces the question whether to prefer multiple receive antennas over transmit antennas, this result clearly suggests to prefer multiple receive antennas for receive diversity.

Nevertheless, if the antenna configuration is fixed and only the transmitter side has two antennas, the Alamouti scheme is one simple and efficient solution to exploit diversity even though no channel knowledge at the transmitter is required, so that the performance is improved compared to the single antenna case.

7 Spatial Multiplexing

Transmit or receive diversity is a means to *combat* fading. By this means, multiple antennas are used to to improve the reliability for one communication channel.

In contrast to this, multiple antennas on both transmitter and receiver sides (figure 7.1) can also be used to turn the single radio link into *multiple parallel channels* [Fos96, Tel99]. This exploits an increase in the available degrees of freedom available for communication. The MIMO channel will then be turned into a Gaussian vector channel, where the parallel channels are multiplexed in space, hence the name *Spatial Multiplexing* [ZT03, TV05]. A technique is said to have a spatial multiplexing gain r if the data rate of this technique scales like $r \log SNR$, compared to the data rate scaling of $\log SNR$ in the single antenna case.

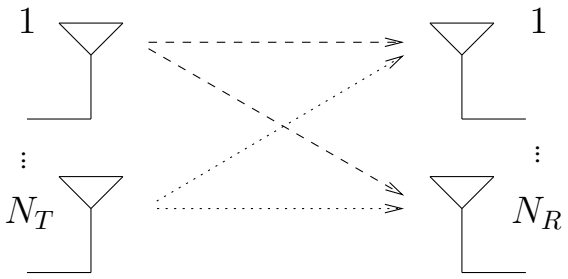

Figure 7.1: Multiple transmitter antennas, multiple receiver antennas

By transmitting independent information symbols over each of these parallel channels, the data rate can be increased. This is evaluated by determining the bandwidth efficiency of this technique over the SNR. This is done in the i.i.d. Gaussian channel model first. The behavior in a MIMO-WSSUS channel model is considered as a second step. It is expected that in a rich scattering channel even the simple Spatial Multiplexing techniques with linear receiver will strongly increase the available data rate when increasing the number of transmit and receive antennas. However, in a more unfriendly radio channel with little scattering as modeled with the new MIMO-WSSUS model, it is expected that Spatial Multiplexing techniques perform not as good anymore. This emphasizes the fact that performance simulations must use a realistic radio

channel model like MIMO-WSSUS in order not to give too optimistic results, as will be seen in the following sections.

7.1 Multiplexing with transmitter channel knowledge

The ideal case for exploiting the available parallel spatial channels is when the *channel state information* (CSI) is known perfectly at both the receiver and the transmitter [Ran08]. For this case the current channel matrix $\boldsymbol{H}$ is known and fixed.

The information theoretical capacity of the MIMO channel has been calculated in literature [Tel99]. It has been shown that the optimum mutual information, hence the capacity, can be reached when the MIMO modulation consists of a multiplication with the Singular Value Decomposition (SVD) at the transmitter side, together with adaptation of the modulation scheme according to some bit loading scheme. For this technique the definition of SVD as explained in section 4.3.2 is used.

7.1.1 Transformed MIMO transmission

With the Singular Value Decomposition, the following transformation will be defined

$$\tilde{\boldsymbol{s}} = \boldsymbol{V}^H \boldsymbol{s} \tag{7.1}$$

$$\tilde{\boldsymbol{r}} = \boldsymbol{U}^H \boldsymbol{r} \tag{7.2}$$

$$\tilde{\boldsymbol{z}} = \boldsymbol{U}^H \boldsymbol{z} \tag{7.3}$$

The MIMO matrix channel of (4.5) and (5.3) can be rewritten as

$$\tilde{\boldsymbol{r}} = \boldsymbol{\Sigma}\tilde{\boldsymbol{s}} + \tilde{\boldsymbol{z}} \tag{7.4}$$

where $\tilde{\boldsymbol{z}}$ has the same distribution as $\boldsymbol{z}$ due to the unitary $\boldsymbol{U}$ and $\|\tilde{\boldsymbol{s}}\|^2 = \|\boldsymbol{s}\|^2$, which means the energy is unchanged. This way, the original MIMO channel is turned into several parallel AWGN channels:

$$\tilde{r}_j = \sigma_j \tilde{s}_j + \tilde{z}_j, \quad j = 1, \ldots, K \tag{7.5}$$

The maximum data rate over these parallel AWGN channels *in space* can be obtained by applying the same techniques that have been described in section 3.2.2 for parallel AWGN channels *in frequency* by OFDM. Namely, the

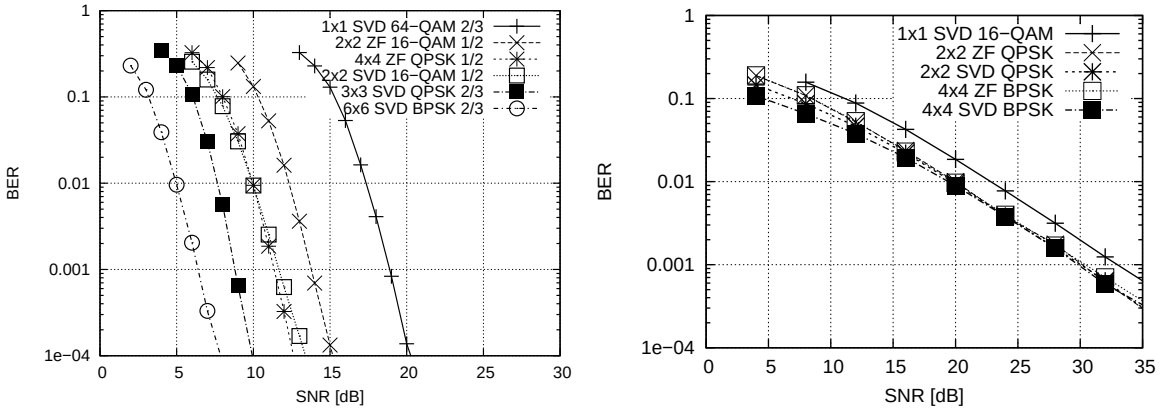

Figure 7.2: BER performance of "naive" SVD without adaptive modulation compared to linear ZF receiver, bandwidth efficiency $E = 4$ bits/s/Hz. Left: Coded, Right: Uncoded.

capacity over parallel channels is the maximization of the sum of bandwidth efficiencies of all the sub-channels (3.16). In the MIMO case the channel transfer factors of OFDM are instead replaced by the squared singular values σ_j^2 of the respective spatial sub-channel. The resulting bandwidth efficiency over the time-invariant known MIMO channel is

$$E_{MIMO} = \sum_{k=1}^{K} \log\left(1 + \frac{P_k \sigma_k^2}{N_0}\right) \text{ bits/MIMO transmission.} \qquad (7.6)$$

Ignoring this result for a moment, (7.4) could naively be used for transmission, which is a system of SVD transmission without adaptive modulation. Its BER performance is shown in figure 7.2.

In the uncoded case (figure 7.2 right), the performance is completely unchanged compared to spatial multiplexing with no channel knowledge at the transmitter (Linear ZF receiver, see section 7.2.1). Changing the transmission vector according to (7.4) does not improve the performance at all, as long as the transmit power is not adapted to the actually available channel quality on the different subchannels. This is because without different power allocation, the performance is limited by the outage events due to channel fading. The outage events due to fading are the limiting factor for the performance in SVD without adaptive modulation.

However, in a coded system (figure 7.2 left) the behavior is not so clear anymore. Some improvement over the ZF system can be observed, but it is not very significant.

In any case, for SVD the channel is assumed to be known anyway and a

capacity-achieving bit and power allocation can be calculated. Hence, in the following sections the technique for exploiting the actual capacity is discussed.

Capacity through Water pouring

Just as in section 3.2, the capacity (which is the maximum bandwidth efficiency) is obtained by solving an optimization problem over the power allocations P_k. The problem formulation leads to the same solution as in the OFDM case. Namely, water pouring and bit loading are needed to achieve the capacity. The water pouring power allocations (3.21) are

$$\hat{P}_k = \max\left(0, \frac{1}{\beta} - \frac{N_0}{\sigma_k^2}\right) \tag{7.7}$$

where the constant β is chosen to satisfy the power constraint

$$\sum_k^K \hat{P}_k = P\,. \tag{7.8}$$

One important difference between OFDM and MIMO-SVD is that in the former, the pre-processing matrices $\boldsymbol{U}, \boldsymbol{V}$ (the IFFT and FFT) do not depend on the channel realization $\boldsymbol{H}$, whereas in the latter they do depend on the specific realization of the MIMO channel.

Expected Capacity Value

The expected capacity that can be achieved in MIMO-SVD has been evaluated analytically by Telatar [Tel99]. The capacity of each of the spatial sub-channels (7.5) is a function of the singular values σ_j of the channel matrix $\boldsymbol{H}$, whose entries are random variables. Hence, the singular values are random and thus *the capacity is a random variable* as well.

In different channel models, the statistics of the singular values are different as well. Figure 4.4 and figure 4.17 show the PDFs of the singular values in various antenna configurations in the Gaussian i.i.d. and the MIMO-WSSUS radio channel model, respectively.

The expected value of the capacity is analyzed by obtaining the PDF of an unordered singular value σ from a WISHART[1] distribution and then integrating

[1] Let $\boldsymbol{H}$ be a random matrix with entries forming a i.i.d. Gaussian collection with zero-mean, independent real and imaginary parts. The matrix $\boldsymbol{W} = \boldsymbol{H}\boldsymbol{H}^H$ is a random non-negative definite matrix. The distribution law of $\boldsymbol{W}$ is called the WISHART distribution, and its joint density of the ordered eigenvalues is known analytically [Ede88, Tel99].

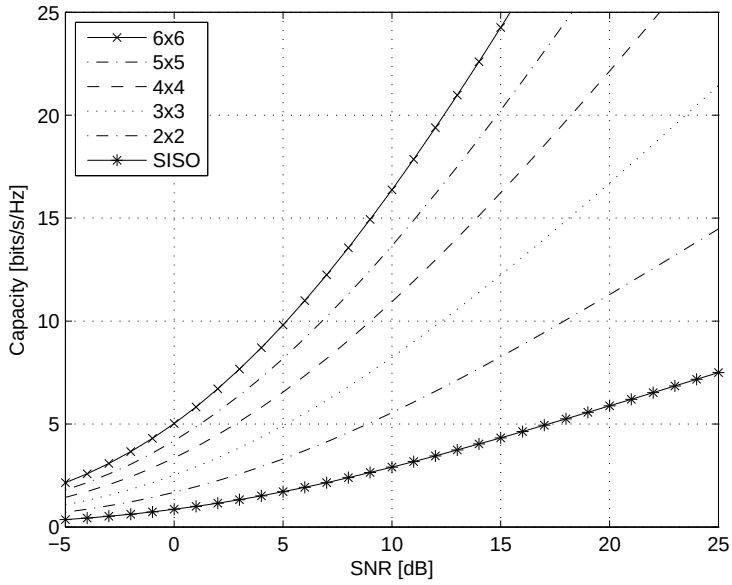

Figure 7.3: Theoretical Capacity of SVD-MIMO and $N_T = N_R = \{1, 2, \ldots, 6\}$

over the PDF of that singular value [Tel99]. The resulting expectation of the capacity for $N_T = N_R$ is

$$C_{SVD}(P) = \int_0^\infty \log(1 + P\lambda/N_R) \sum_{k=0}^{N_R-1} L_k(\lambda)^2 e^{-\lambda} d\lambda \tag{7.9}$$

where $L_k(\cdot)$ is a Laguerre polynomial of order k (see[2] [AS64] §22.3) and P is the total transmit power. The resulting capacity for the first few numbers of antennas with $N_R = N_T$ is shown in figure 7.3, where the single-antenna case is identical to figure 3.4.

These results have been subsequently refined by others [KH05, DM05, Ran08]. With the same number of transmit and receive antennas, in the limit of a large number[3] of antennas the capacity increases *linearly* with the number of antennas N_T:

$$C \sim N_T \int_0^4 \log(1 + SNR \cdot \nu) \frac{1}{\pi} \sqrt{\frac{1}{\nu} - \frac{1}{4}} d\nu \tag{7.10}$$

[2]The first few Laguerre polynomials are $L_0(x) = 1$, $L_1(x) = -x + 1$, $L_2(x) = \frac{1}{2}(x^2 - 4x + 2)$, $L_3(x) = \frac{1}{6}(-x^3 + 9x^2 - 18x + 6)$, $L_4(x) = \frac{1}{24}(x^4 - 16x^3 + 72x^2 - 96x + 24)$

[3]The antennas number where this asymptotical expression comes close to the exact capacity is surprisingly small and for many cases is in the region of 5 to 10 antennas [DM05]

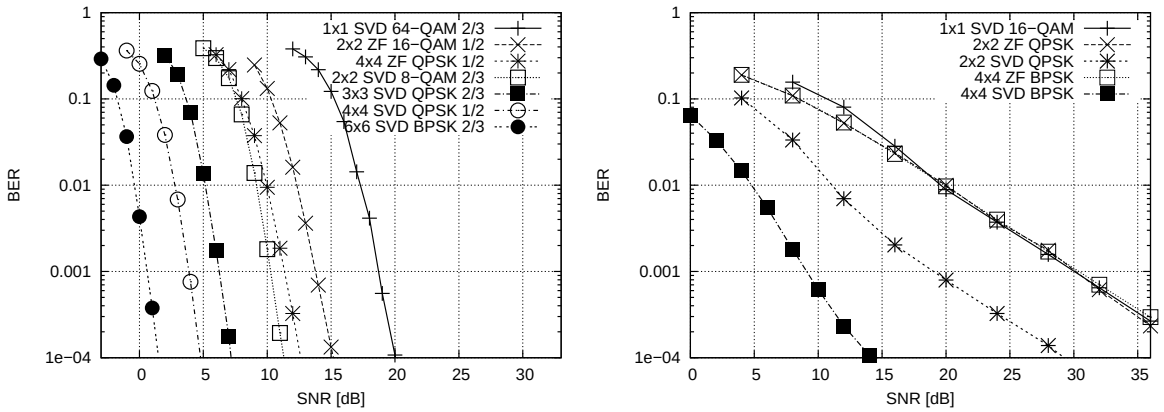

Figure 7.4: BER performance of SVD with adaptive modulation. Bandwidth efficiency $E = 4$ bits/s/Hz, Gaussian i.i.d. Channel. Left: Coded, Right: Uncoded.

The increase in capacity and bandwidth efficiency of figure 7.3 is termed the *spatial multiplexing gain*. By using Singular Value Decomposition with Water Filling and Loading this capacity can be achieved.

7.1.2 Performance

The bit error rate of a MIMO transmission using SVD with water filling and bit loading is shown in figure 7.4. It is clearly visible how SVD with loading improves the performance significantly with increasing numbers of antennas [BVR07, BVR08, Ran08].

In comparison to the linear ZF receiver (see section 7.2.1) even a $N_T = 2, N_R = 2$ system outperforms ZF systems with much higher antenna numbers. In the uncoded case (figure 7.4, right) it can be observed how subchannel-specific adaptive modulation already improves the BER performance significantly. However the full exploitation can be obtained only by the combination of adaptive modulation and channel coding.

The bandwidth efficiency that is actually achieved in these simulation results should now be compared with the theoretical capacity of figure 7.3. The simulated results are being shown in figure 7.5, where the single points represent the bandwidth efficiency due to one particular MIMO configuration at an SNR required for a BER of less than 10^{-4}.

The resulting relation between SNR and achievable bandwidth efficiency already shows the same slope as the theoretical curves, increasing much more steeply with a higher number of antennas available. The simulation results of

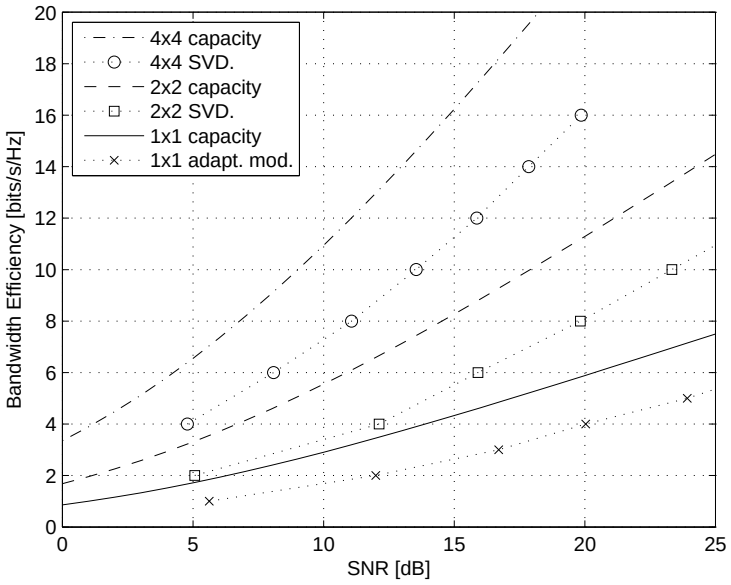

Figure 7.5: Bandwidth Efficiency (at $BER = 10^{-4}$) and Capacity of SVD-MIMO and $N_T = N_R = \{1, 2, 4\}$, Gaussian channel

the MIMO-SVD scheme with water filling, bit interleaving, and channel coding achieves bandwidth efficiencies which are more or less close to the theoretical capacity, although there is still a gap of 4-5 dB due to non-ideal (finite) channel coding and discrete modulation steps.

However, the SNR of these simulation results is to be taken with care. In this case the SNR shown is only the average SNR, but due to water filling, the SNRs of the subset of actually used subcarriers and MIMO subchannels is higher than this average SNR. Hence, the SNR of the simulations does not accurately represent the SNR which would be seen by a system in reality. Nevertheless these results give a clear indication that an MIMO-SVD scheme with ideal channel knowledge can achieve a performance that is rather close to the theoretical capacity.

Also, these results are simulated under the assumption of a perfect channel knowledge at the transmitter. If this assumption no longer holds, the performance degrades significantly and the MIMO technique needs to be modified [BVR07, BVR08], but this was not considered in this thesis.

Performance in MIMO-WSSUS channel

The previous results of figure 7.4 showed a bandwidth efficiency that comes nicely close to the capacity, but in a Gaussian i.i.d. radio channel. The inter-

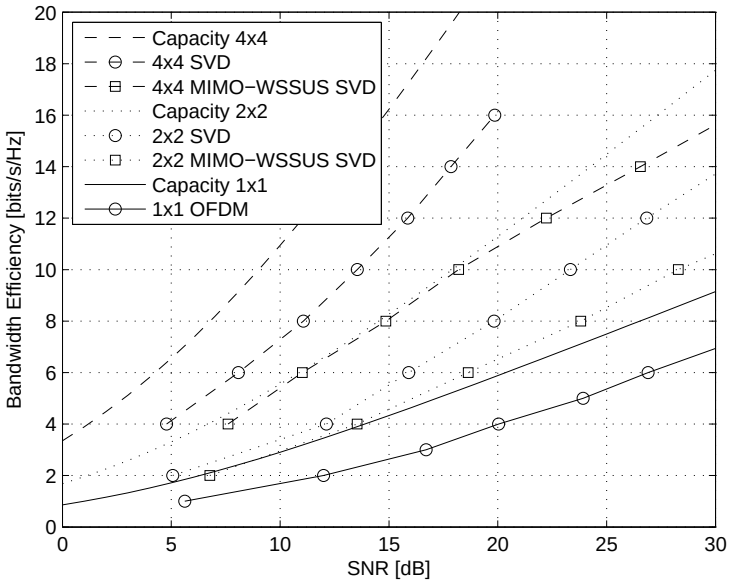

Figure 7.6: Bandwidth Efficiency of SVD-MIMO in Gaussian and in MIMO-WSSUS radio channel

esting question is how this performance looks like if the radio channel does not offer as much statistical independence and the degrees of freedom for spatial multiplexing are much more limited. Hence, the bandwidth efficiency in a MIMO-WSSUS radio channel is the relevant criterion to judge whether this technique can work well in a realistic system as well.

In figure 7.6, this MIMO technique is simulated in a MIMO-WSSUS radio channel with $L_R = L_T = 6$ scatterers. As one can observe, the performance is somewhat degraded compared to the Gaussian channel. Nevertheless the slope of the bandwidth increase is still comparable to the ideal capacity, and increasing the number of antennas still increases the achievable bandwidth efficiency. Hence, SVD-MIMO were a good candidate for increasing the spectral efficiency even in MIMO-WSSUS channels, if the required channel knowledge in the transmitter could be obtained by efficient means.

7.2 Multiplexing without transmitter channel knowledge: Linear MIMO Receivers

The previous technique requires the ideal channel state information (CSI) not only at the receiver, but also at the transmitter. In a realistic system, this is usually not achievable. For this reason, the available spatial multiplexing gain

for receiver CSI only is explained in the following.

Exploiting spatial multiplexing is achieved by transmitting different and independent data symbols from each transmit antenna. Hence, more than one data stream is transmitted in parallel. This is a similar situation to the multi-user channel, where multiple spatially separated users will transmit independent data streams, and a base station receiver has to separate those data streams again.

Receiver structures for separating independently transmitted data streams have been under research for a long time already. Linear structures can easily be thought of, but their performance is limited. Non-linear structures, especially iterative iterative cancellation techniques ("Successive Interference Cancellation", SIC), show huge potential, but are beyond the scope of this thesis.

In this section, linear receiver techniques for spatially multiplexed signals are presented and their BER performance is evaluated. The performance is simulated in both the i.i.d. Gaussian and the MIMO-WSSUS radio channel model, as the behavior will turn out to be rather different in different radio channel models.

7.2.1 Zero Forcing / Matrix Inversion

The straightforward way of separating all parallel original data streams is to invert the channel matrix. This way, all data streams will not interfere with each other at all. This receiver ideally corrects all distortion that has been introduced by the channel matrix, but at the expense of enhanced noise power. The receiver structure is called *Zero Forcing*, or *Interference Nulling*, or *Decorrelator*.

The MIMO demodulator matrix is

$$\boldsymbol{G}_{ZF} = \boldsymbol{H}^{-1} \,. \tag{7.11}$$

In other words, the MIMO demodulator is a matrix multiplication of the received vector with $\boldsymbol{H}^{-1}$, the inverse of the MIMO channel matrix. The received signal on a single OFDM subcarrier results as

$$\tilde{\boldsymbol{s}} = \boldsymbol{H}^{-1}(\boldsymbol{H}\boldsymbol{s} + \boldsymbol{n}) = \underbrace{\boldsymbol{s}}_{\text{Signal}} + \underbrace{\boldsymbol{H}^{-1}\boldsymbol{n}}_{\text{Noise}} \,. \tag{7.12}$$

However, this demodulation technique works only under the assumption that the channel matrix $\boldsymbol{H}$ is invertible, which means it has full rank and (equivalently) it has no singular values close to zero. And even if there is full rank, the inversion of singular values close to zero will result in a large noise amplification in the estimated symbols.

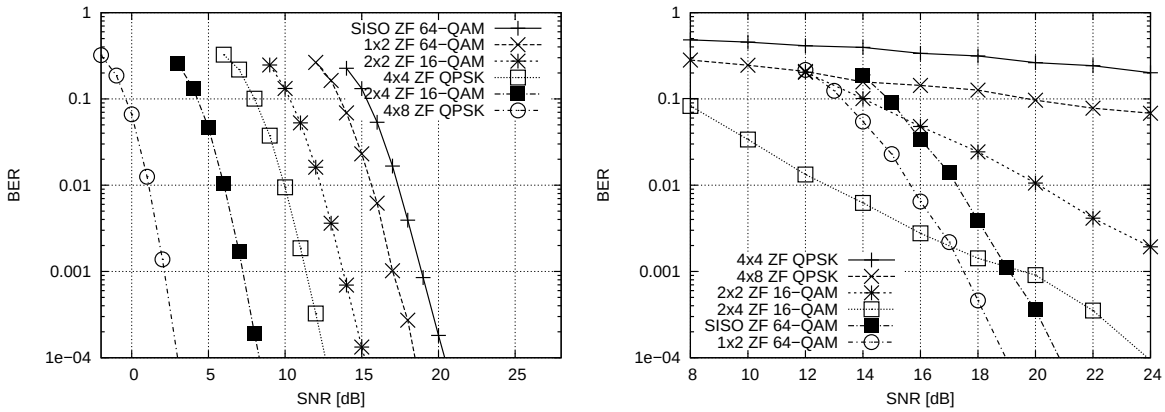

Figure 7.7: Coded BER performance of linear ZF receiver, $E = 4$ bits/sec/Hz. Left: Gaussian channel; Right: MIMO-WSSUS channel.

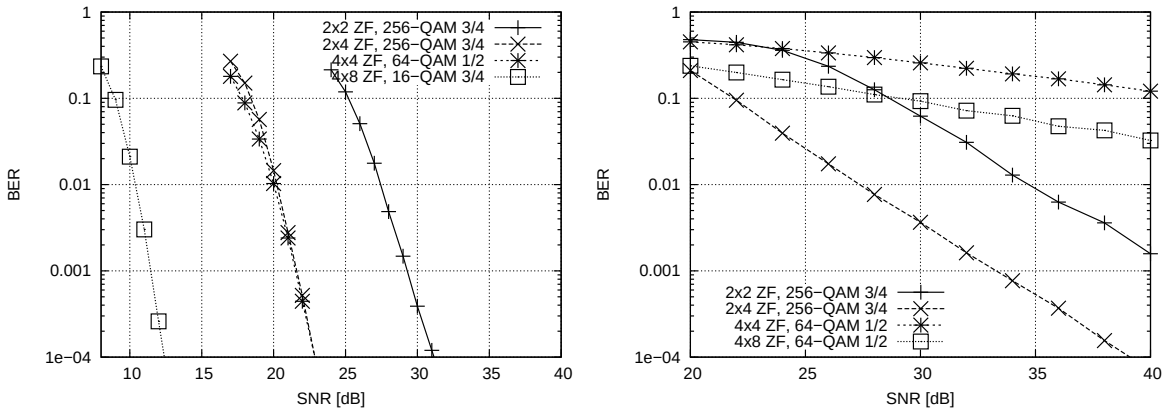

Figure 7.8: Coded BER performance of linear ZF receiver, $E = 12$ bits/sec/Hz. Left: Gaussian channel; Right: MIMO-WSSUS channel.

Performance

The BER performance of this spatial multiplexing with linear zero forcing receiver is shown in figure 7.7, left plot, for an i.i.d. Gaussian channel at bandwidth efficiency $E = 4$. Given the same bandwidth efficiency, in this channel model using some more parallel data streams results in better performance. This demonstrates the potential gain of spatial multiplexing.

For the same efficiency and same number of transmit antennas, increasing the number of receive antennas will additionally improve performance due to the diversity gain. This is no different from what the previous section showed.

Figure 7.8 shows the same comparison but for the higher bandwidth efficiency of $E = 12$ bits/s/Hz.

In terms of increased capacity, figure 7.9 compares the achievable bandwidth

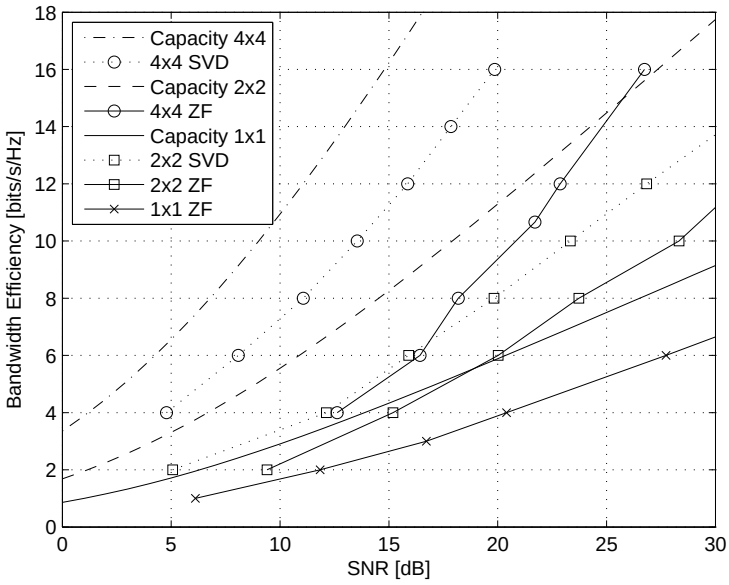

Figure 7.9: Bandwidth Efficiency of MIMO-ZF in Gaussian channel

efficiency to the theoretical capacity of the different antenna configurations. One can nicely see the steepness of the capacity curves reflected in the simulation results, although the linear ZF receiver has a large gap to the capacity: At $N_T = N_R = 2$ the linear ZF receiver has 8dB gap to the optimum, at $N_T = N_R = 4$ the gap is more than 12 dB. Nevertheless this technique can be used to achieve also very high bandwidth efficiencies.

However, this promising performance does not hold anymore if the channel model is not so MIMO-friendly. The same antenna and PHY mode combinations are shown in figure 7.7, right plot, for the MIMO-WSSUS channel model with $L_R = L_T = 6$ scatterers. Diversity-only ($N_T = 1$) shows an unchanged behavior compared to the Gaussian case. But all spatial multiplexing configurations ($N_T \geq 2$) exhibit significantly worse performance than the Gaussian case. For the efficiency shown here one would still have to choose the $N_T = 1$ case to achieve the best performance. The corresponding capacities are shown in figure 7.10, which demonstrates that this linear MIMO receiver will actually decrease the achievable efficiency once such a difficult radio channel is being used.

Discussion

For a channel matrix with i.i.d. Gaussian random variables as entries, the PDF of the singular values have been calculated by [Tel99]. As it turns out, even

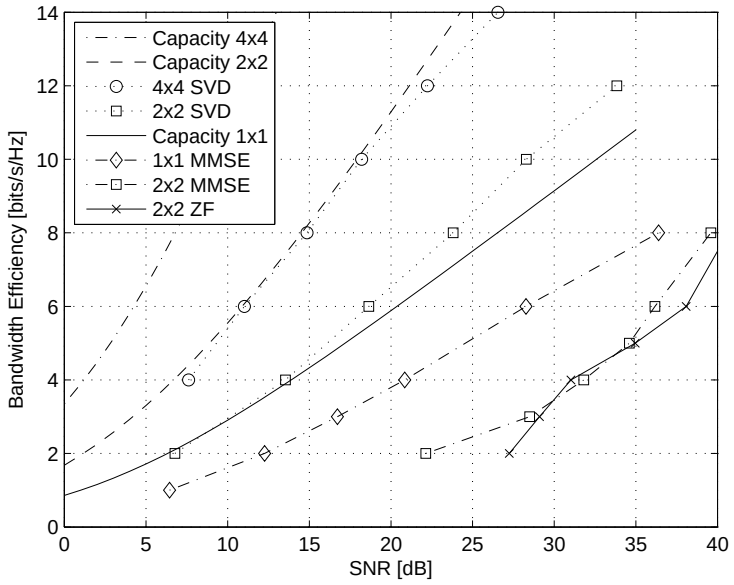

Figure 7.10: Bandwidth Efficiency of MIMO-ZF in MIMO-WSSUS channel

for a small dimension of the matrix $N_T = N_R = 4$ there is already a non-negligible probability for some singular values to be very close to zero. Due to the quantization in any realistic channel estimation device this is a serious issue, and in conclusion the Zero Forcing equalizer will not give any useful performance in a realistic MIMO system.

This effect turns out to be performance limiting once the Gaussian channel model is replaced by the MIMO-WSSUS one. In that case, ill-conditioned channel matrices will occur rather often, and in this case the linear ZF receiver cannot reliably work, as is obvious in figure 7.7, right plot. For this reason, the receiver could be used for some radio channels, but surely not as a general solution for all different radio channels that appear in realistic systems.

7.2.2 Optimum MMSE Receiver

The optimum linear MIMO demodulator for a flat-fading channel is also optimum for the MIMO-OFDM system with subcarrier specific MIMO modulation (section 5.1), which is an obvious outcome of the orthogonality of the subcarriers. In this chapter, the single-user detection case is considered only.

The optimum linear equalizer (and MIMO demodulator) is one that minimizes the mean square error $\boldsymbol{\varepsilon}$ in the received data symbols $\boldsymbol{d}$, i.e. it fulfills the *minimum mean square error* (MMSE) criterion. The error in the received

signal is denoted as

$$\boldsymbol{\varepsilon} = \boldsymbol{d} - \boldsymbol{b} \tag{7.13}$$

and the optimization criterion is to minimize its squared magnitude $E\{\|\boldsymbol{\varepsilon}\|^2\}$. The derivation of such an MMSE equalizer is fairly straightforward, using the orthogonality principle $E\{\boldsymbol{\varepsilon} \cdot \boldsymbol{d}^H\} = \mathbf{0}$ which says that the demodulated signal and its residual error should not be correlated anymore. In other words, after demodulation the residual error "should contain no information" about the actual signal anymore.

The equalized vector $\boldsymbol{d}$ is calculated with equalization matrix $\boldsymbol{G}$ as

$$\boldsymbol{d} = \boldsymbol{GHb} + \boldsymbol{Gn}\,. \tag{7.14}$$

The covariance matrix of the input data symbols is defined as $\boldsymbol{R}_{bb} = E\{\boldsymbol{bb}^H\}$, and $\boldsymbol{R}_{nn} = E\{\boldsymbol{nn}^H\}$ the covariance matrix of the noise samples, and noise and data symbols are assumed to be uncorrelated:

$$\begin{aligned} E\{\boldsymbol{\varepsilon d}^H\} &= 0 \qquad (7.15)\\ &= E\{[(\boldsymbol{HGH} - \boldsymbol{I})\boldsymbol{b} + \boldsymbol{Gn}][\boldsymbol{GHb} + \boldsymbol{Gn}]^H\} \\ &= (\boldsymbol{GH} - \boldsymbol{I})E\{\boldsymbol{bb}^H\}\boldsymbol{H}^H\boldsymbol{G}^H + \boldsymbol{G}E\{\boldsymbol{nn}^H\}\boldsymbol{G}^H \\ 0 &= \boldsymbol{GHR}_{bb}\boldsymbol{H}^H - \boldsymbol{R}_{bb}\boldsymbol{H}^H + \boldsymbol{GR}_{nn}\,. \qquad (7.16) \end{aligned}$$

The optimum matrix-valued MIMO demodulator solution is given by

$$\boldsymbol{G}_{MMSE} = \boldsymbol{R}_{bb}\boldsymbol{H}^H[\boldsymbol{HR}_{bb}\boldsymbol{H}^H + \boldsymbol{R}_{nn}]^{-1}\,. \tag{7.17}$$

This result is in accordance with similar results in [SSB+02] and many others. Further simplifications can be carried out by assuming the transmit symbols to be independent and with power P so that $\boldsymbol{R}_{bb} = P\boldsymbol{I}$, and the noise similarly $\boldsymbol{R}_{nn} = \sigma_n^2\boldsymbol{I}$, which gives

$$\boldsymbol{G}_{MMSE} = \boldsymbol{H}^H[\boldsymbol{HH}^H + \frac{\sigma_n^2}{P}\boldsymbol{I}]^{-1}\,. \tag{7.18}$$

Resulting Signal-to-Interference Ratio

Using such an equalization matrix, it is now the interesting question to see the resulting Signal-to-Interference and Noise Ratio (SINR) after equalization. This SINR of a linear MMSE receiver has been calculated by Tse et al. [TH99, TZ00, DM05].

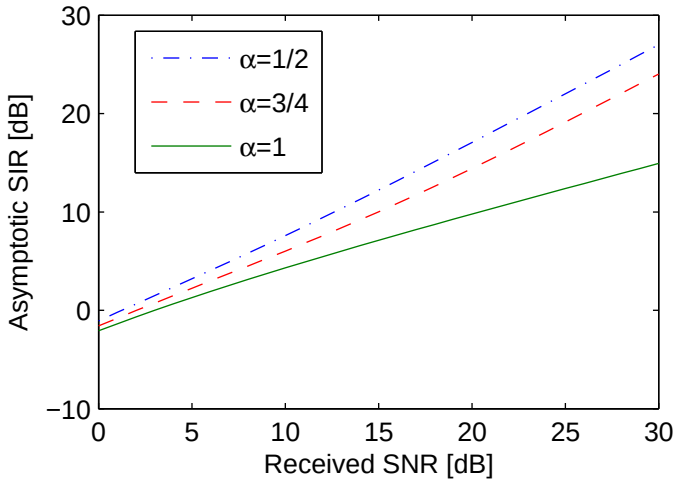

Figure 7.11: Asymptotic limit of the SIR for equal receive powers (7.19) with $\alpha = N_T/N_R$ as the ratio of transmit over receive antenna numbers

Although the actual SINR of the MMSE receiver results in a rather involved expression, the asymptotic Signal-to-Interference (SIR) itself was given in a relatively simple analytical formulation by [TH99]. The surprising result there was that although the MMSE receiver depends on the actual channel realization through the $\boldsymbol{H}$ multiplications, for large antenna numbers ($N_R \to \infty$ with $\alpha = N_T/N_R$ fixed) the SIR will converge to a limit that is independent of the channel realization.

In [TH99] a general solution for this limiting SIR was given, but an explicit solution can be given only for the special case of equal receive powers from all transmit antennas. In this case, the asymptotic SIR is

$$SIR = \frac{1-\alpha}{2}\frac{P}{\sigma_n^2} - \frac{1}{2} + \sqrt{\frac{(1-\alpha)^2}{4}\left(\frac{P}{\sigma_n^2}\right)^2 + \frac{1+\alpha}{2}\frac{P}{\sigma_n^2} + \frac{1}{4}} \tag{7.19}$$

where $\alpha = N_T/N_R$ is the ratio of transmit over receive antenna numbers, and P/σ_n^2 is the average received Signal-to-Noise Ratio (SNR) at the receive antenna of interest. This SIR is plotted in fig. 7.11 over the SNR for several values of α.

BER Performance

The BER performance of this spatial multiplexing with optimum linear receiver is shown in figure 7.12, left plot, for an i.i.d. Gaussian channel at bandwidth efficiency $E = 4$ bits/s/Hz. Similar to the ZF results in the previous section, using

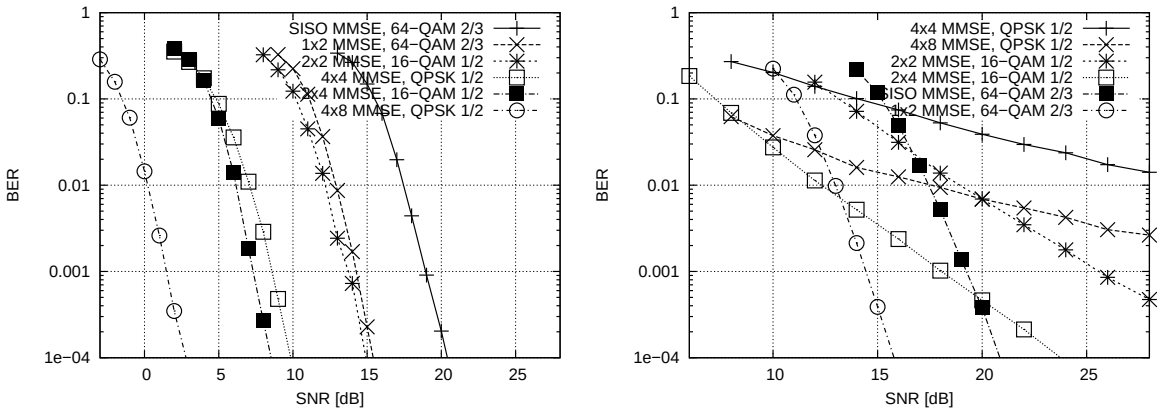

Figure 7.12: Coded BER performance of linear MMSE receiver, $E = 4$ bits/sec/Hz. Left: Gaussian channel; Right: MIMO-WSSUS channel.

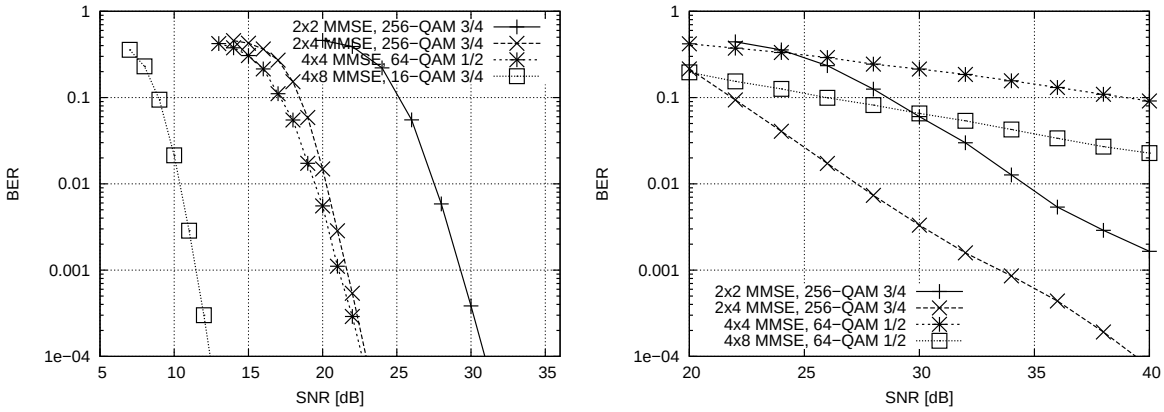

Figure 7.13: Coded BER performance of linear MMSE receiver, $E = 12$ bits/sec/Hz. Left: Gaussian channel; Right: MIMO-WSSUS channel.

some more parallel data streams results in better performance. This demonstrates the potential gain of spatial multiplexing.

However, similar to the ZF receiver this promising performance does not hold in the MIMO-WSSUS channel model with $L_R = L_T = 6$ scatterers, see figure 7.12, right plot. Diversity-only ($N_T = 1$) shows an unchanged behavior compared to the Gaussian case. But all spatial multiplexing configurations ($N_T \geq 2$) exhibit significantly worse performance than the Gaussian case. For the efficiency shown here one would still have to choose the $N_T = 1$ case to achieve the best performance.

For a higher bandwidth efficiencies the same comparison is made for $E = 12$ bits/s/Hz in figure 7.13.

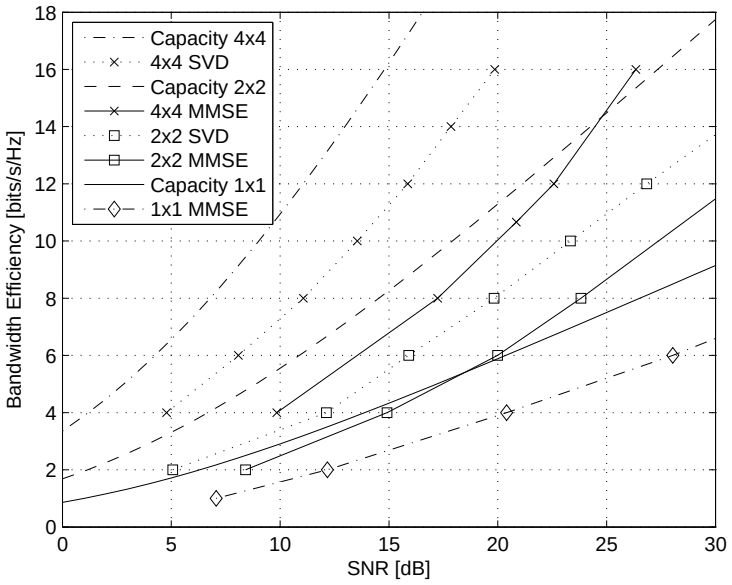

Figure 7.14: Bandwidth Efficiency of MIMO MMSE in Gaussian channel

The achievable bandwidth efficiencies are summarized in the capacity plots of figure 7.14. It turns out the linear MMSE receiver does not perform significantly better than the ZF receiver in the SNR and data rate ranges of interest. The outage events due to ill-conditioned channel matrices are the performance limiting factor in the MMSE receiver as well. For this reason, the receiver could be used for some radio channels, but surely not as a general solution for all different radio channels that appear in realistic systems.

7.2.3 Linear Receivers in MIMO-WSSUS radio channel

The performance of the techniques in the previous sections looked fine when using only the i.i.d. Gaussian radio channel model. In terms of spatial degrees of freedom, this radio channel is an ideal situation. In contrast to this, a realistic system will have to cope with radio channels that do not offer such a high degree of stochastic independence. Hence, all presented linear MIMO receivers are again evaluated in the MIMO-WSSUS radio channel model.

The simulated results indicate problems for Spatial Multiplexing in MIMO-WSSUS channels, figure 7.15. The basic assumption for Spatial Multiplexing is a large number of scatterers in the radio channel, so that the entries of $\boldsymbol{H}$ can assumed to fade independently to begin with. However, when choosing parameters for a MIMO-WSSUS radio channel model which seem reasonable

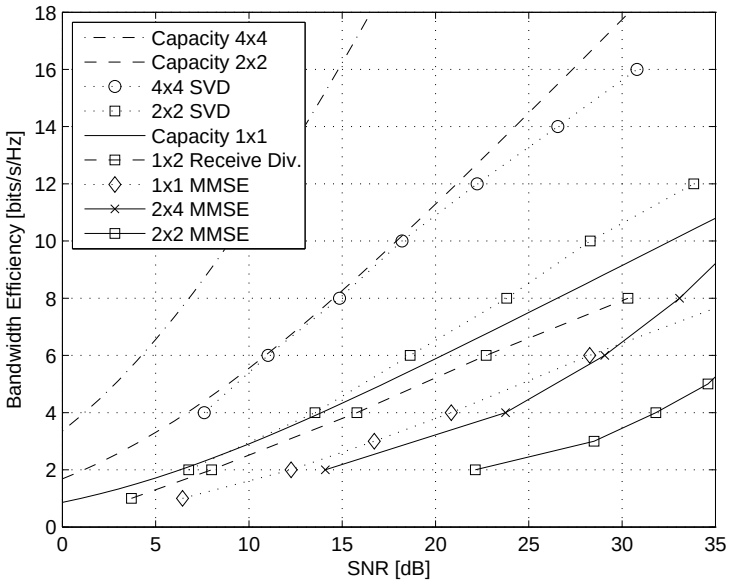

Figure 7.15: Bandwidth Efficiency of MIMO MMSE in MIMO-WSSUS channel

enough (see section 4.4), the performance is already degraded beyond any usable values.

Hence, with the linear receivers investigated in this work, it can be concluded that for realistic non-Gaussian channels, using Receiver Diversity is pretty much all that is possible as MIMO technique. If MIMO techniques should be used with multiple antennas on both sides, non-linear receiver structures will be essential, but these are beyond the scope of this work.

Comparison of Spatial Multiplexing and Alamouti Diversity

An interesting question is the comparison of this simple linear spatial multiplexing scheme with the diversity scheme of Alamouti coding (section 6.2.1). Both schemes assume the same amount of channel knowledge – no knowledge at the transmitter but full knowledge at the receiver. Both schemes can be used with arbitrary numbers of receive antennas to increase the diversity of the system. The actual coded BER performance is shown in figures 7.16 for a bandwidth efficiency of $E = 4$ bits/s/Hz and various antenna configurations.

In a Gaussian radio channel (figure 7.17), for a small number of receive antennas (one or two) the Alamouti scheme slightly outperforms linear MMSE equalization, whereas for a larger number of receive antennas (more than two) MMSE clearly outperforms Alamouti. This demonstrates how the Alamouti

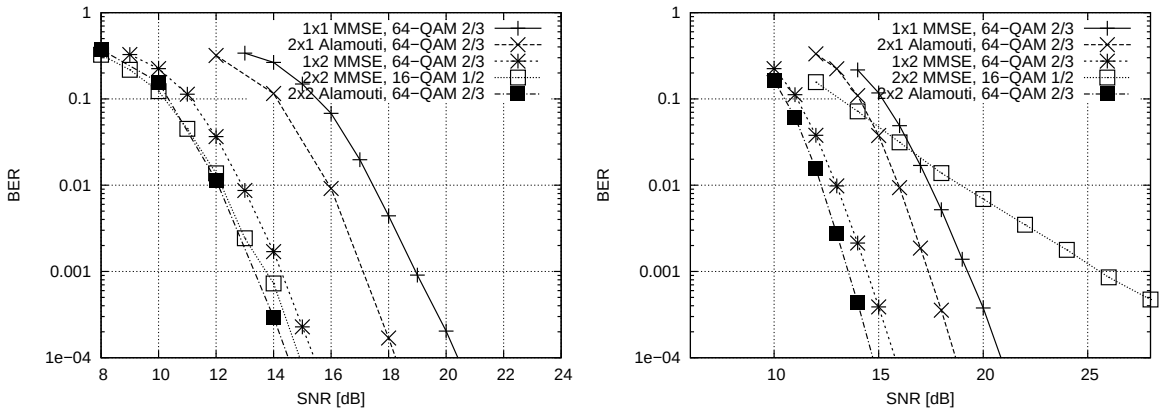

Figure 7.16: Coded BER of Alamouti scheme and linear MMSE spatial multiplexing. Bandwidth efficiency $E = 4$ bits/s/Hz. Left: Gaussian Channel; Right: MIMO-WSSUS channel.

scheme exploits a diversity order of two through the two transmit antennas, but the MMSE system with enough receive antennas can additionally make use of the spatial degrees of freedom through spatial multiplexing.

Figure 7.17 shows how the bandwidth efficiency of Alamouti is an improvement over SISO, but only a small improvement compared to MMSE diversity.

Also, the Alamouti scheme is obviously much less sensitive to the amount of scattering that is available in the MIMO radio channel. This is demonstrated by the fact that the Alamouti curves in the MIMO-WSSUS channel (figure 7.16, right pictures) show almost no degradation compared to the Gaussian channel (left pictures), whereas the MMSE performance is greatly reduced in the MIMO-WSSUS channel. This is confirmed for different bandwidth efficiencies in figure 7.18.

The disadvantage of Alamouti is observable with larger antenna numbers: The receive antennas already provide a lot of diversity and one can observe only a minimal increase in performance because the Alamouti system cannot exploit the additional degrees of freedom. E.g. a 2-by-4 MMSE system improves the performance quite substantial, compared to the Alamouti system with the same antenna numbers.

In summary, the Alamouti scheme is a good choice for one or two receive antennas in any radio channel. Additionally, the Alamouti scheme clearly offers much more robust performance regardless of the MIMO radio channel conditions.

However, in systems with more receive antennas and rich scattering radio channels, other MIMO techniques show better performance, where even linear

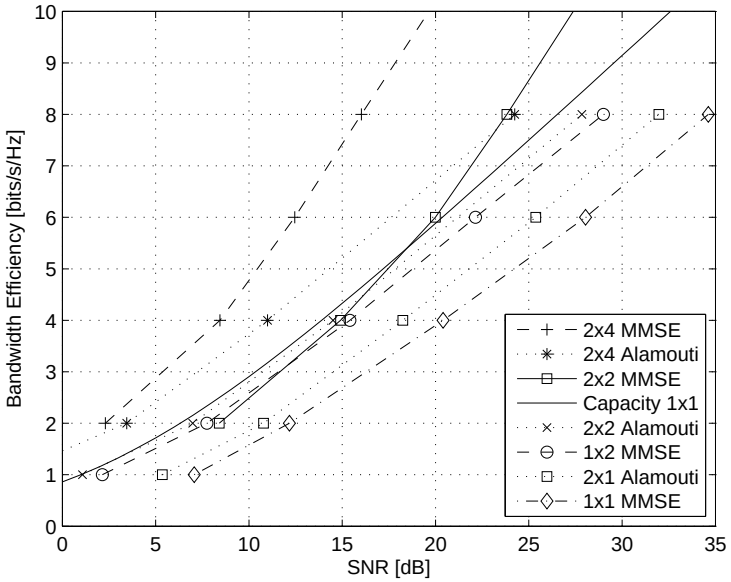

Figure 7.17: Bandwidth Efficiency (at BER=10^{-4}) of Alamouti and MMSE receiver, Gaussian channel

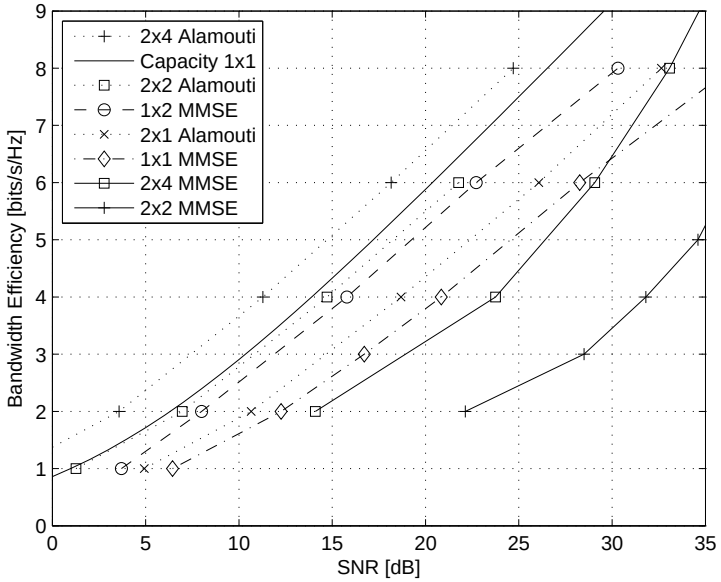

Figure 7.18: Bandwidth Efficiency (at BER=10^{-4}) of Alamouti and MMSE receiver, MIMO-WSSUS channel

MMSE equalization strongly outperforms the Alamouti scheme. Nevertheless one should note the MMSE advantage greatly depends on the rich scattering radio channel and thus cannot be relied upon in general.

7.3 Spatial Multiplexing with variable Channel Knowledge at the Transmitter

The previous sections have introduced several approaches for *linear precoding techniques* in MIMO radio channels. Some of them assumed no channel knowledge at the transmitter, others assumed perfect channel knowledge. In this section, a previously proposed scheme presented in [Tau05] is described that uses a variable amount of radio channel knowledge at the transmitter through the factorization of a matrix and using only a subset of the factors for the channel knowledge at the transmitter.

An improvement to this scheme is also presented that modifies its parameterization of the unitary matrices. The optimum precoding matrix is factorized into several unitary product matrices which are parameterized by simple reconstruction parameters. The modification simplifies the parameterization technique and improves the performance of the original algorithm.

Introduction

The technique described in this section uses linear precoding on the transmitter side [Tau05, SSB+02] which requires the feedback of channel state information (CSI) through a *feedback channel* from the receiver side to the transmitter side. To reduce the amount of required feedback information, a variable amount of CSI is used which is based on a factorization of the precoding matrix. The optimum precoding matrix is factorized into specific unitary product matrices by an algorithm described in [Mur62], where the unitary product matrices are parameterized by simple reconstruction parameters. This scheme enables a flexible *trade-off* between an optimum precoding matrix and the amount of CSI signaling to the transmitter side. Nevertheless, an *ideal* knowledge of the CSI at the *receiver* side is assumed throughout this section.

The matrix parameterization technique of [Mur62] has also been used in [ARU01] and subsequently [MBV02] for finding good packings in complex Grassmannian space. The parameterization scheme has been used to compute gradients in an efficient manner. However, the modifications described in this contribution are not expected to have any significant impact on the optimization outcome in [ARU01, MBV02], although the simplification in the choice of parameters might lead to an easier implementation of the optimization algorithm.

In this contribution, the algorithm of [Tau05, Mur62] is improved by a modified choice of particular parameters during the factorization algorithm. The

resulting performance improvement in the factorized matrix and in a coded MIMO-OFDM system is demonstrated analytically and quantitatively.

7.3.1 Variable Channel Knowledge through Matrix Parameterization

The considered transmission system has N_T transmit and N_R receive antennas and $N_T \leq N_R$. In a vector-matrix notation, the system is shown in figure 7.19.

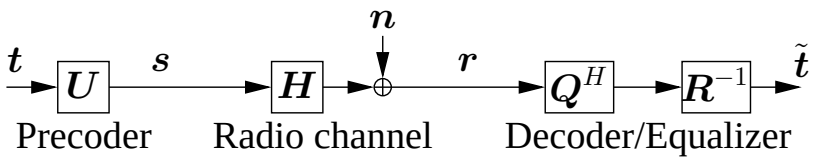

Figure 7.19: Per-subcarrier block diagram of transmission system

At each time step, the symbol vector $\boldsymbol{t} \in \mathbb{C}^{N_T}$ contains N_T modulation symbols in parallel. It is multiplied by the precoding matrix $\boldsymbol{U}$ to give the baseband transmission vector $\boldsymbol{s}$, which is transmitted by N_T antennas simultaneously. The radio channel is described in the baseband by a multiplication with the channel transfer matrix $\boldsymbol{H}$ and the addition of white Gaussian noise $\boldsymbol{n}$.

At the receiver side, the signals from the N_R receive antennas are sampled, giving the baseband receive vector

$$\boldsymbol{r} = \boldsymbol{HUt} + \boldsymbol{n}\,. \tag{7.20}$$

This receive vector $\boldsymbol{r}$ is decoded by the MIMO equalizer. In figure 7.19, it is shown that this equalizer is split into a multiplication with a unitary decoder matrix $\boldsymbol{Q}^H$ and a second multiplication with the equalization matrix $\boldsymbol{R}^{-1}$. These matrices are obtained from the QR decomposition of the matrix product $\boldsymbol{H} \cdot \boldsymbol{U}$

$$\boldsymbol{QR} := \boldsymbol{HU} \tag{7.21}$$

where $\boldsymbol{Q}$ is an unitary and $\boldsymbol{R}$ an upper triangular matrix. Additionally, the equalization block $\boldsymbol{R}^{-1}$ may include non-linear techniques like successive interference cancellation. The MIMO equalization obtains the estimated symbol vector $\tilde{\boldsymbol{t}}$ which is then used for demodulation.

Precoding with variable Channel Knowledge

It is well known that the channel capacity is maximized if the matrix of left singular vectors $\boldsymbol{U}$ from the singular value decomposition (SVD) of the radio

channel matrix $\boldsymbol{H} = \boldsymbol{V}\boldsymbol{\Sigma}\boldsymbol{U}^H$ is used for precoding [RC98, SSB+02]. However, to determine this ideal precoding matrix $\boldsymbol{U}$, the full knowledge of the channel transfer matrix $\boldsymbol{H}$ is necessary at the transmitter, or equivalently, the full matrix $\boldsymbol{U}$ has to be signaled back from the receiver to the transmitter without any errors.

In this proposal, an approximation to the ideal precoding matrix is calculated by the factorization of the ideal precoding matrix $\boldsymbol{U}$ into unitary matrices $\boldsymbol{U}_{pq}$. Since the matrices $\boldsymbol{U}_{pq}$ are all unitary, any subset of the $\boldsymbol{U}_{pq}$ can be used for precoding without losing the unitary property of the linear precoding. Additionally, each of the $\boldsymbol{U}_{pq}$ factors are fully determined by a small set of parameters, which can be signaled back from the receiver to the transmitter with smaller effort than the full matrix. And for a trade-off between signaling effort and performance gain, only a subset of the $\boldsymbol{U}_{pq}$ parameters can be signaled according to different criteria as described below.

In combination, the matrix factorization is a promising technique to achieve a flexible adaptation to the current radio channel situation and to the current possibilities for signaling channel information back from the receiver to the transmitter.

Similar to the previous sections, this technique is proposed to be used on each subcarrier separately, as described in section 5.1. This leads to a system structure as shown in figure 5.2.

7.3.2 Parameterization of Unitary Matrices

Definition of the factorization

Definition 7.1 *Let p and $q > p$ be any two numbers from the set $1, \ldots, n$. Let an unitary* base matrix $\boldsymbol{U}_{pq}(\phi_{pq}, \sigma_{pq}) \in \mathbb{C}^{n \times n}$ *be defined as follows:*

1. *All its diagonal elements are 1 except the pth and qth elements which are $\cos(\phi_{pq})$, and*

2. *All its non-diagonal elements are zero except the element in the pth column and qth row which is $\sin(\phi_{pq})e^{j\sigma_{pq}}$, and the element in the pth row and qth column which is $-\sin(\phi_{pq})e^{-j\sigma_{pq}}$*

These base matrices are "almost" identity matrices, except for the pth and qth row and column, so that a multiplication with such a base matrix will result in a complex rotation in the p, q-plane. Note that $\boldsymbol{U}_{pq}^H(\phi, \sigma) = \boldsymbol{U}_{pq}(-\phi, \sigma)$.

As an example, one such base matrix in $\mathbb{C}^{3\times 3}$ is

$$\boldsymbol{U}_{12}(\phi_{12},\sigma_{12}) = \begin{pmatrix} \cos(\phi_{12}) & -\sin(\phi_{12})e^{-j\sigma_{12}} & 0 \\ \sin(\phi_{12})e^{j\sigma_{12}} & \cos(\phi_{12}) & 0 \\ 0 & 0 & 1 \end{pmatrix} . \tag{7.22}$$

For any dimension n, there are $\binom{n}{2} = n(n-1)/2$ different dimension pairs and hence different base matrices, and each of these base matrix $\boldsymbol{U}_{pq}$ is unambiguously defined by the pair of real-valued parameters ϕ_{pq}, σ_{pq}. In [Mur62] some of the ϕ_{pq}'s are called *longitude angles* and bounded by the parameter range $-\pi \leq \phi_{pq} < \pi$ (notably those with $q = n$), whereas the σ_{pq}'s and the rest of the ϕ_{pq}'s are called *latitude angles* and bounded by the parameter range $-\pi/2 \leq \sigma_{pq} \leq \pi/2$.

Theorem 7.1 (from [Mur62]) *Any unitary matrix $\boldsymbol{S} \in \mathbb{C}^{n\times n}$ can be factorized into a product of base matrices and one diagonal matrix:*

$$\boldsymbol{S} = \boldsymbol{\Delta} \prod_{p=n-1}^{1} \left(\prod_{q=p+1}^{n} \boldsymbol{U}_{pq}(\phi_{pq},\sigma_{pq}) \right) \tag{7.23}$$

(note: the first product term is counting downwards) where

$$\boldsymbol{\Delta} := \begin{pmatrix} e^{j\delta_1} & & 0 \\ & \ddots & \\ 0 & & e^{j\delta_n} \end{pmatrix} \tag{7.24}$$

The first $n-1$ parameters $\delta_1, \ldots, \delta_{n-1}$ of the diagonal matrix $\boldsymbol{\Delta}$ are called latitude angles and bounded by $-\pi/2 \leq \delta_k \leq \pi/2$, $k = 1 \ldots n-1$, whereas the last parameter δ_n is called a longitude angle and bounded by $-\pi \leq \delta_n < \pi$. The parametric space is closed by the identification of the end-points of the interval $-\pi \leq \phi_{pq} < \pi$ and of the interval $-\pi \leq \delta_n < \pi$. The topological character of the parametric space is that of an anchor ring or torus.

The factorization (7.23) *is unambiguous on the understanding that when σ_{11} is indeterminate it is set to zero.*

The proof by construction can be found in [Mur62].

Approximation criteria

With this matrix factorization at hand, in [Tau05] it is proposed to calculate the actual MIMO precoding matrix from a *subset* of the base matrices in (7.23) if

the amount of CSI feedback signaling should be decreased. In this section, a criterion of choosing the "most significant" base matrices of (7.23) is described.

The diagonal matrix $\boldsymbol{\Delta}$ of (7.24) can be ignored for the MIMO precoding. To show this, the factorization (7.23) of the *Hermitian* matrix $\boldsymbol{U}^H$ in the SVD of the channel matrix (section 7.3.1) with $n = N_T$ is calculated as

$$\boldsymbol{U}^H = \boldsymbol{\Delta} \prod_{p=n-1}^{1} \prod_{q=p+1}^{n} \boldsymbol{U}_{pq} \,. \tag{7.25}$$

Inserting this into the equation for the received vector (7.20) gives

$$\boldsymbol{r} = \left(\boldsymbol{V}\boldsymbol{\Sigma}\boldsymbol{\Delta} \prod_{p=n-1}^{1} \prod_{q=p+1}^{n} \boldsymbol{U}_{pq} \right) \cdot \tilde{\boldsymbol{U}}\boldsymbol{t} + \boldsymbol{n} \,. \tag{7.26}$$

This shows that the (potentially approximated) precoding matrix $\tilde{\boldsymbol{U}}$ only needs to cancel the $\boldsymbol{U}_{pq}$ base matrices by their respective Hermitian $\boldsymbol{U}_{pq}^H$ factors but can ignore the diagonal matrix $\boldsymbol{\Delta}$. The effect of $\boldsymbol{\Delta}$ is viewed as a variation of the diagonalized radio channel matrix $\boldsymbol{\Sigma}$, which has to be estimated and compensated for at the receiver side anyway. Therefore the diagonal matrix $\boldsymbol{\Delta}$ will be neglected for the MIMO precoding matrix.

In the product of unitary base matrices $\boldsymbol{U}_{pq}$ in (7.23), the base matrices that are most significant are those most different from an identity matrix. The difference to the identity matrix can be calculated and results in the simple expression[4]

$$\|\boldsymbol{U}_{pq}(\phi_{pq}, \sigma_{pq}) - \boldsymbol{I}\|_F = 2 \sin \frac{|\phi_{pq}|}{2} \,. \tag{7.27}$$

This expression is maximized by the maximum absolute values of ϕ_{pq}.

Therefore if less than the full number of base matrices should be used (say, $k < K = n(n-1)/2$ instead of K), the k base matrices with the largest $|\phi_{pq}|$ are chosen for the approximated precoding matrix.

7.3.3 Matrix Factorization Algorithm

Iteration steps

The algorithm for constructing the factorization (7.23) will be described in the following. The basic idea of the iterative algorithm is to calculate the parameters of a single base matrix per step. In particular, the rightmost base matrix of

[4] $\|\cdot\|_F$ denotes the Frobenius norm which is the square root of the sum of all squared absolute values of the matrix elements

(7.23) is determined in each step, and an algorithm for unambiguously obtaining the resulting $\boldsymbol{U}_{pq}$ matrices will be described.

In the first step this base matrix is $\boldsymbol{U}_{1n}$. Multiplying $\boldsymbol{S}$ by the complex conjugate matrix will then remove this base matrix from the product due to $\boldsymbol{U}\boldsymbol{U}^H = \boldsymbol{I}$, giving the next matrix iterate $\boldsymbol{S}'$ as

$$\boldsymbol{S}[\boldsymbol{U}_{1n}(\phi_{1n}, \sigma_{1n})]^H = \boldsymbol{S}' \,. \tag{7.28}$$

The algorithm is then repeated for the rest $\boldsymbol{S}'$ of the product until the parameters for all base matrices are determined and the diagonal matrix (7.24) is the only remainder on the right hand side of (7.28).

Now it is described how to reduce the product in (7.23) by a single matrix, i.e. how to execute one step (7.28) and determine the matrix $\boldsymbol{U}_{1n}$. The approach is to choose appropriate conditions on the reduced matrix $\boldsymbol{S}'$ in (7.28) to obtain suitable ϕ_{pq}, σ_{pq}, so that the resulting $\boldsymbol{U}_{pq}$ will be of the desired form (7.22).

Two particular matrix elements of $\boldsymbol{S}'$ are considered, namely

$$s'_{11} = s_{11}\cos(\phi_{1n}) - s_{1n}\sin(\phi_{1n})e^{j\sigma_{1n}} \tag{7.29}$$

$$s'_{1n} = s_{11}\sin(\phi_{1n})e^{-j\sigma_{1n}} + s_{1n}\cos(\phi_{1n}) \tag{7.30}$$

which have been obtained from (7.28) by

$$\begin{pmatrix} s'_{11} & \cdots & * & s'_{1n} \\ & \ddots & & * \\ * & \cdots & * & * \end{pmatrix} = \begin{pmatrix} s_{11} & & s_{1n} \\ & \ddots & \\ s_{n1} & & s_{nn} \end{pmatrix} \cdot \begin{pmatrix} \cos(\phi_{1n}) & 0 & \cdots & \sin(\phi_{1n})e^{-j\sigma_{1n}} \\ 0 & 1 & & 0 \\ & & \ddots & \\ -\sin(\phi_{1n})e^{j\sigma_{1n}} & 0 & \cdots & \cos(\phi_{1n}) \end{pmatrix} .$$

Murnaghan algorithm

In [Mur62] the following conditions on the two matrix elements are used for the construction of one base matrix:

c1) $$s'_{1n} = 0$$

c2) $$-\pi/2 \leq \arg(s'_{11}) \leq \pi/2 \text{ or } s'_{11} = 0 \,.$$

These conditions are sufficient to obtain an unambiguous solution for ϕ_{1n}, σ_{1n} so that $\boldsymbol{U}_{1n}$ is of the form (7.22), and the detailed calculation steps are described in [Mur62].

Modified parameterization algorithm

In this contribution, the bounds for the parameter space are chosen differently, resulting in a modified construction of the factorization. According to section 7.3.2, the diagonal matrix $\boldsymbol{\Delta}$ of latitude angles $\delta_1, \ldots, \delta_{n-1}$ and one longitude angle δ_n will not be used for the precoding matrix anyway. This contribution proposes to use *all* angles $\delta_1, \ldots, \delta_n$ as longitude angles and all angles ϕ_{pq} as latitude angles. This is in contrast to the original proposal of [Mur62], where the $\phi_{pq}, q = n$ have been used as longitude angles.

In other words, this contribution proposes a tighter bound on the parameter space of all ϕ_{pq} parameters as follows ("modified" parameterization):

$$-\pi/2 < \phi_{pq} \leq \pi/2\,. \tag{7.31}$$

For the construction of one base matrix, it is sufficient to use only this single condition

$$\text{c3)} \qquad s'_{1n} = 0\,. \tag{7.32}$$

To obtain unique solutions for the parameters so that the resulting $\boldsymbol{U}_{1n}$ is of the desired form (7.22), some case differentiations are necessary:

If $s_{11} = 0$ but $s_{1n} \neq 0$ in (7.30) with (7.32), then $\phi_{1n} = \pi/2$ is chosen. On the other hand if $s_{1n} = 0$ but $s_{11} \neq 0$, then $\phi_{1n} = 0$. And if $s_{11} = s_{1n} = 0$, then ϕ_{1n} becomes irrelevant and is arbitrarily chosen as zero.

If $s_{11} = 0$ or $s_{1n} = 0$ or both, σ_{1n} becomes irrelevant in (7.30) due to the choice of ϕ_{1n} and its value is arbitrarily chosen as zero.

Now the case $s_{11} \neq 0$ and $s_{1n} \neq 0$ is discussed. Inserting (7.32) into (7.30) gives

$$\tan(\phi_{1n}) = -\frac{s_{1n}}{s_{11}} e^{j\sigma_{1n}}\,. \tag{7.33}$$

The right hand side must result in a real valued parameter due to the real-valued ϕ_{1n}. By writing the fraction on the right hand side as $\frac{s_{1n}}{s_{11}} = a + jb$ with $a, b \in \mathbb{R}$, the imaginary part of (7.33) is set to zero by

$$\sigma_{1n} = \begin{cases} \pi/2 & \text{if } a = 0 \\ \arctan(-b/a) & \text{elsewhere.} \end{cases} \tag{7.34}$$

Eventually, the parameter ϕ_{1n} and thus the full base matrix $\boldsymbol{U}_{1n}(\phi_{1n}, \sigma_{1n})$ is obtained by

$$\phi_{1n} = \arctan(a\cos(\sigma_{1n}) - b\sin(\sigma_{1n}))\,. \tag{7.35}$$

Interestingly, this modified parameterization is even easier to implement when compared to the description in [Mur62], but it shows better performance in the later simulations.

7.3.4 Approximation Error

First of all, the approximation error of the approximated precoding matrix $\boldsymbol{U}$ of both parameterizations is checked. The residual error in the received symbols ε is

$$\varepsilon = \tilde{\boldsymbol{t}} - \boldsymbol{t} = \boldsymbol{R}^{-1}(\boldsymbol{R}\boldsymbol{t} + \boldsymbol{Q}^H\boldsymbol{n}) - \boldsymbol{t} = \boldsymbol{R}^{-1}\boldsymbol{Q}^H\boldsymbol{n}$$

where $\boldsymbol{R} = \boldsymbol{Q}^H\boldsymbol{H}\boldsymbol{U}$, and if the noise is assumed uncorrelated ($E\{\boldsymbol{n}\boldsymbol{n}^H\} = \sigma_n^2\boldsymbol{I}$), the error power is

$$E\{\varepsilon\varepsilon^H\} = \sigma_n^2(\boldsymbol{R}^H\boldsymbol{R})^{-1}\,. \tag{7.36}$$

The mean squared error values are the diagonal elements of (7.36).

The matrix $\boldsymbol{R}$ is a direct measure for the error power in the resulting estimated symbols and will be investigated further. The optimum matrix $\hat{\boldsymbol{R}}$ will result if the precoding matrix $\boldsymbol{U}$ is obtained from the Singular Value Decomposition (SVD) as explained in section 7.3.1. In that case the resulting optimum matrix (with additional null columns or rows for $n \neq m$) is identical to the diagonal matrix of the channel matrix' singular values $\hat{\boldsymbol{R}} = \boldsymbol{\Sigma}$, and the expression $\boldsymbol{R}^H\boldsymbol{R}$ in (7.36) is diagonal as well. This is used as the reference case.

The relative Euclidian distance of the diagonal elements of the $\boldsymbol{R}$ matrices to the ideal $\hat{\boldsymbol{R}}$ matrix is calculated according to

$$d_{\text{diag}} = \frac{\|\mathrm{diag}(\boldsymbol{R}) - \mathrm{diag}(\hat{\boldsymbol{R}})\|_2}{\|\mathrm{diag}(\hat{\boldsymbol{R}})\|_2}\,, \tag{7.37}$$

where the diag operator denotes the vector of diagonal elements of a matrix.

The average result is shown in the bottom plots of figure 7.20, calculated as the average over many precoding matrices for random i.i.d. Gaussian matrix realizations. This serves as a comparison for the modified and the original parameterization. In this example with $N_T = N_R = 5$ antennas, $k = N_T(N_T-1)/2 = 10$ different base matrices exist, so with the maximum number of 10 base matrices, both parameterizations enable an ideal reconstruction of the optimum precoding matrix and the distance to $\hat{\boldsymbol{R}}$ converges to zero. For a smaller number of base matrices where the precoding matrix is no longer optimum, it can be seen that the modified parameterization shows a smaller distance to the optimum matrix than the one described in [Mur62].

The same difference can be seen when comparing not only the diagonal values but a Frobenius norm of the *matrix difference*

$$d_{\text{mat}} = \frac{\|\boldsymbol{R} - \hat{\boldsymbol{R}}\|_F}{\|\hat{\boldsymbol{R}}\|_F}\,. \tag{7.38}$$

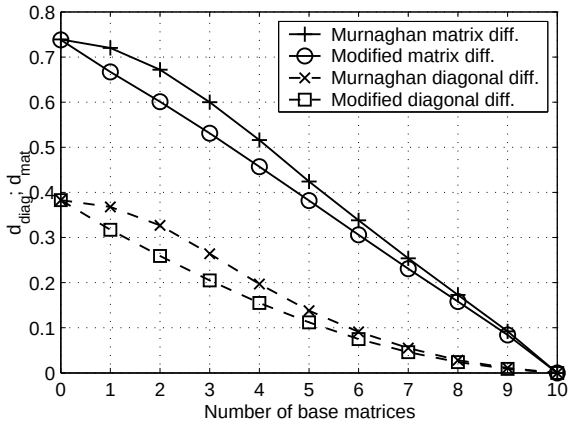

Figure 7.20: Comparison of Murnaghan and modified parameterization. Top: Frobenius norm of matrix difference (7.38) between $\boldsymbol{R}$ and the optimum SVD matrix; Bottom: Relative euclidian distance (7.37) of diagonal elements to optimum SVD diagonal

The top plots of figure 7.20 show a similar result as the previous comparison. With the maximum number of 10 base matrices, both parameterizations enable an ideal reconstruction of the optimum precoding matrix and there is no further distance to $\hat{\boldsymbol{R}}$. For a smaller number of base matrices where the precoding matrix is no longer optimum, it can be seen that the modified parameterization shows a smaller distance to the optimum matrix than the parameterization described in [Mur62].

The differences between the parameterizations can be explained by the choice of latitude and longitude angles. Murnaghan's parameterization chooses some ϕ_{pq} as longitude angles and almost all δ_k as latitude angles. The modified parameterization chooses all ϕ_{pq} as latitude angles and all δ_k longitude angles, i. e. the parameter bounds are distributed differently but in total the same parameter space is used. Since the $\boldsymbol{\Delta}$ matrix is unused for MIMO precoding anyway (see section 7.3.2), the modified parameterization can be said to "shift the approximation error" partly into the unused $\boldsymbol{\Delta}$ matrix. A more smooth approximation as shown in figure 7.20 is the result.

7.3.5 Performance

The linear precoding algorithm has been simulated in the framework that is used throughout this thesis. The OFDM parameters of table 3.2 have been used as well, and an i.i.d. Gaussian MIMO radio channel with independent Rayleigh fading across subcarriers has been assumed. This sections describes

the performance results in terms of the resulting Bit Error Rate (BER).

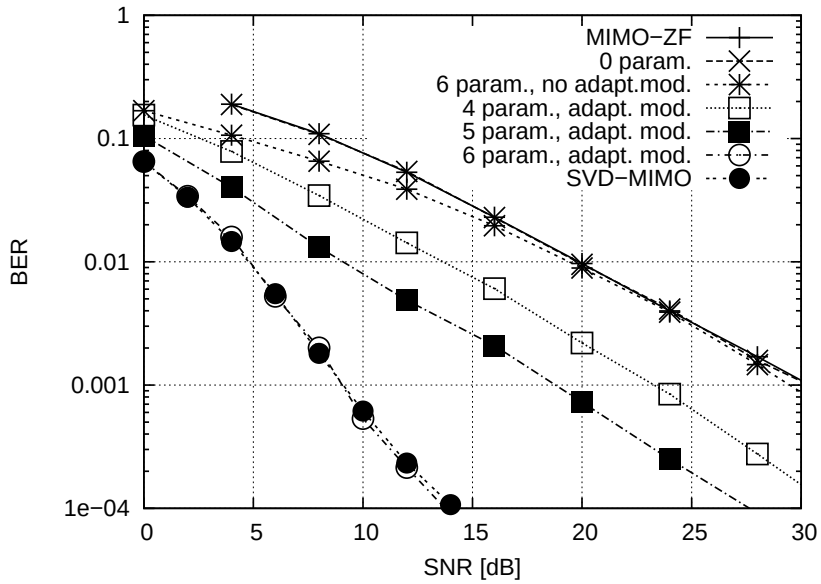

Figure 7.21: Unitary matrix precoding with variable number of base matrices (Bandwidth efficiency $E = 4$ bits/s/Hz; uncoded, 4x4 antennas, Gaussian channel)

In an uncoded MIMO-OFDM system with $N_T = N_R = 4$ antennas, the system performance is shown in figure 7.21. The upper bound for the BER is identical to a linear ZF equalizer as described in section 7.2.1. The lower bound for the BER is identical to SVD transmission as described in section 7.1.

Similar to the investigated SVD system, the linear precoding does give much performance benefit unless combined with Adaptive Modulation. This can be observed by the "6 param., no adapt.mod." curve which shows almost no improvement compared to the "0 param." curve. Instead, when combining the Variable Channel State technique with Adaptive Modulation[5], the performance is improved and eventually reaches that of SVD with Adaptive Modulation, marked by the curve "6 param., adapt.mod." (the factorization consists of $K = N_T(N_T - 1)/2 = 6$ base matrices). The lower bound is identical to an uncoded spatial multiplexing system with matrix inversion, marked by the curve "0 param".

It is visible how a trade-off between a larger amount of feedback information and a better BER performance exists, since any additional base matrix that is used will also improve the performance. In this simulation, no difference between Murnaghan and modified parameterization was observed in the average

[5]This is possible because a feedback channel from the receiver to the transmitter is assumed anyway.

BER results.

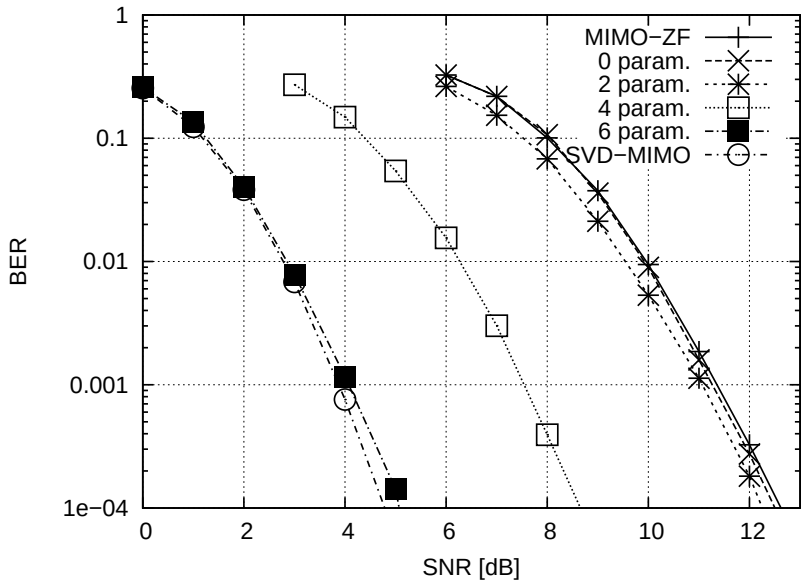

Figure 7.22: Unitary matrix precoding with variable number of base matrices with adaptive Modulation and Channel coding (Bandwidth efficiency $E = 4$ bits/s/Hz; 4x4 antennas, Gaussian channel)

For a comparison in a MIMO-OFDM system, channel coding (convolutional coding with polynomial $171\ 133$) together with adaptive modulation (bit and power loading according to [CCB95]) is considered.

The resulting system performance with $N_T = N_R = 4$ antennas is shown in figure 7.22. Similar to the uncoded case, an increasing number of used base matrices will increase performance (at the expense of increased CSI feedback).

Interestingly, in this simulation there is also a noticeable performance difference between the base matrices obtained by modified versus the ones by the Murnaghan parameterization as can be observed in figure 7.23. In all cases with the approximated precoding matrix, the base matrices calculated by the modified parameterization result in a performance improvement by roughly 1dB compared to the Murnaghan parameterization.

As for the performance in a MIMO-WSSUS radio channel, figure 7.24 clearly shows again how the Variable Channel Knowledge technique varies the performance between Spatial Multiplexing as lower bound and SVD as upper bound. Hence, the best performance in MIMO-WSSUS is simply the case with full channel information at the transmitter (here: “6 param.”). Unfortunately in the MIMO-WSSUS channel even a minor reduction in the channel information (“5 param.”) degrades the performance very much so that this technique is as un-

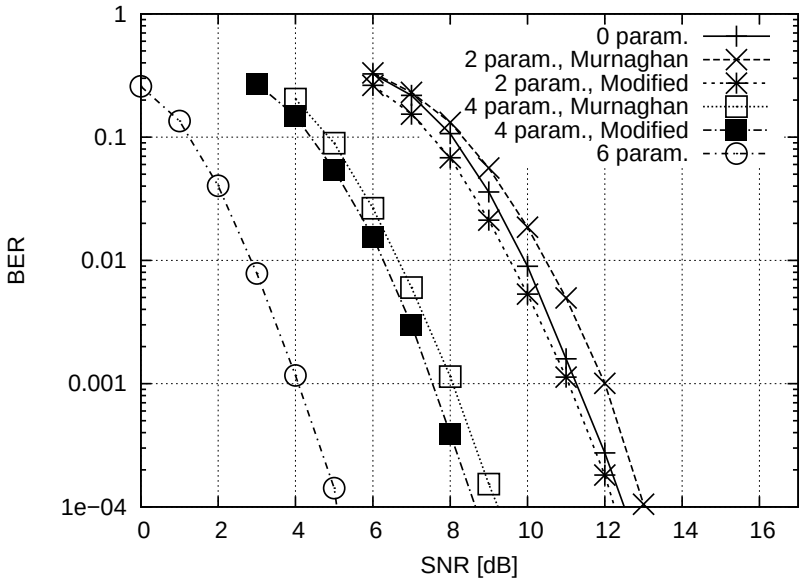

Figure 7.23: Comparison of Unitary matrix precoding with Modified and original Murnaghan factorization. (Coded, Adaptive Modulation, Bandwidth efficiency $E = 4$ bits/s/Hz; 4x4 antennas, Gaussian channel)

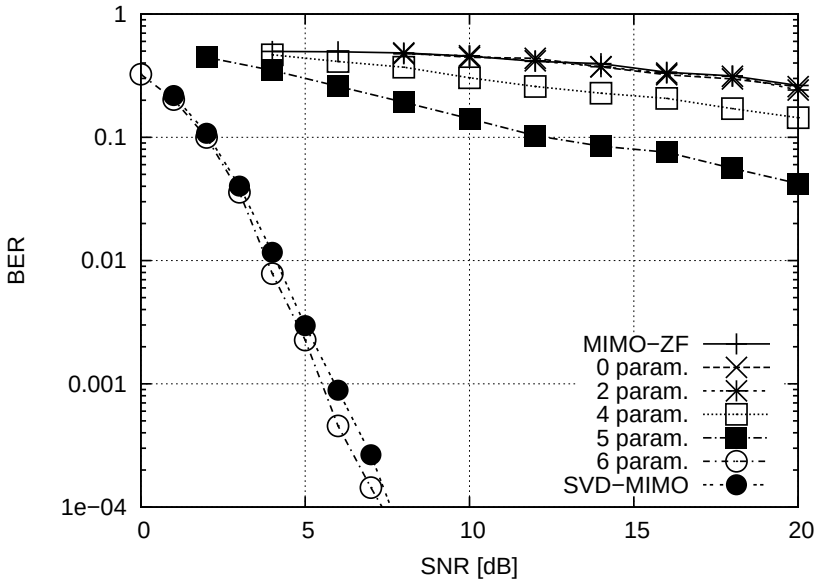

Figure 7.24: Unitary matrix precoding in MIMO-WSSUS channel, with adaptive Modulation and Channel coding (Bandwidth efficiency $E = 4$ bits/s/Hz; 4x4 antennas)

usable as Spatial Multiplexing in the MIMO-WSSUS channel. Nevertheless in some radio channels (like Gaussian) this technique promises to reach similar performance but with reduced feedback requirements.

Discussion

A linear MIMO precoding technique with variable feedback information proposed by [Tau05] has been investigated. The optimum precoding matrix is factorized into unitary product matrices, some or all of which can be used for the approximation of the optimum precoding matrix. For the case of full feedback information and ideal reconstruction of the precoding matrix, no difference between the investigated algorithms and SVD precoding could be observed, as had been expected. In the approximated case with limited feedback information, the matrix factorization enables a trade-off between the amount of feedback information and the system performance. In this contribution, a modification to the matrix parameterization of [Mur62, ARU01, MBV02] has been described. The modified parameterization shows a performance gain over the original parameterization in terms of matrix norms and also in the BER performance of a coded MIMO system.

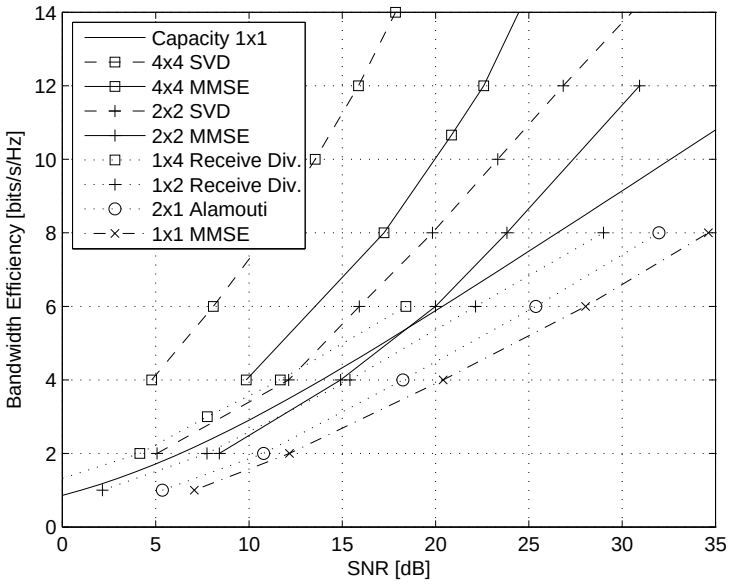

Figure 7.25: Bandwidth Efficiency of MIMO techniques at BER=10^{-4}, Gaussian channel

7.4 Conclusion

Many different techniques have been proposed that exploit various aspects of multiple antennas. All techniques can be combined with OFDM to form a broad-band communication system for high data rates. The bandwidth efficiency of them is summarized in figure 7.25 (Gaussian channel) and figure 7.26 (MIMO-WSSUS channel).

The OFDM transmission technique enables an efficient implementation of MIMO techniques in a broad-band radio channel. The intersymbol-interference will be equalized by the frequency domain equalization of the OFDM technique. This simplification is important because otherwise, the equalizer needs to take into account the whole length of the channel impulse response for all MIMO radio channels in parallel. The algorithmic complexity of such an equalizer will grow too large for broad-band systems. But OFDM is an effective technique to avoid such complexities, and in combination with MIMO even a large number of parallel radio channels can be processed with realistic implementation complexity.

In a rich scattering radio channel represented by the Gaussian model, even the simple Spatial Multiplexing with simple linear receivers can strongly increase the available bandwidth efficiency when increasing the number of transmit and receive antennas. Using ideal channel knowledge at the transmitter in

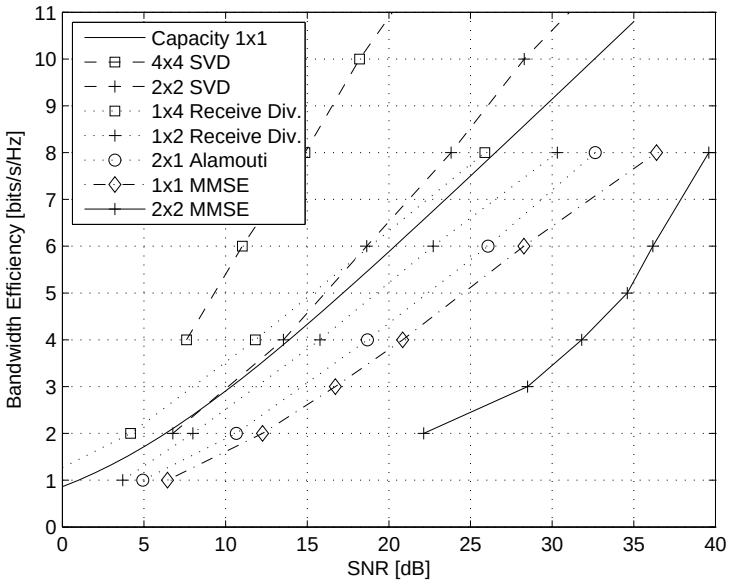

Figure 7.26: Bandwidth Efficiency of MIMO techniques, MIMO-WSSUS channel

SVD would still give additional performance gain, but even without this transmitter knowledge the Spatial Multiplexing techniques improve the data rate. This gives new opportunities in designing a system, where simple algorithms can be used at the expense of additional hardware for multiple antennas. The results of figure 7.25 confirm that a linear ZF receiver and a transmitter without channel knowledge would be sufficient in such a radio channel.

However, in a more unfriendly radio channel with little scattering represented by the MIMO-WSSUS model, the picture is rather different. The simulated results indicate problems for any Spatial Multiplexing technique in MIMO-WSSUS channels, figure 7.26. The assumed large number of scatterers for Spatial Multiplexing is no longer available, and its performance is degraded beyond any usable values in the MIMO-WSSUS radio channel. Only by using transmitter channel knowledge it would be possible to reach usable data rates through SVD, but only with a larger number of antennas where the effort to obtain an accurate channel prediction at the transmitter is prohibitive in reality.

Hence, with the linear receivers investigated in this work, it can be concluded that for realistic non-Gaussian channels, using Receiver Diversity is pretty much all that is possible as MIMO technique. If MIMO techniques should be used with multiple antennas on both sides, non-linear receiver structures will be essential, but these are beyond the scope of this work.

Additionally, it can be concluded that MIMO performance simulations must

be aware of using a MIMO radio channel model that adequately models the correlation between the different channel coefficients, as otherwise unrealistically optimistic performance results will occur. The MIMO-WSSUS radio channel model is a simple modeling approach that enables this choice by the single parameter of the number of scatterers. This way, the performance of the investigated techniques could be evaluated in a realistic radio channel behavior.

8 System Performance and Radio Channel Models

In this work, the information-theoretical channel capacity is not the most important performance measure; instead, the Bit Error Rate (BER) of the complete communication system is the much more important performance figure.

This section uses the BER performance of the MIMO techniques introduced in chapter 7 as a comparison criterion of the MIMO-WSSUS radio channel model of chapter 4 with some other channel models from literature. The communication technique in question is the simple Spatial Multiplexing with linear MMSE demodulation.

It is expected that in a rich scattering channel this simple Spatial Multiplexing technique will strongly increase the available data rate when increasing the number of transmit and receive antennas. Each radio channel model in the following sections should be able to represent this data rate gain. However, in a more unfriendly radio channel with little scattering, it is expected that Spatial Multiplexing techniques perform not as good anymore. Realistic radio channel models should be able to model this performance degradation as well. The MIMO-WSSUS radio channel model introduced in this thesis is a simple modeling approach that represents these statistical properties accurately enough and is still easily configurable.

8.1 Gaussian I.I.D. Radio Channel Model

The Bit Error Rate (BER) of Spatial Multiplexing from section 7.2.2 is evaluated here as an example in various radio channel models.

The performance simulations of this Spatial Multiplexing technique demonstrate that the MIMO channel model shows a noticeable impact on the performance results. In Figure 8.1 (left plot), the i.i.d. Gaussian model from section 4.3 has been used.

In the i.i.d. Gaussian model, the channel transfer matrix $\boldsymbol{H}$ always has full rank and all singular values will be nonzero (see section 4.3.2). For a larger

number of antennas, this means the simulations will show a huge potential for the parallel transmission of data. But this is a much more optimistic performance than what could be expected in realistic radio channels. In fact, this channel model is so optimistic that the performance increases significantly with an increasing number of antennas in figure 8.1, hence increasing the bandwidth efficiency enormously – which is contrary to what has been expected.

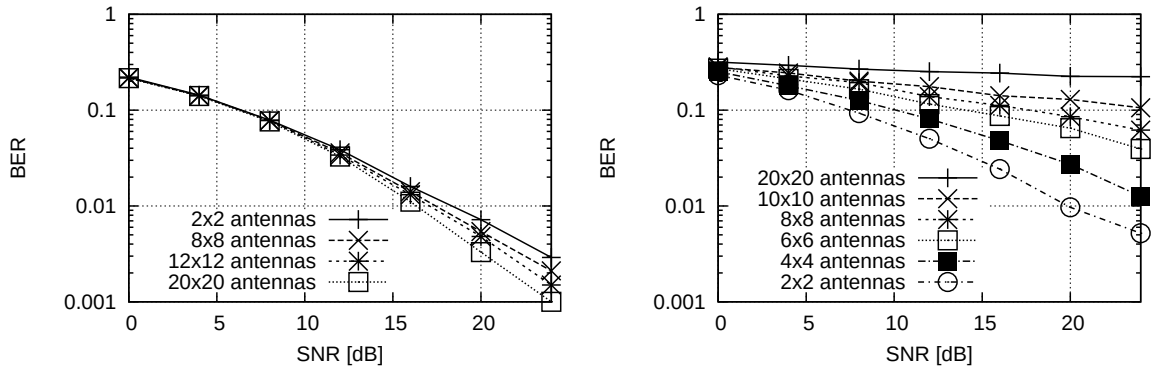

Figure 8.1: Spatial Multiplexing BER. Left: Unrealistically good performance in i.i.d. Gaussian radio channel model. Right: Realistic performance in MIMO-WSSUS channel model, 10 scatterers. (QPSK uncoded)

In contrast to these unrealistically optimistic results, the same simulations have been performed in the MIMO-WSSUS channel model described in section 4.4, here with 10 scatterers. The results in figure 8.1 (right plot) show a behavior completely different from the Gaussian model: For a small number of antennas, Spatial Multiplexing shows an acceptable performance, but as the number of antennas grows larger than the expected rank of the channel matrix (corresponding to the 10 scatterers in the MIMO-WSSUS radio channel model), the performance is no longer acceptable and different MIMO techniques would be required for useful communication. This is the realistic performance that is expected from such a simple MIMO technique in radio channels with realistic correlation among the channel matrix elements.

8.2 MIMO-WSSUS Radio Channel Model

The significant parameter of the MIMO-WSSUS model is the number of scatterers. The influence of this particular parameter on the overall Bit Error Rate (BER) of a MIMO-OFDM system with spatial multiplexing and linear MMSE receiver is investigated in the following.

The BER with various choices of the number of scatterers can be seen in figure 8.2 and 8.5, where a larger number of scatterers leads to a better BER performance of this example MIMO-OFDM system. (For simplicity, $L_T = L_R = L$ is chosen in these examples.) The other radio channel parameters are of less importance for this MIMO performance difference – only this number of scatterers is the relevant parameter to distinguish different channel realizations.

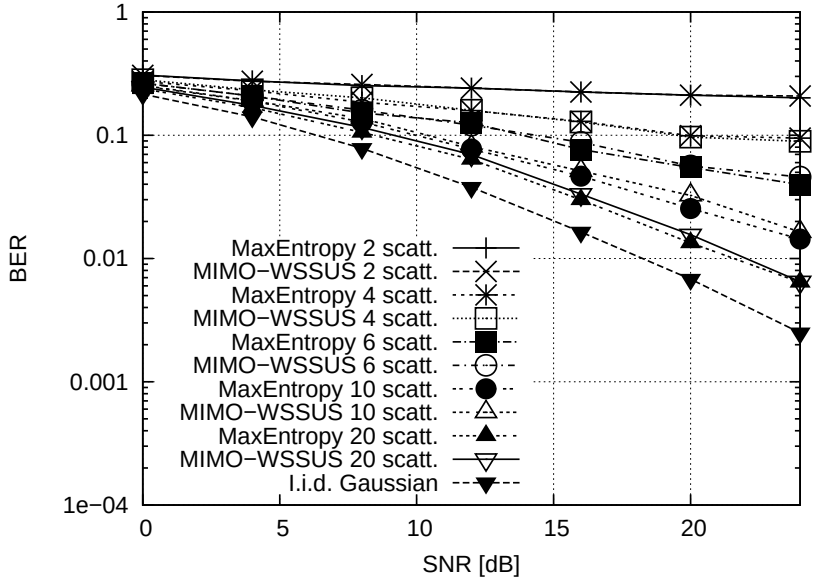

Figure 8.2: Spatial Multiplexing performance in MIMO-WSSUS and Maximum Entropy channel models (4x4 QPSK uncoded, MMSE receiver)

8.3 Maximum Entropy Radio Channel Model

In [DM03, DM05], a different channel model is derived on the basis of maximizing the entropy that is represented by the model, see figure 8.3. Based on the available knowledge in an MIMO-OFDM system setting with s close scatterers at the receiver and s_1 at the transmitter, the resulting channel model is expressed by

$$\boldsymbol{H} = \frac{1}{\sqrt{ss_1}} \boldsymbol{\Psi}_{r\times s} \boldsymbol{\Theta}_{s\times s_1} \boldsymbol{\Phi}_{s_1\times t} \tag{8.1}$$

where $\boldsymbol{\Theta}$ is a matrix of i.i.d. Gaussian random variables, $\boldsymbol{\Phi}$ is the matrix of steering vectors to the closely located scatterers at the transmitter and $\boldsymbol{\Psi}$ at the receiver.

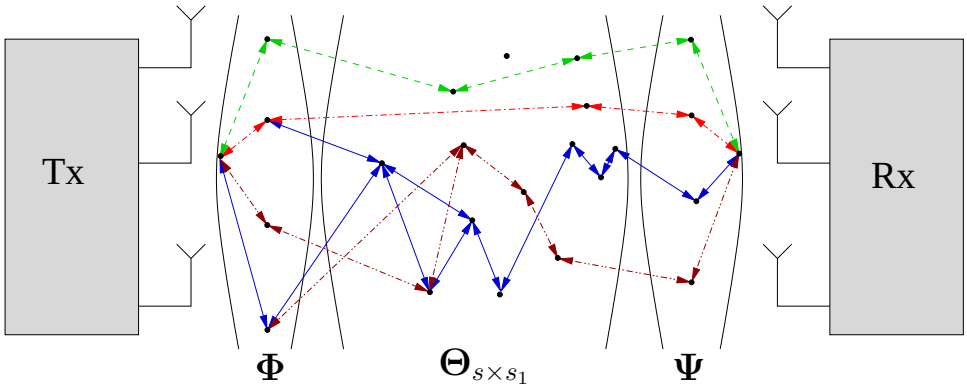

Figure 8.3: Maximum Entropy channel model

The MIMO characteristics of this channel model can be changed by the same two parameters as described in the MIMO-WSSUS model: The number of closely located scatterers s on the transmitter side and s_1 on the receiver side of the radio link. (For the sake of brevity $s = s_1$ is chosen for the rest of this section.)

In figure 8.2, the BER of a spatial multiplexing MIMO-OFDM system is shown. The number of scatterers s in the Maximum Entropy channel model is used as a parameter. Also, the BER of the same system but with the MIMO-WSSUS model is calculated, and the number of WSSUS scatterers L is used as a parameter. As one can observe, the system shows the very same behavior in both channel models, and the parameter in each model shows the same impact on the performance of the system.

In figure 8.4, the same comparison is made for a system employing Space-Time-Block codes (STBC) according to the Alamouti scheme, as explained in section 6.2.1. In figure 8.5, the system of figure 8.2 now uses additional channel coding.

In all cases, the resulting performance behaves the same in both channel models, depending on the single parameter of number of scatterers. Nevertheless the Maximum Entropy channel model has been designed with an Information-Theoretic approach, which means the MIMO-WSSUS channel model approach for broad-band communications was not used here. Therefore this confirms the choice in this work to prefer the MIMO-WSSUS model when the actual system performance of a broad-band MIMO system is the investigated criterion.

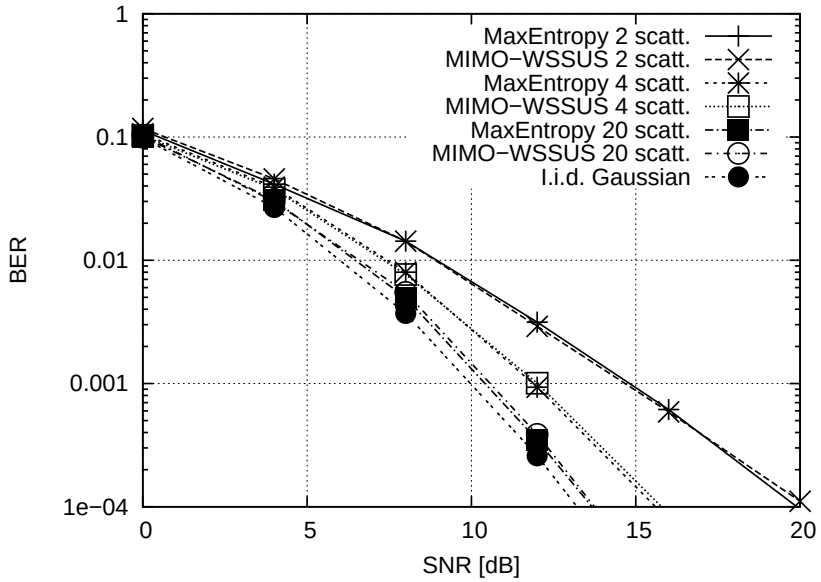

Figure 8.4: Alamouti-coded system in MIMO-WSSUS and Maximum Entropy radio channel model (2x2 QPSK uncoded)

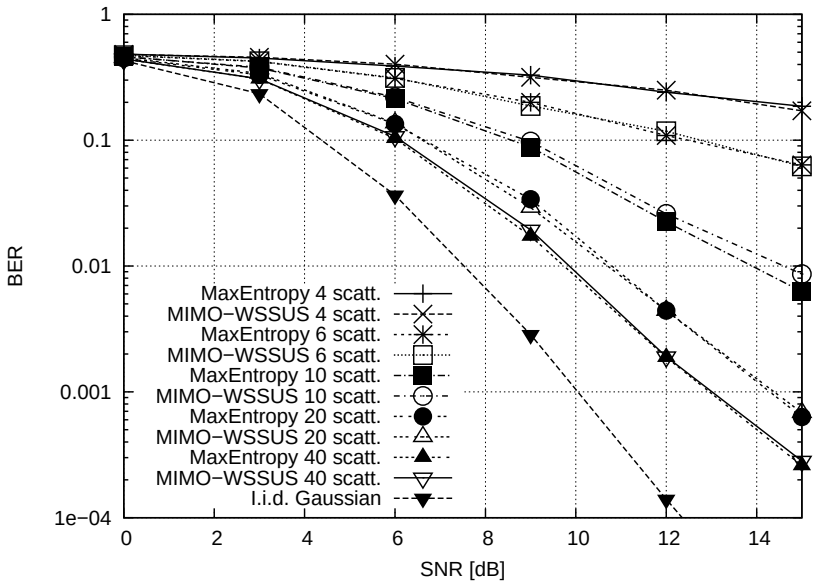

Figure 8.5: Spatial Multiplexing in MIMO-WSSUS and Maximum Entropy radio channel model (4x4 QPSK, $r = 1/2$ channel coding, $E = 1$)

8.4 Wide-band Double-directional Radio Channel Model (WDDCM)

In [GC02, GC04], yet another MIMO channel model is proposed based on an exact geometrical description of the area used for transmission.

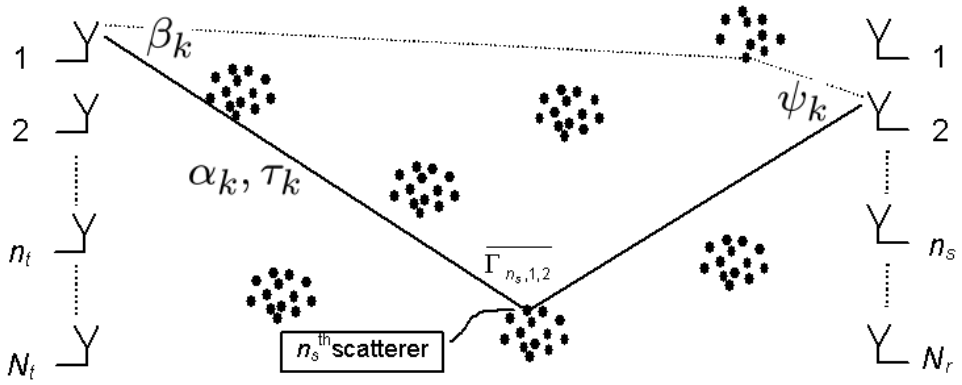

Figure 8.6: WDDCM channel model

In this model, a number of clusters N_C is chosen (fig. 8.6). For each realization of the channel model, each cluster is assigned randomly a place on the two-dimensional plane of the transmission area. In each cluster, some scatterers are randomly located, but close to each other. Then, the actual propagation rays of radio transmission are calculated by the geometry from one transmit antenna over the scatterers to the receive antenna, so that for each path a delay τ_k, a phase shift θ_k, an angle of departure β_k and arrival ψ_k is calculated. These values are used in equation (4.12) to calculate the channel impulse response from antenna n to antenna m.

In figure 8.7, the BER of the spatial multiplexing MIMO-OFDM system from figure 8.2 is shown. The number of clusters N_C in the WDDCM channel model is used as a parameter (solid lines). Also, the BER of the same system but with the MIMO-WSSUS model is calculated, and the cardinality of the set of angles L is used as a parameter (dotted lines). In this case as well, the resulting performance behaves the same in both channel models.

However, the WDDCM channel model requires much more parameters to be chosen, which means that the results depend on the accurately chosen parameters. From our point of view this is a distraction from the actual system performance evaluation and should be avoided.

It can be concluded that for the BER comparison of MIMO-OFDM systems, the actual details of the MIMO channel model are of less importance, and any of the three radio channel models could have been used to evaluate the perfor-

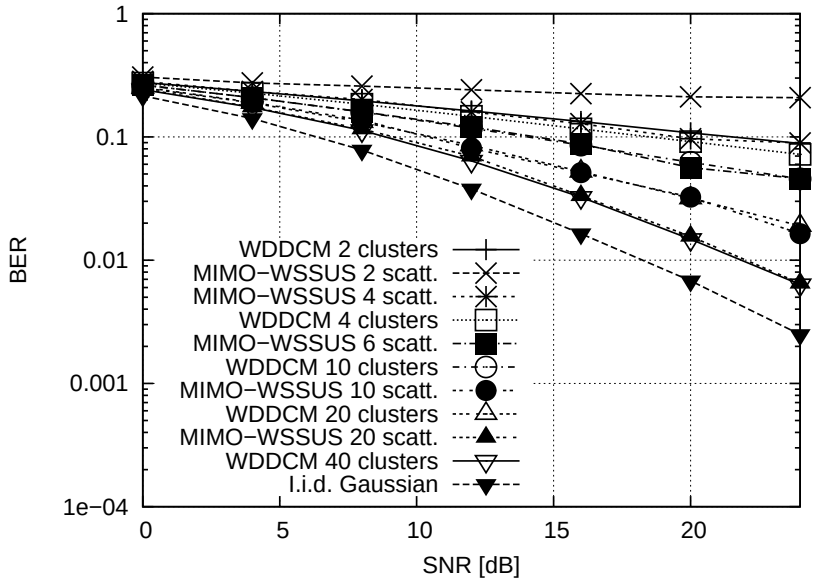

Figure 8.7: Spatial Multiplexing performance in MIMO-WSSUS and WDDCM MIMO channel models (4x4 QPSK uncoded)

mance of the system in different MIMO environments. But for the evaluation in an OFDM system, the MIMO-WSSUS model seems the best compromise between simple parameter choices and meaningful performance results. This confirms the usage of the MIMO-WSSUS radio channel model as an evaluation criterion for the performance of MIMO transmission techniques in realistic radio channels.

9 Conclusion

Multi-antenna (MIMO) communication is a proposed technology to increase the capacity of wireless links. The prerequisite for evaluating the performance of MIMO techniques is a profound knowledge of the MIMO radio channel and an adequate statistical model for the essential properties of this channel. Several MIMO radio channel models have been discussed in this thesis, starting from the well-known Gaussian model with completely uncorrelated fading, and eventually introducing a MIMO-WSSUS channel model with the correlation chosen by the single parameter of the number scatterers. Using an appropriate radio channel model is a crucial component when evaluating candidate technologies for future radio communication systems.

OFDM is the signal processing technique of choice to communicate with a high data rate over broadband channels, either in single antenna or in MIMO systems. This multicarrier technique enables a simple equalization even in strong multi-path radio channels where an equalizer of the inter-symbol interference would be prohibitively complex. But with OFDM the equalization can be done with moderate complexity, even in MIMO systems.

Several basic MIMO techniques were presented in this work. The performance of them depend strongly on the assumed radio channel model. In a rich scattering radio channel represented by the Gaussian model, no correlation between the radio channels occurred and even simple linear MIMO techniques can strongly increase the available bandwidth efficiency when increasing the number of transmit and receive antennas. This gives new opportunities in designing a system, where simple algorithms can be used at the expense of additional hardware for multiple antennas.

However, in a more difficult radio channel with only little scattering as represented by the MIMO-WSSUS model (figure 9.1), the picture is rather different. With a small number of scatterers, the correlation between the radio channels becomes significant and the performance of any linear Spatial Multiplexing technique is degraded beyond any usable values in the MIMO-WSSUS channel. Hence, it can be concluded that for realistic non-Gaussian channels, using Receiver Diversity is basically all that is possible as MIMO technique. If MIMO techniques should be used with multiple antennas on both sides, non-

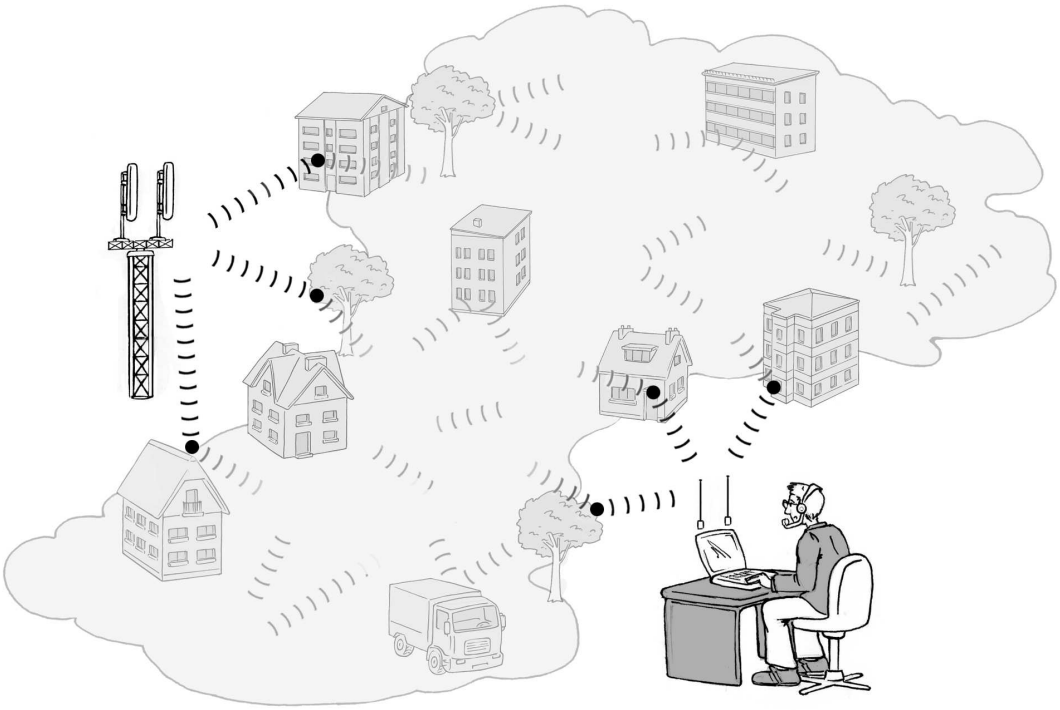

Figure 9.1: MIMO radio channel with a small number of scatterers (here $L = 3$) as represented by the MIMO-WSSUS channel model

linear receiver structures could be a solution to this problem, but those were not covered in this work.

Additionally, a linear precoding technique with variable amount of feedback was explained and improved. All or only a subset of factorization matrices of the unitary matrix factorization can be fed back to the transmitter to reduce the required feedback data rate. This enables a trade-off between the amount of feedback information and system performance. In this thesis, an improvement to the matrix parameterization was presented, which shows a performance gain over the original parameterization. However, in radio channels with little scattering, this technique suffered the same performance degradation as the other spatial multiplexing techniques and is not usable in those radio channels.

It can be concluded that MIMO performance simulations must use a MIMO radio channel model that adequately models the channel conditions with little scattering. Otherwise unrealistically optimistic performance results will occur.

This has been verified by evaluating the system performance degradation with different MIMO radio channel models as taken from literature. All of them enabled an adequate representation of the correlation and performance degradation of simple MIMO techniques. The MIMO-WSSUS model is a sim-

ple modeling approach that enables this choice by the single parameter of the number of scatterers. This way, the performance of the investigated techniques could be evaluated in a realistic radio channel context. The introduced MIMO-WSSUS radio channel model represents these statistical properties accurately and is easily configurable.

OFDM can be used in MIMO systems and enables using MIMO techniques in broadband channels. Receive diversity as a simple MIMO technique can be used always, but other MIMO techniques do not seem to give enough performance benefit in realistic radio channels. OFDM is a very good candidate for future radio communication systems.

A Derivations

This chapter derives the Probability Density Functions of the random phase shifts and gives an analytical expression for its mean value.

A.1 PDF of random phases

A.1.1 PDF of $Y = \sin U$

Given a uniformly distributed random variable $U \sim Unif(-\pi, \pi)$, this section derives the PDF of the transformed random variable $Y = \sin U$.

For the transformation function $y = \sin(u)$ the inverse exists and is $f(y) = u = \arcsin(y)$. Its derivative is $f'(y) = 1/\sqrt{1-y^2}$. The PDF of the transformed random variable is

$$f_Y(y) = f_U(u = f(y)) \cdot |f'(y)| \,.$$

This results in the following PDF for the transformed random variable Y:

$$f_Y(y) = \frac{1}{\pi\sqrt{1-y^2}} \quad \text{for } |y| < 1, \text{ 0 elsewhere} \tag{A.1}$$

This PDF is plotted in figure A.1. It is still symmetric, just like the input random variable U.

A.1.2 PDF of $\Re\{\exp(j\pi \sin U)\}$

This transformed random variable is now used as an angle on the unit circle, resulting in the complex-valued random variable $Z = \exp(j\pi Y) = \exp(j\pi \sin U)$. The PDF of Z can also be calculated analytically.

The polar coordinates of the result are immediately obvious: The magnitude is unity, the argument is πY. But the interesting question is the mean value in Cartesian coordinates. To obtain this, the PDF of the real and imaginary part (i.e. in Cartesian coordinates) is needed.

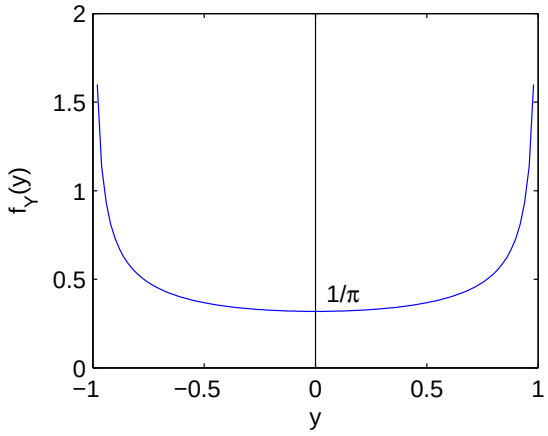

Figure A.1: PDF of $Y = \sin(U)$ from (A.1)

For the real part $f_{Re}(x)$ the transformation function is $x = g(y) = \cos \pi y$ where $y \in [-1, 1]$. Its derivative is $g'(y) = -\pi \sin \pi y$. Its inverse has multiple solutions in the co-domain of y:

$$f(x) = \begin{cases} y_1 = \frac{1}{\pi} \arccos x & \text{for } 0 < y < 1 \\ y_2 = -\frac{1}{\pi} \arccos x & \text{for } -1 < y < 0 \end{cases}$$

The PDF of the transformed random variable must take into account all those solutions of the inverse, giving

$$\begin{aligned} f_{Re}(x) &= \left.\frac{f_Y(y_1)}{|g'(y_1)|}\right|_{y_1 = g^{-1}(x)} + \left.\frac{f_Y(y_2)}{|g'(y_2)|}\right|_{y_2 = g^{-1}(x)} \\ &= \frac{1}{\pi\sqrt{1 - (\frac{1}{\pi}\arccos x)^2} \cdot |-\pi \sin \arccos x|} \\ &\quad + \frac{1}{\pi\sqrt{1 - (\frac{1}{\pi}\arccos x)^2} \cdot |\pi \sin \arccos x|} \,. \end{aligned}$$

The result for the PDF of the real part is

$$f_{Re}(x) = \frac{2}{\pi^2\sqrt{1 - \left(\frac{1}{\pi}\arccos x\right)^2} \cdot \sin \arccos x} \,. \tag{A.2}$$

This PDF is plotted in figure A.2, left picture. The function is not symmetric! It has a nonzero mean, calculated below.

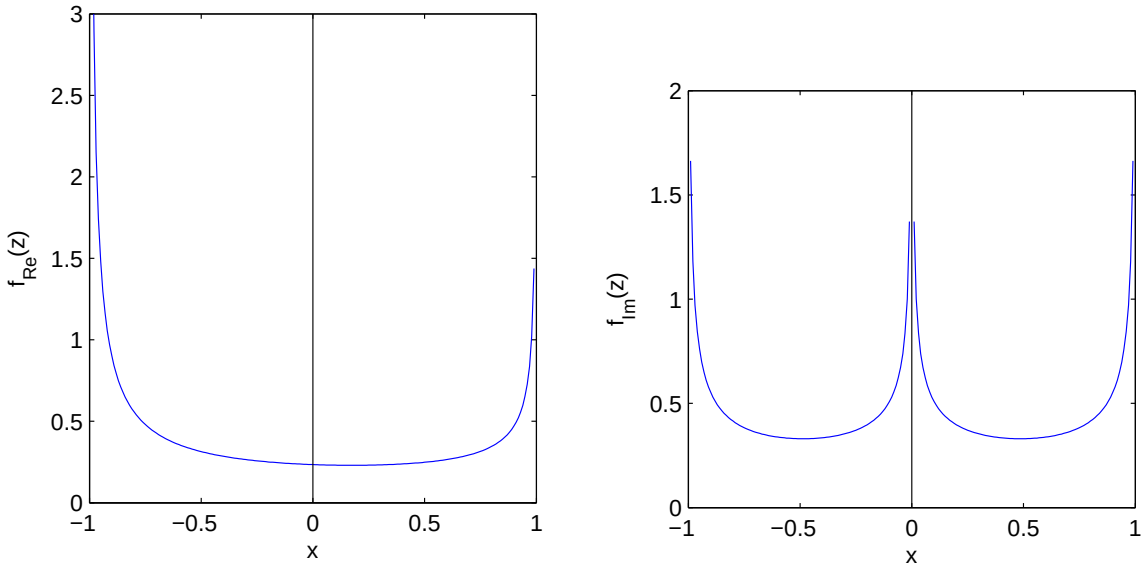

Figure A.2: PDF of real (left) and imaginary (right) part of Z, (A.2) and (A.4)

A.1.3 PDF of $\Im\{\exp(j\pi \sin U)\}$

To calculate the imaginary part, the transformation function is $x = g(y) = \sin \pi Y$, again $y \in [-1, 1]$. Its derivative is $g'(y) = \pi \cos \pi y$. Its inverse again has multiple solutions in the co-domain of y,

$$f(x) = g^{-1}(x) = \begin{cases} y_1 = \frac{1}{\pi}(-\arcsin x - \pi) & \text{for } -\pi < \pi y < -\frac{\pi}{2} \\ y_2 = \frac{1}{\pi}\arcsin x & \text{for } -\frac{\pi}{2} < \pi y < \frac{\pi}{2} \\ y_3 = \frac{1}{\pi}(-\arcsin x + \pi) & \text{for } \frac{\pi}{2} < \pi y < \pi \end{cases} .$$

The PDF of the transformed random variable must take into account all three solutions of the inverse.

$$f_{Im}(x) = \sum_k \frac{f_Y(y_k)}{|g'(y_k)|}\bigg|_{y_k = g^{-1}(x)}$$

$$= \frac{1}{\pi^2 \cos \arcsin x} \left[\frac{1}{\sqrt{1 - (\frac{1}{\pi}\arcsin x)^2}} + \begin{cases} \frac{1}{\sqrt{1-(1-\frac{1}{\pi}\arcsin x)^2}} & \text{for } x > 0 \\ \frac{1}{\sqrt{1-(1+\frac{1}{\pi}\arcsin x)^2}} & \text{for } x < 0 \end{cases} \right] \tag{A.3}$$

By merging the last term with the case distinction into an absolute value of the $\arcsin$, the result for the imaginary part is

$$f_{Im}(x) = \frac{1}{\pi^2 \cos\arcsin x}\left[\frac{1}{\sqrt{1-(\frac{1}{\pi}\arcsin x)^2}} + \frac{1}{\sqrt{1-\left(1-\frac{1}{\pi}|\arcsin x|\right)^2}}\right]. \tag{A.4}$$

This PDF is plotted in figure A.2, right picture. This function is symmetric and has zero mean.

A.1.4 Mean value of $\Re\{\exp(j\pi \sin U)\}$

The mean value of the random phase shift Z is the goal of this derivation. Above, the imaginary part of Z was shown to be symmetric, hence it has zero mean. For the mean value of Z only its real part is relevant anymore. This mean value of the real part part $\gamma = \overline{f_{Re}(x)}$ is obtained by solving the integral for the mean,

$$\gamma = \int x f_{Re}(x)\, dx = \frac{2}{\pi^2}\int_{-1}^{1} \frac{x}{\sqrt{1-(\frac{1}{\pi}\arccos x)^2}\cdot \sin\arccos x}\, dx\,.$$

This integral is simplified using integration by parts,

$$\begin{aligned}
&= \frac{2}{\pi^2}\left[\int_{-1}^{1} \pi \arcsin\frac{\arccos x}{\pi}\, dx - \pi x \arcsin\frac{\arccos x}{\pi}\Big|_{-1}^{1}\right] \\
&= \frac{2}{\pi}\int_{-1}^{1} \arcsin(\frac{1}{\pi}\arccos x)\, dx - 1\,.
\end{aligned}$$

The remaining integral is solved by solving the integral over its inverse, which is possible because graphically one can observe how the inverse must be chosen over the various co-domains. This way, to solve the integral over $y = \arcsin(\frac{1}{\pi}\arccos x)$ in $x \in [-1,1]$, instead an integral over $x = \cos(\pi \sin y)$ is solved over suitable argument ranges, giving

$$\int_{-1}^{1} \arcsin(\frac{1}{\pi}\arccos x)\, dx = \frac{\pi}{2} + \int_{0}^{\pi/2} \cos(\pi \sin y)\, dy\,.$$

Inserting this into γ above gives the mean value

$$\gamma = \frac{2}{\pi} \int_0^{\pi/2} \cos(\pi \sin y)\ dy = \frac{1}{\pi} \int_0^{\pi} \cos(\pi \sin y)\ dy$$

where in the second equation the integral borders could be doubled due to the symmetry of $\sin y$ with respect to $y = \pi/2$. This last expression is identical to the integral form of the Bessel function of the first kind with $z = \pi$,

$$J_0(z) = \frac{1}{\pi} \int_0^{\pi} \cos(z \sin \theta)\ d\theta\,.$$

The final result for the overall mean value is

$$\gamma = \overline{f_{Re}} = J_0(\pi)\,.$$

Even in the generalization of the random phases where an integer multiple k of Y occurs in the exponent and the transformation is $\exp(jk\pi \sin U)$ (note the k), the resulting mean value of this PDF is still the Bessel function of the first kind,

$$\overline{f_{Re}} = J_0(k\pi)\,. \tag{A.5}$$

Again, $J_0(\cdot)$ is the Bessel function of the first kind of order zero. Its first few values are listed in table A.1.

k	$J_0(k\pi)$
1	-0.3042
2	0.2203
3	-0.1812
4	0.1575
5	-0.1412

Table A.1: First few values of the Mean of $f_{Re}(x)$, the real part of the random phase shift distribution

B Simthetic: A programming framework for multiple contributors in OFDM and MIMO simulations

Research work often involves the programming of computer simulations for the evaluation of proposed algorithms. In this chapter, a programming framework is described that simplifies the creation of computationally intensive simulations. This framework supports especially the combination of programming contributions by several different researchers into the same simulation. This is very common in a University context, where multiple PhD candidates and other students work together on the same algorithmic problems. The presented Simthetic software is publicly available as Open Source Software and already includes many building blocks for OFDM and MIMO simulations.

B.1 Introduction

For any kind of proposed transmission system it is vital to demonstrate the actual benefit of one approach versus others. In order to show this comparison under controllable conditions, it is necessary to use a simulation environment in which the algorithms and systems can be implemented.

A plethora of different simulation environments exist in the computer world, and many researchers will simply produce their own simulation tools tailored to their specific needs. It is an open question whether such a simulation environment can be designed in a way so that it has re-usable and universal components. Additionally, a simulation tool should also support an easy combination of contributions by several different researchers. This aspect is especially common in a University context, where multiple PhD candidates and other students work together on the same simulation problems.

The Technische Universität Hamburg-Harburg (TUHH, Hamburg University

of Science and Technology) created the Simthetic[1] Open Source software for Windows and Linux operating systems in order to find a common framework for base-band system simulations [SR04, SR06]. The framework and first steps for programming OFDM systems with or without MIMO techniques will be described below.

B.2 Software

B.2.1 Simulation Structure

The simulation software Simthetic implements a stream-driven model of computation. The system is divided into "`Devices`" which exchange data by means of stream "`Interfaces`", figure B.1. These are classes in the programming language C++ and a UML class diagram is shown in figure B.2 [Fow03]. Connections between `Interfaces` are specified at run-time by a simulation parameter file in XML format and are strongly type-checked at run-time as well. Every `Device` can be freely exchanged by other `Devices`, as long as the connections between `Interfaces` remain type-correct. It is therefore very easy to re-use existing systems or parts of systems, and directly extend them by new algorithms.

Figure B.1: Example `Devices` in Simthetic

To combine the contributions by several independent researchers, each one would be asked to work on a different `Device` class. The C++ language will enforce the same data interfaces and configuration mechanisms on all contributed C++ classes, so that eventually every `Device` can be easily exchanged by functionally equivalent alternative implementations. For example, a `Device` for PSK modulation can easily be exchanged by an alternative `Device` that implements a QAM modulation (figure B.3), and similar `Devices` on the receiver side can be exchanged as well. This way, the performance comparison between two modulation approaches can be achieved while all the rest of the simulation parameters are completely unchanged.

[1] http://simthetic.sourceforge.net

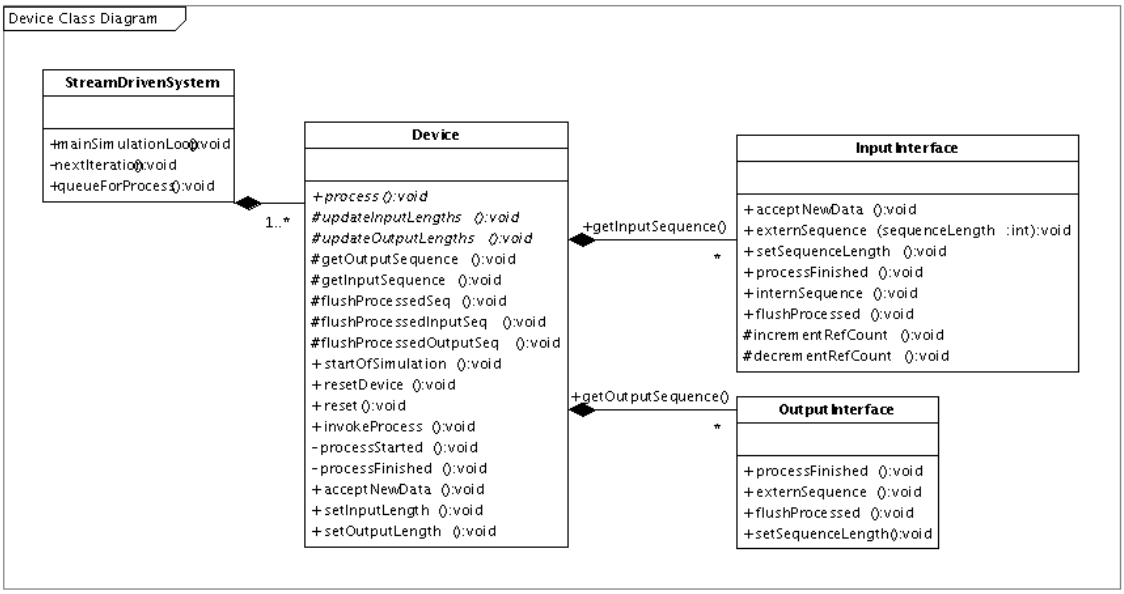

Figure B.2: UML Class Diagram [Fow03] of main classes in Simthetic

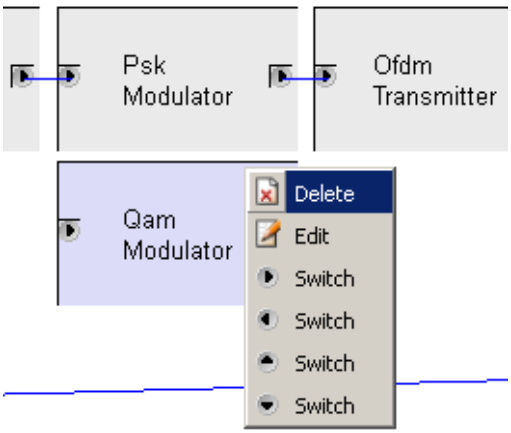

Figure B.3: Exchanging `Devices` in the graphical user interface

B.2.2 Graphical user interface KSimthetic

Additionally, a graphical user interface named *KSimthetic* is available, see figure B.5. In this graphical user interface, a simulation is composed by two steps:

1. Connections between `Interfaces` are created, figure B.5,

2. and the settings (the so-called `Properties`) of each `Device` are specified, figure B.4.

This simulation setup is saved in an XML file. At run-time of Simthetic, this XML file is loaded. The Simthetic system will then instantiate the specified `Device` objects with the given `Properties` according to the simulation XML file. Then, the connections between the `Interfaces` will be created and the simulation starts by calling the processing code of the first `Device`. This first device will create a data stream that is passed through the `Interface` to the second `Device`, whose processing code will be called next, and so forth. This simulation loop will be repeated until the BER counting `Device` sends a special signal to the simulation system so that the simulation ends and the final results are written into output files.

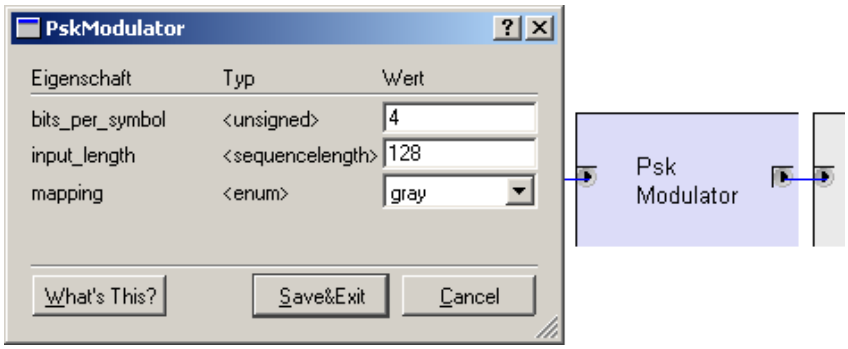

Figure B.4: Setting the `Properties` of a `Device`

Many different system blocks for coded OFDM with coherent, differential or adaptive modulation and convolutional or turbo codes are available. For MIMO-OFDM, various MIMO techniques and MIMO radio channel models are available. Since the software is licensed under the LGPL (GNU Lesser Public License [GNU99]), the full source code of the simulation blocks can be downloaded by everyone from http://simthetic.sourceforge.net. Every interested person can install, use, modify, or redistribute the software for themselves.

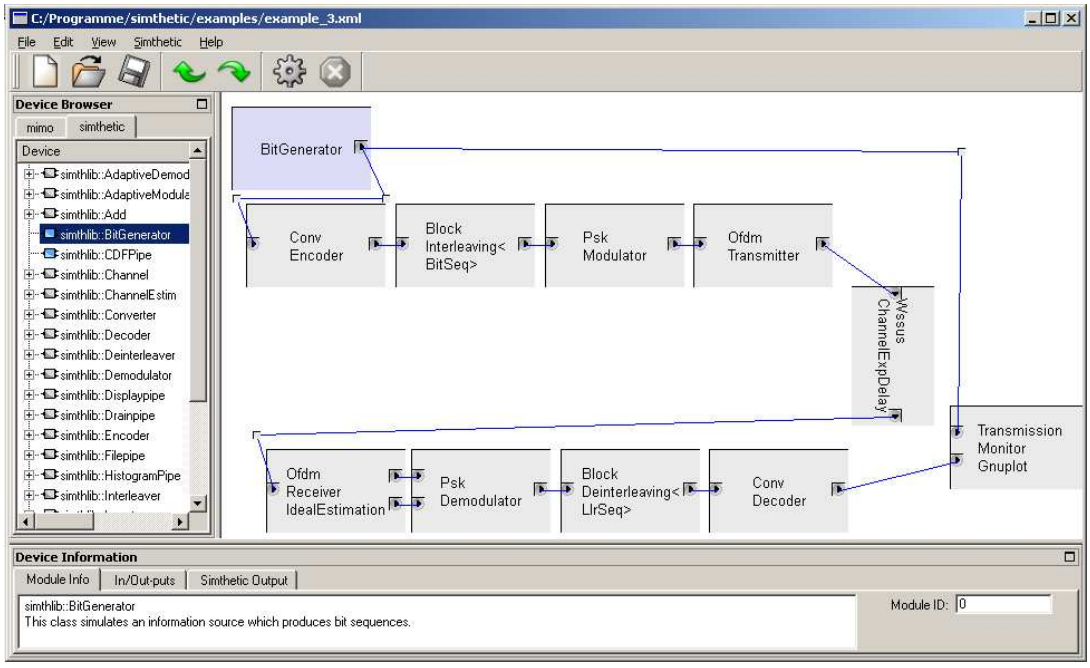

Figure B.5: Creating simulations in the graphical user interface (KSimthetic)

B.3 OFDM

For future communication systems, the OFDM transmission technique is of special interest [RGG01]. The principle of multi-carrier modulation and OFDM in particular is to map a serial high rate source bit stream onto multiple parallel low rate sub-streams. Each subcarrier is modulated individually based on a single sub-stream. Since the symbol rate on each subcarrier is considerably smaller than the serial symbol rate, the effects of delay spread significantly decrease which reduces the equalizer computation complexity.

Every OFDM system consists of similar building blocks. In Simthetic, most of the commonly proposed blocks are already available, figure B.5.

On the left side of the block diagram, a bit sequence is generated randomly. The input bit sequence is then coded by a convolutional channel code, bit interleaved, modulated into complex modulation symbols, and transmitted by the OFDM transmission technique (IFFT and guard interval).

The time continuous signal that is transmitted through the radio channel can be approximated using oversampling techniques. Time shifts of non-integer duration are represented by appropriate oversampling in the radio channel model. It is also possible to display particular signals graphically and in animated form, for example the radio channel transfer function, figure B.6.

At the receiver side, each transmitter block has its corresponding receiver

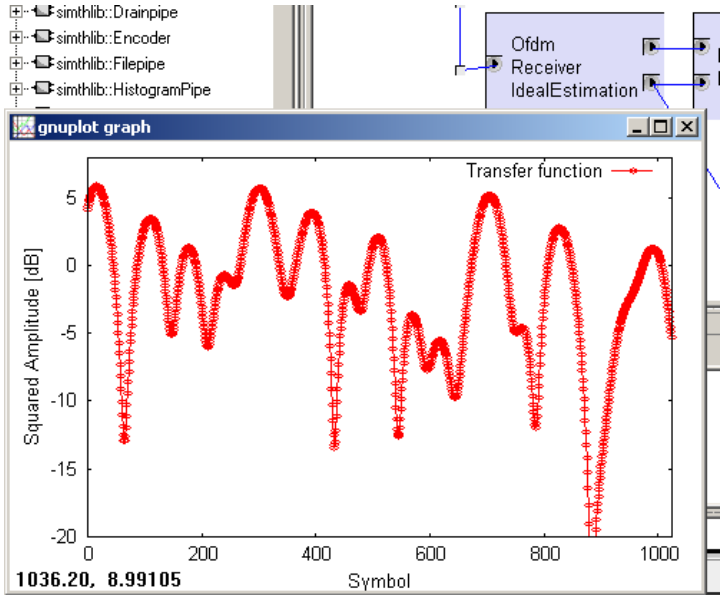

Figure B.6: Example radio channel transfer function animation

block. The received baseband signal is OFDM processed, demodulated, and transmission errors are corrected by a Viterbi decoder. In the end, the bit errors are counted, written into a file, and (optionally) displayed, figure B.7.

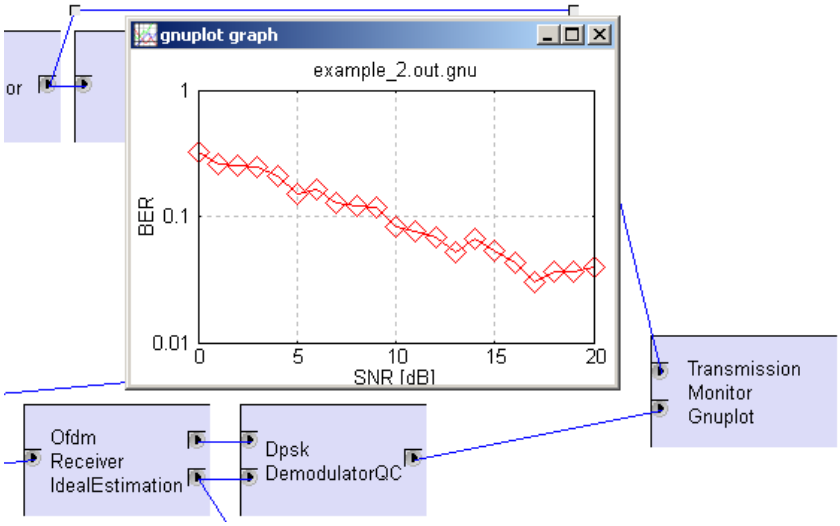

Figure B.7: Example Bit Error Rate

B.4 Getting Started with Programming

This section should explain the necessary steps to follow when somebody intends to add new processing code into the Simthetic system. As an example, it

is explained how a new MIMO radio channel model would be implemented.

First of all one should start to read the existing HTML-documentation[2] where the "Alphabetical List" of classes quickly shows the existing `MIMOChannel` class for a MIMO radio channel. In the documentation of that class, one can see that all MIMO-Channels which are already implemented in Simthetic are subclasses of the basic class `simth::Device`. One can check for functions of the base class that are available in all subclasses by clicking on the `Device` button. At the beginning those functions are usually not needed.

Back in the documentation of the `MIMOChannel` class, one can look under "Public Methods" for the functions `getTransfer()` and `transmit()`. Those are the functions that one has to implement in a new channel class, indicated by the `=0` at the end of the function which declares these functions as purely virtual. The function `transmit()` should define how the transmission of the symbol-sequence from the transmitting antennas (variable `insym`) to the receiving antennas (`outsym`) is done. `transmit()` does its operation in the time domain, because the function arguments are time domain signals. `getTransfer()` is used for an ideal estimation of the channel transfer function and should return the channel transfer matrices $H(f)$ in the frequency domain, because the function argument is a frequency signal.

Now one should open the source code file `src/mimo-channel.cpp` and take a look at the source code of these functions in existing classes. For the implementation of a MIMO channel normally several mathematical operations from linear algebra are needed. The MIMO library of Simthetic uses data types from the Lapack++ library[3] for those operations.

At the beginning one can easily build a "perfect" MIMO Channel, which of course only works for an equal number of transmitting and receiving antennas (set by the Properties in the simulation XML file). In `transmit()` every sample from the incoming `VectorTimeSignal insym` is directly given to the outgoing `VectorTimeSignal outsym`:

```
// The "transmission"
for(size_t k; k!=insym.size(); k++)
   outsym[k] = insym[k];
```

Starting with this simple channel one can extend it step by step. It can be helpful to look at the work by others in the existing source code files. Also, for many people it has been helpful to print intermediate values by `std::cout` to

[2] http://simthetic.sourceforge.net/mimolib/api-doc/html

[3] http://lapackpp.sourceforge.net

double-check the results with a calculator or a mathematical program. As soon as a new class has been added with the virtual functions implemented, this new class is available in the graphical tool KSimthetic and it can be used in own simulations.

B.5 Conclusion

The behavior and performance of any simulation algorithm needs to be confirmed by quantitative simulation results. The Open Source simulation software Simthetic offers a platform for many different communication system evaluations, especially for OFDM systems and MIMO techniques. This simulation framework additionally supports an easy integration of contributions by different researchers. This aspect is especially common in a University context, where multiple PhD candidates and other students work together on the same simulation problems. All the described algorithms and systems can directly be downloaded with the full program source code for Windows and Linux operating systems, so that tests and modifications are available for every interested reader.

List of Figures

List of Tables

Bibliography

[Ala98] S. M. Alamouti. A simple transmitter diversity scheme for wireless communication. *IEEE Journal on Selected Areas in Communication*, 16(8):1451–1458, October 1998.

[ARU01] D. Agrawal, T. Richardson, and R. Urbanke. Multiple-antenna signal constellations for fading channels. *IEEE Trans. Inform. Theory*, 47(6):2618–2626, September 2001.

[AS64] M. Abramowitz and I. A. Stegun. *Handbook of Mathematical Functions with Formulas, Graphs, and Mathematical Tables*. Dover, New York, 1964.

[BBP03] H. Bölcskei, M. Borgmann, and A. J. Paulraj. Impact of the propagation environment on the performance of space-frequency coded MIMO-OFDM. *IEEE Journal on Selected Areas in Communications*, 21(3):427–439, April 2003.

[Bel63] P. A. Bello. Characterization of randomly time-invariant linear channels. *IEEE Transactions on Communications*, 11:360–393, December 1963.

[BVR07] H. Busche, A. Vanaev, and H. Rohling. SVD-based MIMO precoding on equalization schemes for realistic channel estimation procedures. *Frequenz*, 7–8:146–151, July/August 2007.

[BVR08] H. Busche, A. Vanaev, and H. Rohling. SVD-based MIMO precoding and equalization schemes for realistic channel knowledge: Design criteria and performance evaluation. *Wireless Personal Communications*, published online, June 2008.

[CCB95] P. Chow, J. Cioffi, and J. Bingham. A practical discrete multitone transceiver loading algorithm for data transmission over spectrally shaped channels. *IEEE Trans. Commun.*, 43(234):773–775, Feb.-Apr. 1995.

[CGR02] B. Chen, R. Grünheid, and H. Rohling. Scheduling policies for joint optimization of DLC and physical layer in mobile communication systems. In *Proc. of the 13th IEEE International Symposium on Personal, Indoor and Mobile Radio Communications (PIMRC 2002)*, Lissabon, Portugal, September 2002.

[Cim85] L. J. Cimini. Analysis and simulation of a digital mobile channel using orthogonal frequency division multiplexing. *IEEE Transactions on Communications*, 33:665–675, July 1985.

[CKBS04] M. Capstick, B. Kemp, A. Burr, and C. Stimming. Multiband MIMO antenna arrays. In *13th IST Mobile Communications Summit*, Lyon, France, 27-30 June 2004.

[DM03] M. Debbah and R. Müller. Capacity complying MIMO channel models. In *37th Annual Asilomar Conference on Signals, Systems and Computers*, Pacific Grove, California, USA, 2003.

[DM05] M. Debbah and R. Müller. MIMO channel modelling and the principle of maximum entropy. *IEEE Transactions on Information Theory*, 51(5):1667–1690, May 2005.

[Ede88] A. Edelman. Eigenvalues and condition numbers of random matrices. *SIAM Journal on Matrix Analysis and Applications*, 9(4):543–560, October 1988.

[FH96] R. F. H. Fischer and J. B. Huber. A new loading algorithm for discrete multitone transmission. In *IEEE Globecom*, London, 1996.

[Fos96] G. J. Foschini. Layered space-time architecture for wireless communication in a fading environment when using multi-element antennas. *Bell Labs Technical Journal*, 1(2):41–59, 1996.

[Fow03] M. Fowler. *UML Distilled: A Brief Guide to the Standard Object Modeling Language, Third Edition*. Addison-Wesley Professional, 2003.

[Gal06] D. Galda. *Ein Beitrag zum Vielfachzugriff, zur Synchronisation und Kanalschätzung in einem OFDM-basierten Mobilfunksystem*. Dissertation, Technische Universität Hamburg-Harburg, Germany, 2006. Cuvillier Verlag, ISBN 3-86537-996-6, Göttingen.

[GBGP02] D. Gesbert, H. Bölcskei, D. A. Gore, and A. J. Paulraj. Outdoor MIMO wireless channels: Models and performance prediction. *IEEE Trans. Commun*, 50(12):1926–1934, December 2002.

[GBR01] R. Grünheid, E. Bolinth, and H. Rohling. Blockwise loading algorithm for the adaptive modulation technique in OFDM systems. In *IEEE VTC-2001, Atlantic City, USA*, April 2001.

[GC02] J. Gil and L. Correia. Impact of wideband directional propagation channel characteristics on adaptive beamforming. *IEICE Trans. on Communications*, E85-B(12):2640 – 2647, December 2002.

[GC04] J. Gil and L. Correia. Fundamental wideband and directional channel parameters ruling adaptive beamforming performance in micro- and macro-cells. In *VTC 2004 Spring*, Genova, Italy, 2004.

[Gie06] T. Giebel. *Kanaladaption und adaptiver Vielfachzugriff in codierten OFDM-Datenübertragungssystemen*. Dissertation, Technische Universität Hamburg-Harburg, Germany, 2006. Cuvillier Verlag, ISBN 3-86537-739-4, Göttingen.

[GNU99] GNU Lesser General Public License, Version 2.1. Website, 1999. Published by the Free Software Foundation. Available online at http://www.gnu.org/licenses/licenses.html; visited on July 14th 2006.

[Grü00] R. Grünheid. *Vielfachzugriffsverfahren für die Multiträger-Übertragungstechnik*. Dissertation, Technische Universität Hamburg-Harburg, Germany, 2000. VDI Verlag, ISBN 3-18-363610-7, Düsseldorf.

[Hat80] M. Hata. Empirical formula for propagation loss in land mobile radio services. *IEEE Transactions on Vehicular Technology*, 29(3):317–325, August 1980.

[HH87] D. Hughes-Hartogs. Ensemble modem structure for imperfect transmission media. Technical report, U.S. Patent No 4,679,227 (July 1987), 4,731,816 (March 1988), and 4,833,706 (May 1989), 1987.

[IYTU84] F. Ikegami, S. Yoshida, T. Takeuchi, and M. Umehira. Propagation factors controlling mean field strength on urban streets. *IEEE*

Transactions on Antennas and Propagation, 32(8):822–829, August 1984.

[KH05] M. A. Kamath and B. L. Hughes. The asymptotic capacity of multiple-antenna rayleigh-fading channels. *IEEE Transactions on Information Theory*, 51(12):4325–4333, December 2005.

[Lam04] M. Lampe. *Adaptive Techniques for Modulation and Channel Coding in OFDM Communication Systems*. Dissertation, Technische Universität Hamburg-Harburg, Germany, 2004. GCA-Verlag, ISBN 3-89863-163-X, Herdecke.

[MBV02] M. L. Mccloud, M. Brehler, and M. K. Varanasi. Signal design and convolutional coding for noncoherent space-time communication on the block-rayleigh-fading channel. *IEEE Trans. Inform. Theory*, 48(5):1186–1194, May 2002.

[Mur62] F. D. Murnaghan. *The Unitary and Rotation Groups, vol III of Lectures on Applied Mathematics*, volume III of *Lectures on Applied Mathematics*. Spartan Books, Washington DC, USA, 1962.

[OOKF68] Y. Okumura, E. Ohmori, T. Kawano, and K. Fukuda. Field strength and its variability in VHF and UHF land-mobile radio service. *Review of the Electrical Communication Laboratory*, 16(9-10):825–873, Sept./Oct. 1968.

[Pap84] A. Papoulis. *Probability, Random Variables, and Stochastic Processes (McGraw-Hill Series in Electrical Engineering)*. McGraw-Hill Companies, 1984.

[PL95] K. Pahlavan and A. Levesque. *Wireless Information Networks*. John Wiley, Chicester, UK, 1995.

[Pro00] J. Proakis. *Digital Communications*. McGraw-Hill Science/Engineering/Math, 2000.

[Pät02] M. Pätzold. *Mobile Fading Channels: Modelling, Analysis & Simulation*. John Wiley & Sons, 2002.

[Ran08] J. Ran. *Signal Processing, Channel Estimation, and Link Adaptation in MIMO-OFDM Systems*. Dissertation, Technische Universität Hamburg-Harburg, Germany, 2008.

[Rap01] T. S. Rappaport. *Wireless Communications: Principles and Practice (2nd Edition)*. Prentice Hall PTR, 2001.

[RC98] G. Raleigh and J. Chioffi. Spatio-temporal coding for wireless communication. *IEEE Transactions on Communications*, 46:357–366, March 1998.

[RG05] H. Rohling and R. Grünheid. Cross layer considerations for an adaptive OFDM-based wireless communication system. *Wireless Personal Communications*, 32(1):43–57, January 2005.

[RGG01] H. Rohling, R. Grünheid, and D. Galda. OFDM air interface for the 4th generation of mobile communication systems. In *6th International OFDM-Workshop*, Hamburg, Germany, 2001.

[SCR05] C. Stimming, T. Chen, and H. Rohling. Flexible self-organized resource allocation in cellular OFDM systems. In *10th International OFDM-Workshop*, Hamburg, Germany, September 2005.

[Sha48] C. E. Shannon. A mathematical theory of communication. *Bell System Technical Journal*, 27:379–423 and 623–656, 1948.

[SR04] C. Stimming and H. Rohling. Evaluation of MIMO-OFDM and MIMO channel models in the open-source simulation software simthetic. In *9th International OFDM-Workshop*, Dresden, Germany, September 2004.

[SR06] C. Stimming and H. Rohling. Simthetic: A programming framework for multiple contributors in OFDM and MIMO simulations. In *11th International OFDM-Workshop*, Hamburg, Germany, August 2006.

[SSB+02] A. Scaglione, P. Stoica, S. Barbarossa, G. Giannakis, and H. Sampath. Optimal designs for space-time linear precoders and decoders. *IEEE Transactions on Signal Processing*, 50(5):1051–1064, May 2002.

[Tau05] G. Tauböck. *Wireline Multiple-Input/Multiple-Output Systems*. PhD thesis, Vienna University of Technology, 2005.

[Tel99] I. E. Telatar. Capacity of multi-antenna gaussian channels. *European Transactions on Communication*, 10:585–595, November/December 1999.

[TH99] D. N. Tse and S. Hanly. Linear multi-user receiver: Effective interference, effective bandwidth and user capacity. *IEEE Trans. on Information Theory*, 45(6):641–657, March 1999.

[TJC99] V. Tarokh, H. Jafarkhani, and A. R. Calderbank. Space-time block codes from orthogonal designs. *IEEE Transactions on Information Theory*, 45(5):1456–1467, July 1999.

[TSC98] V. Tarokh, N. Seshadri, and A. Calderbank. Space-time codes for high data rate wireless communication: performance criteria and code construction. *IEEE Trans. Information Theory*, 44(2):744–765, March 1998.

[TV05] D. N. Tse and P. Viswanath. *Fundamentals of Wireless Communication*. Cambridge University Press, Cambridge, UK, 2005.

[TZ00] D. N. Tse and O. Zeitouni. Linear multiuser receivers in random environments. *IEEE Trans. on Information Theory*, 46(1):171–188, January 2000.

[WB88] J. Walfish and H. Bertoni. A theoretical model of UHF propagation in urban environments. *IEEE Transactions on Antennas and Propagation*, 36(12):1788–1796, December 1988.

[WDM05] T. Weber, S. Deng, and M. Meurer. Dynamic resource allocation in JOINT. In *10th International OFDM-Workshop*, Hamburg, Germany, 2005.

[WE71] S. B. Weinstein and P. M. Ebert. Data transmission by frequency-division multiplexing using the discrete fourier transform. *IEEE Transactions on Communications*, 19:628–634, 1971.

[ZT03] L. Zheng and D. Tse. Diversity and multiplexing: a fundamental tradeoff in multiple-antenna channels. *IEEE Transactions on Information Theory*, 49(5):1073– 1096, May 2003.

Index